Microfluidic development of a pneumolysin-responsive liposomal platform for selective treatment of *Streptococcus pneumoniae*

by

Ethan Watt

A thesis

presented to the University of Waterloo

in fulfilment of the

thesis requirement for the degree of

Master of Science

in

Pharmacy

Waterloo, Ontario, Canada, 2024

© Ethan Watt 2024

Author's Declaration

I hereby declare that I am the sole author of this thesis. This is a true copy of the thesis, including any required final revisions, as accepted by my examiners.

I understand that my thesis may be made electronically available to the public.

Abstract

The bacterium *Streptococcus pneumoniae* has become a leading cause of meningitis, sepsis, and bacterial pneumonia worldwide, with increased prevalence of antibiotic-resistant serotypes only serving to exacerbate the issue. This imposes a significant public health threat and growing economic burden, spurring research into alternative treatments. One effective route to bypass resistance development is through the targeting of virulence factors essential for bacterial pathogenesis, comprising cellular structures, regulatory systems, and molecules produced by the bacterium. The main factor responsible for colonization and immune response escape in pneumococcal infections is the secreted molecule pneumolysin, which is a subset within a family of related toxins that form transmembrane pores in biological membranes through cholesterol recognition and binding. The conserved activity and structure of pneumolysin between all observed *S. pneumoniae* serotypes, along with its requirement for pathogenicity, has made this molecule an attractive target for vaccination, diagnostic, and sequestration platforms, but not yet as a facilitative agent for therapeutic treatment.

The present work aimed to take advantage of pneumolysin's dependencies through the fabrication of cholesterol-rich liposomes, a natural mimic of the external surface of mammalian cells, to elicit pore formation and subsequent release of an encapsulated peptide. A custom microfluidic system was manufactured to enable rapid and consistent liposomal synthesis, with key formulation parameters optimized through a Box-Behnken response surface design. The vesicles themselves were comprised of naturally-derived phospholipids and varying levels of cholesterol (30/45/60/75 mol%), which displayed desirable physical properties and high encapsulation rates of the bacteriocin nisin. A liposomal cholesterol content above 45 mol% was determined necessary to facilitate interactions with both purified pneumolysin toxin and *S. pneumoniae* culture, as demonstrated through enhanced nisin release and a reduction in hemolytic rates upon exposure of the toxin with cholesterol-rich vesicles.

Antibacterial testing highlighted the ability of the developed platform to elicit a potent and specific bactericidal response *in vitro* against *S. pneumoniae* when compared to a control strain, *Staphylococcus epidermidis*. It further improved viability of a fibroblast cell line upon *S. pneumoniae* challenge, outperforming free nisin via the synergistic impact of simultaneous bacterial clearance and pneumolysin neutralization. This study indicates that cholesterol-rich liposomes hold promise as a treatment platform against pneumococcal infections, with potential for expansion to other pathogenic bacteria known to produce similar cholesterol-dependent toxins.

Acknowledgements

I would like to firstly express my deepest gratitude to my supervisor Dr. Emmanuel A. Ho for his consistent and unwavering support, mentorship, and funding throughout the duration of this project. He has left a lasting impact on my career development as a scientist and without him, none of this would be possible. I would also like to extend many thanks to my advisory committee, Dr. Praveen P. Nekkar Rao and Dr. Juewen Liu, for their valuable advice and encouragement throughout the project.

I would also like to extend appreciation to all staff at the School of Pharmacy as they play an integral role to the daily function of the laboratory and building. Special thanks go out to my graduate coordinator Melinda Recchia for her continual support, as well as the School of Pharmacy research technician Dr. Monica Tudorancea for ensuring an efficient and safe work environment. Beyond that, morphological analysis would not have been possible without the highly skilled Mishi Groh in the Department of Biology. I would of course like to also thank all members of the Ho research group, both past and present. I have grown very close bonds with you all and your continual guidance and support has been integral over the past two years. Special thanks go out to Ilinca Andriescu, Kaidy Orellana, Ryan Nodder, Jin Wang, Alistair Chan, Calvin Wong, Qi Sun, Dr. Chen Sun, and Dr. Yannick Traore.

Thank you to Tara Prica for your constant support and companionship – I am so fortunate to have been able to go through this experience with you by my side. Finally, I am especially thankful for my loving family who have never waivered in their support of my studies. All my progress throughout the past two years would not have been possible without this wide network of talented individuals, for which I am eternally grateful.

Table of Contents

Author's Declaration ii

Abstract iii

Acknowledgements iv

List of Figures viii

List of Tables xi

List of Abbreviations xii

Chapter 1 : Introduction 1

1.1 Pneumococcal Disease 1

1.1.1 Epidemiology 1

1.1.2 Virulence Factors 2

1.1.3 Prevention and Treatment 4

1.2 Pneumolysin as a Therapeutic Target 6

1.2.1 Structure and Function 6

1.2.2 Pneumolysin-Responsive Nanosystems 8

1.3 Liposomal Synthesis 11

1.3.1 Conventional Preparation Techniques 11

1.3.2 Microfluidics 12

1.3.3 Optimization via Response Surface Methodology 15

1.4 Research Framework 16

1.4.1 Project Rationale 16

1.4.2 Hypothesis 17

1.4.3 Objectives 18

Chapter 2 : Methodology 19

2.1 Materials 19

2.2 Liposome Synthesis & Characterization 20

2.2.1 Experimental Microfluidic Setup 20
2.2.2 Dried Film Preparation 21
2.2.3 Physical Particle Characteristics 22
2.2.4 Encapsulation Efficiency 22
2.2.5 Physical Stability 23
2.3 Box-Behnken Response Surface Design 23
2.4 Bacterial Studies 24
2.4.1 Bacterial Strains and Growth Conditions 24
2.4.2 Hemolytic Activity Assay 25
2.4.3 Morphological Analysis 26
2.4.4 Liposomal Release Assay 26
2.4.5 Minimum Inhibitory and Bactericidal Concentrations 27
2.4.6 Time-Kill Kinetics Assay 27
2.5 Cell Studies 28
2.5.1 Cell Culturing 28
2.5.2 Cell Viability Testing 29
2.6 Statistical Analysis 30

Chapter 3 : Results and Discussion 31
3.1 Liposomal Synthesis and Optimization 31
3.1.1 Microfluidic System Development 31
3.1.2 Box-Behnken Design Model Construction 34
3.1.3 Optimization of Box-Behnken Design 39
3.1.4 Variation of Liposomal Cholesterol 41
3.2 Pneumolysin Interactions 44
3.2.1 Optimization of Bacterial Culture 44
3.2.2 Hemolytic Activity 45
3.2.3 Pneumolysin-Induced Liposomal Burst Release 49
3.2.4 Morphological Analysis of Liposomal Pneumolysin Binding 50

3.3 Antibacterial Activity 53
3.3.1 Minimum Inhibitory and Bactericidal Concentrations 53
3.3.2 Time-Kill Kinetics 55
3.4 Cell Protective Impact 57
3.4.1 Nisin Cytotoxicity 57
3.4.2 Bacterial Challenge Protection 58

Chapter 4 : Conclusions 62
4.1 Findings and Significance 62
4.2 Limitations and Future Directions 63

References 66

Appendix 80

List of Figures

Figure 1.1. Illustration of genera and species of bacteria that produce CDCs alongside their associated toxin [24, 25]. 4

Figure 1.2. Schematic of PLY pore formation process, initiated by membrane binding within cholesterol-rich domains and followed by subsequent oligomerization and insertion. Created with BioRender.com and adapted from [48]. 7

Figure 1.3. Schematic representation of a typical staggered herringbone micromixer from both (a) top-down and (b) side profiles, with relevant parameters identified, including channel width (w) and height (h), as well as herringbone depth (d) and width (a). Adapted from [91]. 13

Figure 1.4. Comparison of three-factor design methods, including (a) three-level FFD, (b) Box-Wilson CCD, and (c) BBD. The scale has been coded to range from -1 to 1, with total trials assuming one centre point measurement. 16

Figure 2.1. Experimental setup of the microfluidic system. 21

Figure 3.1. Impact of ethanol content on viability of cultured IMR-90 cells. Values represent mean ± SD (n=3). 33

Figure 3.2. Standard curve of nisin measured via CBQCA assay, with the line of best fit, its equation, and R^2 value displayed. Values represent mean ± SD (n=3). 34

Figure 3.3. Measured responses of randomized three-factor BBD for (a) EE (b) LC, (c) PS, and (d) PDI. Values represent mean ± SD (n=3). 35

Figure 3.4. Contour plots highlighting the influence and interactions between different independent variables in the BBD model. This includes the correlation between (a, d, g, j) FRR and nisin concentration, (b, e, h, k) FRR and EPG molar concentration, and (c, f, i, l) nisin concentration and EPG molar concentration. Specifically, the contour plots give indications on the impact these variables have on (a-c) EE, (d-f) LC, (g-i) PS, and (j-l) PDI. All hold values were set to their median coded level. For interpretation, dark blue colours represent the lowest values for each response variable while dark green represents the highest, with legends displayed for each contour plot. 38

Figure 3.5. Liposomal characteristics of the optimization solutions, including (a) EE and LC, (b) PS and PDI, as well as (c) encapsulated nisin and ZP. Values represent mean ± SD (n=3)..... 40

Figure 3.6. Impact of cholesterol content on liposomal (a) EE and LC, as well as (b) PS and PDI. Statistical analysis was carried out via one-way ANOVA followed by Tukey's multiple comparison test for both EE and PS, where *$p < 0.05$. Values represent mean ± SD (n=3). 42

Figure 3.7. Physical stability of liposomes in terms of (a,b) PS and (c,d) PDI at storage temperatures of (a,c) 4°C and (b,d) 37°C, measured at varying timepoints over a 14-day period. Statistical analysis was carried out via one-way ANOVA followed by Tukey's multiple comparison test from initial measurements against each timepoint, where *$p < 0.05$. Values represent mean ± SD (n=3). 43

Figure 3.8. Growth curves of cultured (a) *S. pneumoniae* and (b) *S. epidermidis* as measured through both OD at 600 nm and CFU via serial plate dilutions, with initial inoculums diluted to a 0.5 McFarland standard density. A standardization curve within regions of logarithmic growth was then developed to contrast OD at 600 nm vs CFU/mL for both (c) *S. pneumoniae* and (d) *S. epidermidis*, with a line of best fit, its equation, and R^2 displayed for each. Values represent mean ± SD (n=3). 45

Figure 3.9. Hemolytic activity of (a) varying concentrations of purified PLY toxin and *S. pneumoniae* culture load against human RBCs. This was then compared to hemolytic activity of (b) purified PLY toxin (200 ng/mL) and (c) *S. pneumoniae* culture (3.0×10^7 CFU/mL) against RBCs in the presence of liposomes at varying cholesterol content. Values represent mean ± SD (n=3). 47

Figure 3.10. Liposomal solution at varying molarities were affixed to the bottom of a 96-well plate and fully dried, with (a) visible changes in opacity within the well evidence of lipid film formation at 1000 µM. Following this, the protective effect of the films was examined through (b) hemolytic assays of the treated wells at varying cholesterol content when incubated with PLY capable of inducing full lysis of human erythrocytes (200 ng/mL). Values represent mean ± SD (n=3). 48

Figure 3.11. Liposomal release of nisin induced by PLY incubation (4 µg/mL) at 37°C, measured at varying timepoints over a 1 h duration at differing molar cholesterol content (200 µM liposomal dose). Values represent mean ± SD (n=3). 50

Figure 3.12. TEM images of both (a,c,e,g) untreated and (b,d,f,h) PLY-incubated (4 μg/mL) liposomes at varying molar cholesterol compositions (200 μM), ranging from (a,b) 30 mol%, (c,d) 45 mol%, (e,f) 60 mol%, and (g,h) 75 mol%. Red arrows indicate potential PLY-induced liposomal pores. All scale bars are equivalent to 100 nm. 52

Figure 3.13. Time-kill plots for both (a,c) *S. pneumoniae* and (b,d) *S. epidermidis* over a 24 h incubation period and initial load of $8.6x10^5$ CFU/mL. The effectiveness of (a-b) free nisin at various factors of the MIC was examined, as well as (c-d) liposome-encapsulated nisin at varying molar compositions of cholesterol at a concentration of 1X the MIC. Values represent mean ± SD (n=3), with a limit of quantitation of 100 CFU/mL. 56

Figure 3.14. Cytotoxicity assay examining the impact of unencapsulated and liposome-encapsulated nisin on cultured IMR-90 cell viability at varying concentrations over a 24 h incubation period. Statistical analysis was carried out through one-way ANOVA followed by Tukey's multiple comparison test between free nisin and the liposomal samples at each concentration, where $*p < 0.05$, $**p < 0.01$. Values represent mean ± SD (n=3). 58

Figure 3.15. Impact on IMR-90 cell viability through inoculation with varying bacterial loads of cultured *S. pneumoniae* and *S. epidermidis* for 24 h. Values represent mean ± SD (n=3). 59

Figure 3.16. Protection studies examining viability of IMR-90 cells challenged by $7.5x10^6$ CFU/mL of *S. pneumoniae* culture in the presence of free nisin, empty liposomes, or nisin-loaded liposomes. This study was conducted for liposomes containing a molar composition of (a) 30 mol%, (b) 45 mol%, (c) 60 mol%, and (d) 75 mol% cholesterol. Statistical analysis was carried out through one-way ANOVA followed by Tukey's multiple comparison test between free nisin and loaded liposomal samples at each concentration, where $*p < 0.05$, $**p < 0.01$. Values represent mean ± SD (n=3). 61

List of Tables

Table 1.1. Pneumococcal virulence factors and their role in pathogenesis. 3

Table 1.2. Overview of nanosystems utilizing PLY for biomedical applications. 9

Table 1.3. Relevant parameters for consideration during development of a microfluidic workflow. . 14

Table 2.1. Independent variables and their corresponding levels utilized in the BBD. 24

Table 3.1. Coefficients for the second-order polynomial equations for all four response variables (EE, LC, PS, PDI) and associated *p*-values as determined in Minitab® software (X_1 – FRR, X_2 – Nisin concentration, X_3 – EPG molar composition). All coefficients are displayed in coded units to maintain orthogonality, with each model's R^2 identified. All *p*-values < 0.05 have been highlighted under the assumption of significance. 36

Table 3.2. A series of optimization solutions given varying goals for each response variable in the developed polynomial model, including minimization (-), maximization (+), and set targets, along with corresponding fit and desirability values. 39

Table 3.3. Response results of the O3 formulation and agreeance as compared to the predicted model outputs. Observed data values represent mean ± SD (n=3). 41

Table 3.4. MIC and MBC for *S. pneumoniae* and *S. epidermidis* against both free and liposome-encapsulated nisin at varying molar compositions of cholesterol (n=3). Initial bacterial load equated to $8.6x10^5$ CFU/mL. 54

List of Abbreviations

ANOVA	Analysis of variance
BBD	Box-Behnken design
BHI	Brain heart infusion
CBQCA	3-(4-carboxybenzoyl) quinoline-2-carboxaldehyde
CCD	Central composite design
CDC	Cholesterol-dependent cytolysin
CFU	Colony forming units
DLS	Dynamic light scattering
DMSO	Dimethyl sulfoxide
DNA	Deoxyribonucleic acid
DTT	Dithiothreitol
EDTA	Ethylenediaminetetraacetic acid
EE	Encapsulation efficiency
EMEM	Eagle's minimum essential medium
EPC	Egg L-α-phosphatidylcholine
EPG	Egg L-α-phosphatidylglycerol
FBS	Fetal bovine serum
FDA	United States Food and Drug Administration
FFD	Full factorial design
FRR	Flow rate ratio
IPD	Invasive pneumococcal disease
LC	Loading capacity

LytA	Lytic amidase
MBC	Minimum bactericidal concentration
MIC	Minimum inhibitory concentration
MM	Molar mass
MTS	3-(4,5-dimethylthiazol-2-yl)-5-(3-carboxymethoxyphenyl)-2-(4-sulfophenyl)-2H-tetrazolium
MWCO	Molecular weight cut-off
NP	Nanoparticle
OD	Optical density
P/S	Penicillin/streptomycin
PBS	Phosphate-buffered saline
PDI	Polydispersity index
PLY	Pneumolysin
PS	Particle size
RBC	Red blood cell
RSM	Response surface methodology
SD	Standard deviation
T_m	Phase transition temperature
TEM	Transmission electron microscopy
TFR	Total flow rate
TSA	Tryptic soy agar
TSB	Tryptic soy broth
ZP	Zeta potential

Chapter 1: Introduction

1.1 Pneumococcal Disease

1.1.1 Epidemiology

The gram-positive *Streptococcus pneumoniae* is an opportunistic pathogen that maintains a commensal relationship with the host when colonized on mucosal surfaces of the human upper respiratory tract, with over 97 characterized serotypes [1]. This bacterium has been found to be carried by 20-50% of children and 5-20% of adults, with this asymptomatic presence allowing for rapid aerosol transmission within a community to eventual elicit infection [2, 3]. Invasive pneumococcal disease (IPD) involves spreading of the bacterium to normally sterile bodily fluids, with examples being sepsis, bacteremic pneumonia, septic arthritis, and meningitis. Alternatively, non-IPD typically occurs outside of major organs and tend to be less serious, including bronchitis, sinusitis, and otitis media [4].

Due to its opportunistic nature, hosts with weakened, deteriorating, or underdeveloped immune systems are at the greatest risk to *S. pneumoniae* colonization and proliferation, with the highest rates of incidence found in the elderly, immunocompromised individuals, and children under the age of two [2]. The susceptibility of a host to disease varies on their demographic and the colonizing pneumococcal strain, as different serotypes have been seen to vary in their pathogenicity [5]. Beyond this, the bacterium is a common secondary infection in individuals with influenza A due to upregulation of epithelial receptors used for *S. pneumoniae* binding, leading to elevated mortality rates when compared to the isolated virus [6].

Pneumonia can be caused by viruses and fungi but is most often bacterial in origin, with several different types being identified depending on where the infection is contracted and the bacterium that causes it. Pneumococcal pneumonia, caused by the migration of *S. pneumoniae* to the lungs, is responsible for roughly two-thirds of all bacterial cases and attributable to 55% of all lower respiratory tract infection deaths in 2015 [7, 8]. The disease state is typically characterized by inflammation of pulmonary tissue and difficulty breathing due to elevated fluid levels, worsened by the potential for person-to-person spread via aerosols [9]. *S. pneumoniae* is also naturally competent, giving it a higher capacity to remodel its genome through uptake of exogenous deoxyribonucleic acid (DNA), promoting antibiotic resistance and limiting vaccine-induced immunity [10]. As a result of this and high carriage

rates in healthy hosts, the World Health Organization has identified *S. pneumoniae* as one of twelve priority pathogens that urgently requires more effective treatment methods [11].

1.1.2 Virulence Factors

The effectiveness of *S. pneumoniae* arises due to the range of produced colonization and virulence factors described in Table 1.1, which serve to give insight towards disease pathogenesis and, consequently, potential points of treatment and intervention. This has been an area of growing interest, as it has been found that these virulence factors are typically essential for growth and highly specific to the host bacterium. These traits make them promising therapeutic targets, as it both limits selection pressure towards resistant strains and reduces damage to commensal microbiota in the host through more specific targeting [12]. The virulence factors of *S. pneumoniae* have implications ranging from adherence, colonization, bacterial spreading, and avoidance of host immune defences, serving to highlight the importance of understanding their mechanisms when designing a therapeutic platform [2].

Overall, pathogenesis of *S. pneumoniae* is largely controlled by release of the protein pneumolysin (PLY), which is part of a pore-forming toxin family referred to as cholesterol-dependent cytolysins (CDCs). Over 20 species of pathogenic bacteria have been associated with the production of CDC toxins that demonstrate largely conserved structure and function, as outlined in Figure 1.1. These protein toxins act mainly to recognize and bind to cholesterol-rich regions within cellular membranes, at which point they reassemble into a pore complex and insert within the lipid bilayer to cause membrane disruption [13]. In particular, PLY can act in concert with proteases, invasins, and adhesins to damage membranes, modulate inflammation, aid bacterial escape, and increase host-to-host transmission of pneumococcal disease [14]. Interestingly, unlike all other studied CDCs that are secreted from the bacterium as soluble monomers through a type II signal peptide, PLY utilizes the autolysin lytic amidase (LytA). LytA is able to degrade bacterial peptidoglycan to induce lysis and subsequently release various pneumococcal antigens [15]. As such, it has been found to be vital for *S. pneumoniae* virulence and can be found in nearly all pneumococcal isolates [16].

Table 1.1. Pneumococcal virulence factors and their role in pathogenesis.

Virulence Factor	Location	Primary Function	Reference
Capsule	Polysaccharide layer on cell wall	Aids in adherence and inhibits phagocytosis	[5]
Biofilm	Surrounding bacterium	Protects bacteria and reduces recognition by host	[17]
Pili	Cell surface	Inhibits phagocytosis and promotes colonization	[18]
Choline-Binding Proteins	Surface of cell wall	Aids host cell receptor binding and protects from complement system	[19]
Metal-Binding Proteins	Surface of cell wall	Transports magnesium and zinc into cytoplasm	[20]
Other Surface Proteins	Surface of cell wall	Protects against complement system and act as adhesins	[2]
Neuraminidase	Surface of cell wall	Degrades mucus to improve adherence and colonization	[21]
Lytic Amidase	Intracellular	Breaks down bacterial peptidoglycan to release toxins	[15]
Bacteriocins	Secreted by bacteria	Inhibit growth of competing bacteria and act as signaling peptide	[22]
Pneumolysin	Secreted by bacteria	Induce pore formation and limit immune cell response	[14]

The previously highlighted virulence factors are but a subset of those crucial for colonization and pathogenesis of *S. pneumoniae*. However, bacterial genomics have indicated that two of the most promising vaccine and treatment targets include PLY and LytA, as mutations in their corresponding genes have led to reduced pneumococcal virulence [23]. Of particular interest is PLY due to its presence

in all studied strains and direct impact on disease severity and progression. Further, the conserved structure and function to other CDCs implies the potential for development of a broad-spectrum treatment platform that can selectively target various pathogenic bacterial strains.

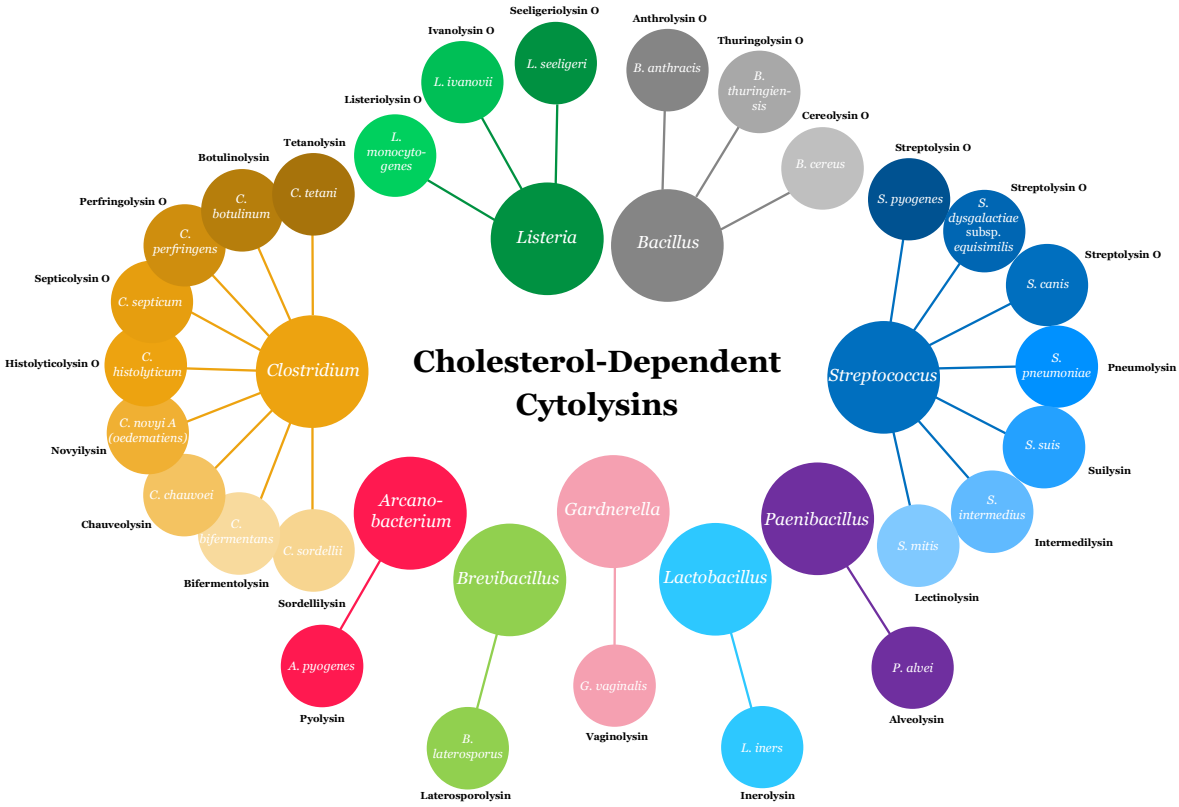


Figure 1.1. Illustration of genera and species of bacteria that produce CDCs alongside their associated toxin [24, 25].

1.1.3 Prevention and Treatment

To date, there has been the development of three major pneumococcal vaccines, including a 23-valent pneumococcal polysaccharide vaccine and both a 13- and 7-valent pneumococcal conjugate vaccine [26]. Vaccine effectiveness varies between patients, but serotypes covered under the conjugate series in children under 5 years of age have been seen to range between 89-97% effectiveness [27]. In comparison, polysaccharide vaccination in elderly and high-risk groups is estimated to only be around

54% effective, with a further decline in efficacy over time [28]. A key issue in using pneumococcal capsules as a therapeutic target is the wide variety of available serotypes, all of which have different variations in their polysaccharide structure [23]. Furthermore, under harsh conditions *S. pneumoniae* promotes biofilm formation by downregulating capsular protein expression, making it more difficult to target [2]. The focus on specific serotypes can also consequently increase prevalence of non-targeted *S. pneumoniae* strains, which in conjunction with vaccine hesitancy has led to the continued presence of IPD [29, 30].

Conventional strategies to detect bacterial respiratory tract infections involves isolation of the organism or a related capsular antigen from bodily fluid at the disease site, as chest x-rays are unable to determine the causative agent for pneumonia [31]. Typical antibiotic therapies include macrolides, fluoroquinolones, or β-lactams either on their own or in combination, but their effectiveness is limited due to 15-30% of all *S. pneumoniae* strains being classified as multi-drug resistant [32]. Further, antibiotic therapy faces long development cycles, low bioavailability, barrier challenges in pulmonary delivery, and adverse side effects [33]. To address these limitations, there has been research into the antibacterial properties of various alternative therapeutics, including antimicrobial peptides, bacteriophages, adjuvants, probiotics, and essential oils [34].

Some of the most promising emerging therapeutic molecules are antimicrobial peptides, owing to their natural production, low observed levels of resistance development, and their ability to break down into non-toxic metabolites. They typically function by disrupting bacterial membranes or interacting with intracellular components, and due to their short amino acid sequences they can be easily synthesized [35]. One such molecule, nisin, is a 3.5 kDa type A lantibiotic naturally produced by *Lactococcus* and *Streptococcus* species, having been approved for use by the United States Food and Drug Administration (FDA) as a food preservative for the past few decades. However, nisin's applications have recently been extending into the biomedical field due to its anti-biofilm properties and ability to inhibit growth of drug-resistant pathogens [36]. It displays strong antimicrobial activity against *S. pneumoniae* strains through both pore formation and inhibition of peptidoglycan biosynthesis via lipid II binding in the bacterial membrane, but has thus far been limited by poor targeting to infection sites [37].

To address limitations in the delivery of therapeutic to multi-drug resistant pneumococcal strains, research has been focusing on the implementation of nanomaterials. The ability of these systems to

release drugs within the site of infection dramatically increases bioavailability of the therapeutic and reduces off-target effects. Nanomaterials are also desirable in that they are often able to effect bacterial metabolism as a whole, thereby allowing them to evade existing resistance mechanisms and lower the likelihood of effective mutations [38]. Pulmonary inhalation for delivery of nanosystems is gaining popularity as it has potential to increase local targeting and provide faster onset times as compared to systemic delivery [33]. However, this route poses several key barriers, as it has been found that only particle sizes (PS) below 260 nm can effectively penetrate deep into alveoli and reduce macrophage clearance [33, 39]. Beyond this, it has been found that hydrophobic and/or cationic formulations are readily captured by respiratory mucus, thereby limiting effectiveness [40].

The most common nanoparticle (NP) systems under current study for the delivery of antibacterial agents include inorganic NPs, polymeric NPs, and liposomes. Of particular interest are liposomes, which are spherical vesicles compromised of one or more concentric phospholipid bilayers and an inner aqueous core. This imparts a structural similarity to cellular membranes, giving liposomes a unique ability to initiate fusion and promote high bactericidal potency while maintaining low toxicity to mammalian cells [41]. These systems have also demonstrated the capability to detect and interact with virulence factors produced by pathogenic bacteria, serving to aid in targeted therapy within infection sites [42].

1.2 Pneumolysin as a Therapeutic Target

1.2.1 Structure and Function

As one of the major virulence factors of *S. pneumoniae*, PLY has become a potential therapeutic target. To effectively target this virulence factor, knowledge of its structure and function is imperative. The protein is comprised of 471 amino acids with four main structural domains, where D_1 and D_3 are commonly considered together as a membrane attack complex/perforin, while D_2 serves to link the rest of the protein to D_4 [43]. This fourth domain of PLY contains an undecapeptide sequence conserved among all CDCs for cholesterol recognition and binding [14]. To form pores through the target membrane, this binding is followed by structural reconfiguration to a pre-pore complex with a ring-like structure comprised of roughly 30-50 PLY subunits [44]. In detail, D_4 facilitates perpendicular membrane binding, upon which intermolecular contacts leads to collapse of the pre-pore to bring the

attack domain in proximity of the membrane. Following this, α-helical bundles unfurl to produce two adjacent β-strands to form a large β-barrel transmembrane pore with an average diameter of 35 nm, as outlined in Figure 1.2 [45]. This insertion often occurs in lipid rafts, being laterally organized regions rich in various phospholipids and 3- to 5-fold higher cholesterol concentrations [46]. Repeated insertions can lead to a loss of ion homeostasis and membrane destabilization, thereby allowing for bacterial spread. The likelihood of cell lysis relies on cholesterol content and other physical properties of the membrane, such as electrostatic properties and rigidity [47].

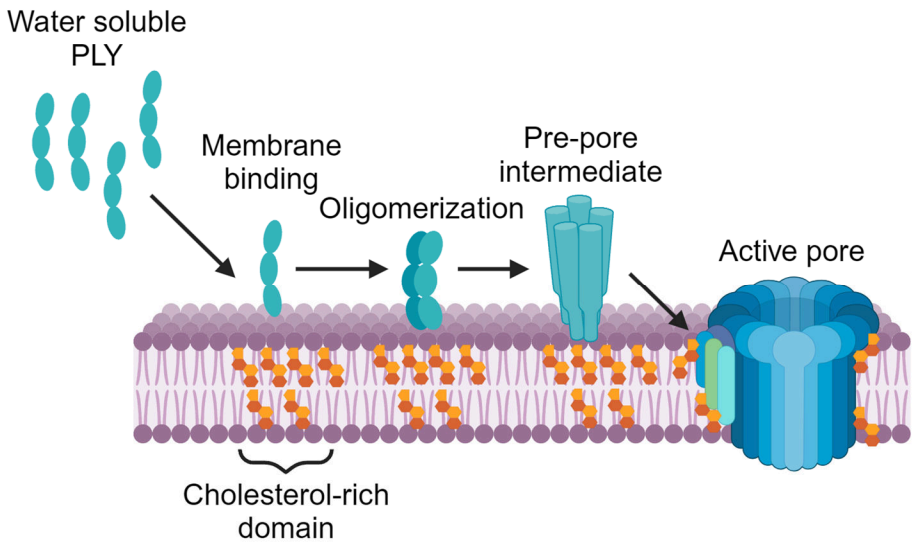


Figure 1.2. Schematic of PLY pore formation process, initiated by membrane binding within cholesterol-rich domains and followed by subsequent oligomerization and insertion. Created with BioRender.com and adapted from [48].

S. pneumoniae can naturally be found either as planktonic diplococci or in sessile microbial biofilms. Pneumococcus present in biofilms have shown to be far less virulent than their planktonic counterparts, thereby acting as a reservoir for virulent bacteria to seed off from under optimal conditions [49]. Associated with this loss in virulence is downregulation of genes involved in PLY production, thereby indicating that there is less presence of the toxin in proximity to avirulent biofilms [50]. Conversely, during IPD progression PLY can be found in the cytoplasm surrounding the pneumococcal colonies

due to its release via LytA-induced autolysis. The location of infection is dependent on the disease state, and can include the lungs, ears, spinal fluid, lining of the brain, and blood. The amount of PLY released into the cytoplasm has been found to vary between 20-700 ng/mL depending on infection severity, but is most commonly reported around or below 200 ng/mL [51, 52]. This heterogeneity in expression depends on the location and stage of pathogenesis of the bacterium, with the highest PLY expression often found during colonization of the nasopharynx and initial stages of IPD due to its metabolically demanding nature [53].

PLY is lytic to cells at high concentrations via its pore-forming properties, while at sublytic concentrations it can induce proinflammatory reactions and activate the host complement [54]. The toxin can increase release of platelet activating factor via calcium influx and promote vascular permeability to induce acute lung or cardiomyocyte injury, as well as interfere with leukocyte migratory ability to promote bacterial survival [14]. Beyond this, PLY can aid in bacterial translocation across the blood-brain barrier through disruption of endothelial tight junctions and has also been associated with improved biofilm growth in acute otitis media [55, 56]. It is interesting to note that the majority of testing on PLY to date has been through murine models that exhibit stronger inhibition of hemolytic activity as compared to human serum, indicating potential underestimation of virulence [57].

1.2.2 Pneumolysin-Responsive Nanosystems

A major benefit in the targeting of PLY for treatment of *S. pneumoniae* is that the toxin shows little variation between different pneumococcal strains and serotypes [58]. However, while PLY has been of interest as a vaccine candidate, it is not expressed on the pneumococcal capsule but rather found in the supernatant after release, making antibody-induced opsonization more difficult [59, 60]. Various other pharmacological agents have also been observed to inhibit the cytolytic activity of PLY either directly or indirectly, including statins, corticosteroids, macrolides, and monoclonal antibodies, but these have yet to be evaluated in clinical settings and concerns over their efficacy exist due to limited bioavailability [47]. As such, there has been recent interest in developing nanosystems capable of more efficiently reaching pneumococcal infection sites and facilitating interactions with PLY for a variety of biomedical applications, as summarized in Table 1.2.

Table 1.2. Overview of nanosystems utilizing PLY for biomedical applications.

Purpose	Nanosystem	Brief Description	Reference
Ligands	Ovalbumin-$CaCO_3$-PLY complex	Anti-tumor applications through improved antigen delivery	[61]
	PLY-DNA-origami complex	Formation of nanopores with precise dimensions and gating	[62]
Detection	Au@Ag core-shell NPs	Plasmonic platform for ultrasensitive detection of PLY	[63]
	Spherical iron oxide nanoclusters	Conjugation to anti-PLY antibodies for remote detection	[64]
	Mixed hybrid bilayer lipid membrane	Damage-induced electrochemical impedance signal source for biosensors	[65]
Capture	Liposomes	Decoy targets to uptake and neutralize PLY as adjunct therapy	[66–71]
	Erythrocyte-derived nanosponge	Polymeric cores surrounded by rabbit erythrocyte membranes for PLY uptake	[72]
	Multi-bilayer polymeric membrane	Brush copolymer films containing lipid and cholesterol for PLY adsorption	[73]

The research to date on PLY-interacting nanosystems can be divided into three main categories, notably being the toxin's use as a functionalization agent, systems capable of detecting PLY presence, and those capable of PLY capture and subsequent neutralization. Firstly, there has been some research into the use of PLY as a ligand for nanosystem functionalization, largely due to its facilitation of lysosomal escape for improved drug delivery and ability to form well-behaved transmembrane pores for diagnostic research [61, 62]. However, in this field another CDC, listeriolysin O, has displayed the greatest promise for anti-tumor applications through its role in immune response modulation [74, 75].

Another major target for PLY-responsive nanosystems is for the diagnosis of IPD through detection of PLY at infection sites. Classical detection of *S. pneumoniae* is often accomplished through Gram stains of a sputum sample or antigen detection in urine, but these methods often lack rapidity and sensitivity [64]. As such, there has been development of a range of different nanosystems that utilize PLY binding to quickly generate a detectable signal, be it through plasmonic, magnetic, or electrochemical means, at comparatively low limits of detection [63–65].

The final major avenue of nanosystems consists of those capable of sequestering PLY and neutralizing its toxic effects. This work was largely pioneered by a series of publications from Babiychuk et al., in which empty cholesterol-rich liposomal formulations led to preferential CDC toxin binding. This reduced levels of PLY and allowed for bacterial clearance in mouse models, giving it potential as an adjunctive therapy to minimize the effect of toxin burst release during antibiotic treatment [66]. While sequestration studies have since been expanded to nanosponges and polymeric membranes, liposomes with high cholesterol saturation remain the most studied target [69].

Beyond the applications identified, there has also been limited research into toxin-responsive systems that utilize the pore-forming ability of CDCs to selectively release therapeutics in proximity to pathogenic bacteria. This has been displayed with the CDC listeriolysin O, as liposomal formulations have seen effective delivery of nutmeg and lemongrass oil to inhibit the growth of *Listeria monocytogenes* on various food products [76, 77]. In contrast, several studies have utilized nanocarriers as a delivery vehicle of various PLY neutralization agents, but lack a responsive form of release within infection sites and act instead as an adjunctive therapy acting in concert with antibiotics [78, 79].

To the authors knowledge, there are no studies to date on PLY-induced therapeutic release for the treatment of *S. pneumoniae*, despite similar release kinetics proven to be effective for listeriolysin O. Targeted therapy poses several advantages, such as protection from degradation, improved delivery to infection sites, modulation of release kinetics, and a high safety profile [80]. Liposomes have shown the most promise to date for use in PLY-responsive systems, owing to their ability to mimic cellular membranes and incorporate high levels of cholesterol to facilitate PLY binding. As such, further study on PLY-responsive liposomal systems appears warranted.

1.3 Liposomal Synthesis

1.3.1 Conventional Preparation Techniques

Beyond research demonstrating liposomes can facilitate CDC toxin interactions, they also benefit from high bioavailability, biocompatibility, stability, and the ability to encapsulate both hydrophobic and hydrophilic molecules [81]. There are various different liposomal classifications based on size and the number of bilayers present, but in general it has been found that small (50-200 nm), unilamellar vesicles are preferred for drug delivery applications [82, 83]. The final structure, organization, and physicochemical properties of a given liposome solution is highly variable on a number of factors, including the choice, charge, and concentration of phospholipids and other constituents, as well as the ionic strength, pH, and temperature of the solution [84].

Common liposomal constituents typically include a mix of natural and/or synthetic lipids, steroids, and surfactants at varying molar composition [81]. Phospholipids, which are conventionally the main component of liposomes, orient themselves into lipid bilayers once in an aqueous solution due to their amphiphilic nature. The following self-assembled curvature of these bilayers into a spherical, hollow vesicle comes at an intrinsic energy cost, thereby making liposomes metastable states whose properties largely depend on the method of synthesis [84].

There are a variety of bulk methods employed for the fabrication of liposomes, with PS ranging from tens of nanometers to microns depending on the approach used. Conventional methods typically involve dissolution of the lipids in organic solvent and subsequent evaporation, rehydration in aqueous media, size reduction, and additional purification steps [84]. Some of the most common methods include thin-film hydration, reverse-phase evaporation, detergent depletion, injection, heating, and membrane extrusion techniques [82]. A key issue with these approaches is that self-assembly of the particles occurs in the bulk phase, leading to local fluctuation in lipid and payload concentrations that result in heterogeneous and multilamellar particles. As a result, size reduction is required and can include sonication, extrusion, homogenization, or freeze-thawing, but these techniques are often time-consuming, induce liposomal damage, and produce polydisperse size distributions [85]. Beyond this, these workflows are often hampered by various drawbacks depending on the method utilized, ranging from complex procedures, the use of harsh organic solvents, and/or poor drug encapsulation [82].

1.3.2 Microfluidics

Owing to the discussed drawbacks of conventional liposomal synthesis techniques, there has been the recent development of various novel preparation methods [86]. Of these, microfluidic approaches have boasted some of the most progress both academically and industrially. There are a number of available microfluidic techniques for the production of liposomes, including emulsion templates, pulsed flow jetting, droplet emulsion transfer, hydration techniques, electroformation, and the use of micromixers [87]. However, many of these systems have limited feasibility for biomedical applications as they are only able to produce large vesicle systems, with an exception being those that utilize micromixers [88].

Microfluidic mixing involves the rapid merging of different fluid streams, conventionally an ethanolic phase with dissolved lipid solution and an aqueous phase containing therapeutic, within a confined microchannel typically on the scale of tens of micrometers [89]. The small channel size results in a lowered Reynolds number and, consequently, laminar flow within the fluidic domain such that mass transfer can only occur through diffusion and molecular advection [89]. The diffusion of the alcohol stream in water will eventually reach the lipids solubility limit, causing them to precipitate and form intermediate micelles that subsequently become liposomes. There are typically microstructures inside the mixer to induce the formation of helical and chaotic flow within the laminar stream, increasing mixing rates and giving the geometry of a given chip dramatic influence on particle properties [90].

There are innumerable different chip designs available, with some of the most common including T-shaped, hydrodynamic flow focusing, bifurcating, herringbone, and baffle micromixers [89]. Of these, staggered herringbone micromixers, with a general structure as displayed in Figure 1.3, have displayed efficient chaotic mixing owing to their asymmetric protrusions, with an ability to control sizes anywhere between 20-140 nm through adjustment of microfluidic workflow parameters. The major drawbacks of such mixers, however, are slow total flow rates (TFR), low lipid concentration, and the requirement for regular purge cycles to remove any potential lipid blockage within the internal grooves that would hinder flow through the chip [89]. However, despite these limitations, they are still widely used due to their excellent control over particle properties, simple fabrication, and mixing efficiency [90].

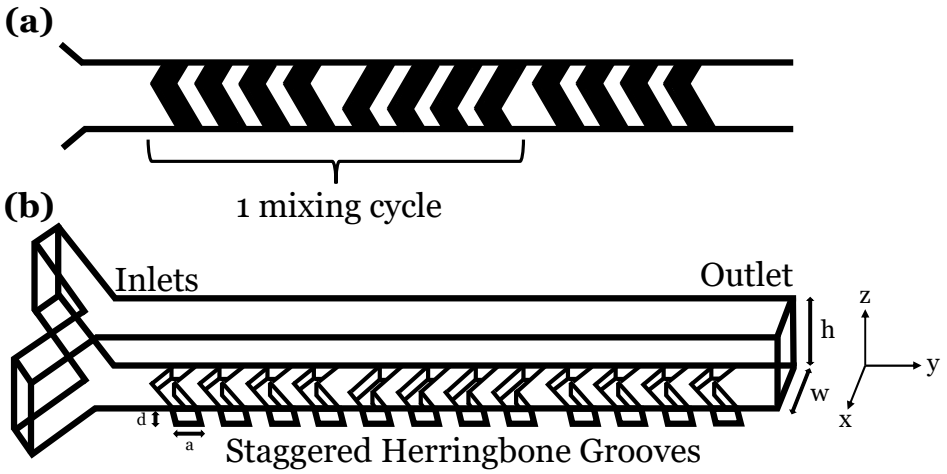


Figure 1.3. Schematic representation of a typical staggered herringbone micromixer from both **(a)** top-down and **(b)** side profiles, with relevant parameters identified, including channel width (w) and height (h), as well as herringbone depth (d) and width (a). Adapted from [91].

While the selection of micromixer plays a major role in synthesized liposomal properties, various other parameters and components identified in Table 1.3 also have influence. Firstly, there are passive and active approaches to direct flow within microfluidic systems, with the latter being more popular due to its precise control. In more detail, they allow for the variation of the ethanol-to-aqueous flow rate ratio (FRR) and TFR of the system, two parameters that can directly modulate rate of mixing and precipitation kinetics [88]. These approaches include pressure-driven, centrifugal, electrokinetic, and acoustic systems [92]. Other relevant parameters for a given formulation are the liposomal constituents used, concentrations of both the lipid and therapeutic, buffers and their exchange techniques, and post-processing conditions. Notably, as therapeutic agents are incorporated into liposomes through either encapsulation, surface attachment, or entrapment, careful consideration of the properties of both the therapeutic and lipid components are required to facilitate interactions [81]. Further, there is the availability of several separation techniques for liposomes, including ultracentrifugation, dialysis, centrifugal filtration, and pressure filtration. The method chosen must be carefully considered against the given system as it can directly impact separation efficiency, PS, and therapeutic encapsulation [93]. As such, microfluidic device design is often complicated and requires numerous optimization procedures to produce particles with desirable characteristics.

Table 1.3. Relevant parameters for consideration during development of a microfluidic workflow.

Component	Purpose	Importance	Reference
Mixer	Accelerates liposome formation via chaotic mixing	Varying geometry influences liposomal properties	[90]
Pump	Generates flow within a microfluidic system	Choice of driving force influences fluid dynamics	[92]
Tubing	Ensures water-tight flow between all components	Impact on void volume and solvent interactions	[88]
Lipid Components	Liposomal constituents required for self-assembly	Significant influence on properties and interactions	[81]
Lipid Concentration	Influences concentration of liposomes in solution	Implications on particle lamellarity and encapsulation	[94]
Therapeutic Concentration	Controls the amount of therapeutic in solution	Impact on encapsulation efficiency and efficacy of carrier	[95]
TFR	Total speed both fluid streams are pumped at	Influence on liposomal size and system throughput	[88]
FRR	Volumetric ratio of aqueous to organic fluid stream	Shortens diffusion length and impacts physical properties	[96]
Buffer	Added to dilute residual ethanol content	Implications on liposomal stability and pH-mediated release	[97]
Buffer Exchange	Separation of dispersion medium from liposomes	Impact on particle properties and separation efficiency	[93]
Filtering	Removes contaminants and induces sterility	Improved homogeneity but potential filter interactions	[98]
Storage	Temperature and additives that influence stability	Impact on hydrolysis rate and particle quality	[99]

1.3.3 Optimization via Response Surface Methodology

As previously discussed, there are a wide array of parameters within a given microfluidic system that can directly impact particle properties and quality. While some parameters are more standardized (e.g. use of ethanol), others like FRR, charged lipid concentration, and therapeutic concentration can be highly variable for any given system [88, 100]. This makes them important considerations when designing a standalone microfluidic process and are often optimized via experimental designs [101]. The most basic three-factor system is a three-level full factorial design (FFD), with a graphical representation visible in Figure 1.4a. For a FFD, owing to the fact that every factor combination is tested, the number of experiments required is described as $N = 3^k$, where k is the number of parameters. This quickly becomes laborious for complex systems, and as such is rarely used. Instead, response surface methodology (RSM) is commonly employed for factor optimization, consisting of a set of advanced design of experiment techniques [102]. These designs are able to more efficiently construct models of a given system based on collected data to describe the relationship among independent factors and their dependent responses. For any given RSM, factors should have defined low and high levels, as well as a centre point at the average of the two extremes. These values are generally encoded -1, 1, and 0 respectively within design software to aid with model computation for subsequent transformations.

The choice between available RSM designs should be tailored to the specific system being studied, as each pose distinct properties and potential advantages. Perhaps the most common three-factor RSM is a central composite design (CCD), displayed in Figure 1.4b, which is a first-order factorial design (2^k) that includes axial points (2k) and an evaluation of centre points (n_o), making its total number of experiments $N = 2^k + 2k + n_o$. The axial points are at a distance α from the centre point of the design and represent new extremes for each factor, with the chosen value describing the CCD as either circumscribed, inscribed, or face centred [103]. An added benefit is that both the circumscribed and inscribed version of CCDs are rotatable, meaning that prediction variance stays equivalent for all points at a given distance from the centre point. This is desirable for optimization, as estimation has equal precision in all directions along the surface of the design space [104].

Another rotatable RSM is a Box-Behnken design (BBD), with its design space visible in Figure 1.4c. This is a quadratic design that differs in that it avoids extreme treatment conditions and instead evaluates the edge midpoints and centre of the given process space, with the total number of

experiments defined as $N = 2k(k-1) + n_o$. The major advantages for such a system are that it requires the least amount of treatment combinations and avoids the evaluation of impractical extreme values for each factor that would be otherwise be considered in CCDs. As a direct result of this however, BBDs can contain areas of poor prediction quality near these extremes. To diminish this impact, careful selection of the high and low levels for each independent factor to be within feasible ranges is imperative [102]. Overall, due to their efficiency and greater evaluation of the intermediate design space, BBDs have seen use for microfluidic liposomal optimization [105].

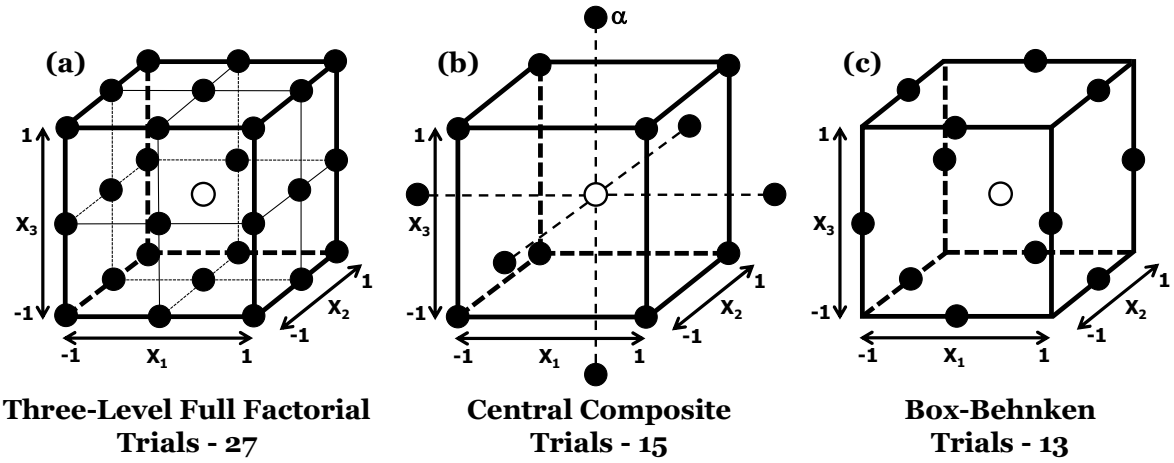


Figure 1.4. Comparison of three-factor design methods, including **(a)** three-level FFD, **(b)** Box-Wilson CCD, and **(c)** BBD. The scale has been coded to range from -1 to 1, with total trials assuming one centre point measurement.

1.4 Research Framework

1.4.1 Project Rationale

As the third deadliest bacterium responsible for over 800,000 deaths worldwide in 2019 alone, development of more efficacious and cost-effective antimicrobial platforms for treatment of *S. pneumoniae* is of global concern [106]. Conventional antibiotic treatments are hindered by the development of resistant strains and low bioavailability, while vaccination strategies targeting only specific capsular serotypes promote proliferation of non-targeted forms and lowered efficacy [107].

Improved control over the synthesis and modification of nanomaterials has seen their rapid expansion into clinical applications, with one target being pneumococcal disease. Due to its ubiquitous presence in all strains, there has been interest in the development of nanomaterials responsive to PLY toxin for biosensing, functionalization, and sequestration applications. Liposomes have shown great promise as such systems through their ability to facilitate PLY binding to cholesterol-rich domains, but initial clinical studies have showed relatively low efficacy of toxin-trapping as a treatment form [71].

There has recently been development of liposomal formulations that interact with listeriolysin O, a CDC which functions in a similar fashion as PLY, to utilize its pore-forming abilities for selective therapeutic release in proximity to bacterial colonies as a form of food preservation [76, 77]. This, along with the development of more potent antimicrobial agents in recent years, suggests a currently unexplored avenue of PLY-responsive therapeutic release for more efficacious and specified *S. pneumoniae* treatment. Currently, few experimental therapies under development ever reach clinical trials, indicating that there is a clear need for the emergence of novel methods and molecules to effectively treat pneumococcal infections. To account for this, the developed system should be non-toxic, especially as the primary target demographic are young or immunocompromised individuals, display a PS under 260 nm to effectively penetrate the alveoli, and be of hydrophilic nature [2, 33, 39]. To be clinically relevant, it is also imperative the proposed nanosystem be homogeneous, consistent, and readily scalable, to which recently developed microfluidic systems hold promise. As such, the present work aims to develop and optimize liposomal NPs prepared on an in-house microfluidic system. These will be used to facilitate PLY-responsive therapeutic release of an antimicrobial peptide, nisin, in proximity to *S. pneumoniae* to facilitate bacterial clearance, improve specificity of treatment, and neutralize toxin activity all within one platform.

1.4.2 Hypothesis

It is hypothesized that BBD models can be used to optimize microfluidic-prepared liposomes and that modulation of compositional cholesterol content can facilitate PLY binding, thereby promoting the therapeutic release of nisin through pore formation.

1.4.3 Objectives

To investigate the potential of a PLY-responsive antibacterial liposome system, this research project has been divided into the four subsequently listed main objectives. **O1:** Optimize an in-house microfluidic system for the production of unilamellar liposomes capable of nisin encapsulation via BBD RSM techniques. **O2:** Identify the influence of liposomal cholesterol on PLY binding and subsequent nisin release kinetics. **O3:** Evaluate antimicrobial efficacy and specificity of the liposomal formulations for cultured *S. pneumoniae* as compared to a commensal bacterial strain. **O4:** Examine cytotoxicity of the platform against a lung fibroblast cell line and its protective ability upon bacterial challenge.

Chapter 2: Methodology

2.1 Materials

Sheep-wool derived cholesterol, L-α-phosphatidylcholine harvested from egg yolk (EPC), Amicon Ultra-15 and Ultra-0.5 centrifugal filters with a 30kDa molecular weight cut-off (MWCO), Triton X-100, potassium cyanide, brain heart infusion (BHI) broth, tryptic soy broth (TSB), yeast extract, dithiothreitol (DTT), dimethyl sulfoxide (DMSO), and glycerol were all purchased from Millipore Sigma. Defibrinated sheep blood, heat-inactivated fetal bovine serum (FBS), penicillin/streptomycin (P/S; 10,000 U/mL), surface-treated T-75 Nunc™ EasYFlask™ cell culture flasks, trypan blue (0.4%), Falcon™ 96-well cell culture-treated flat-bottom microplates, and agar (bactericidal grade) were all purchased from Thermo Fisher Scientific.

S. pneumoniae (strain 23F-1, 700669™), *Staphylococcus epidermidis* (strain Fussel, 14990™), IMR-90 human fibroblast cells (CCL-186™), Eagle's minimum essential medium (EMEM), and trypsin-ethylenediaminetetraacetic acid solution (EDTA; 1x) was purchased from ATCC. Recombinant *S. pneumoniae* serotype 2 PLY (*E. coli* host expression) was purchased from MyBioSource, while the CellTiter 96® Aqueous One Solution Reagent consisting of the compound 3-(4,5-dimethylthiazol-2-yl)-5-(3-carboxymethoxyphenyl)-2-(4-sulfophenyl)-2H-tetrazolium (MTS) was bought from Promega. Phosphate-buffered saline (PBS; 1x, pH 7.2) was purchased from Wisent, while single donor washed human red blood cells (RBCs) was purchased from Innovative Research.

Nisin Z was purchased from TOKU-E, while ATTO-TAG™ 3-(4-carboxybenzoyl) quinoline-2-carboxaldehyde (CBQCA) reagent was purchased from ABP Biosciences and sodium borate decahydrate was purchased from MP Biomedicals. L-α-phosphatidylglycerol harvested from chicken eggs (EPG) was purchased from Avanti Polar Lipids, while polyethersulfone syringe filters (0.45µm membrane) were purchased from Montreal Biotech. For the microfluidic system, the dual channel syringe pumps (NE-4000) were purchased from New Era Pump Systems Inc., while the microfluidic mixer chip (MIX-4) was purchased from PreciGenome. Polytetrafluoroethylene tubing (1/16" outer diameter, 1/32" internal diameter) was purchased from Fluorostore while Idex Leur adapters and perfluoroalkoxy alkane flangeless fittings (1/16" outer diameter) were purchased from Cole-Parmer.

2.2 Liposome Synthesis & Characterization

2.2.1 Experimental Microfluidic Setup

The developed microfluidic system, as displayed in Figure 2.1, utilized two dual channel syringe pumps connected to a microfluidic mixer chip that featured an internal herringbone geometry. Three pieces of nonreactive tubing were cut to exactly 21 mm to minimize the amount of dead volume and attached to the inlets and outlet of the chip. All ports were fitted with a series of Idex Leur adapters and flangeless fittings to ensure a watertight system. Two 15 mL syringes were then loaded with the aqueous and ethanolic phase respectively. The aqueous phase contained nisin dissolved in neutral Milli-Q water at a known concentration, while the ethanolic phase contained the lipids EPG, cholesterol, and EPC dissolved in ethanol at a known concentration.

Each lipid solution was warmed in a water bath set to 50^{o}C to ensure full dissolution in ethanol prior to mixing at the desired molar concentrations and initial lipid content of 20 mM. The syringes were then tilted and flicked vertically to remove any air bubbles that may hinder the mixing process and the liquid was pushed manually to the edge of the outlet [108]. After securely mounting the syringes on the pumps and connecting them to the tubing, the speed and volumes were set accordingly to match a TFR of 6 mL/min, a FRR varying between 2:1 and 4:1 for aqueous:ethanol content, and a 1.5 mL total formulation volume. Injection of the solutions was then initiated simultaneously and the liposomal solution was collected from the outlet in a reservoir.

Newly formed liposomes underwent a series of wash cycles with Milli-Q water through the use of Amicon Ultra-15 centrifugal filter units (MWCO 30kDa) spun at 3000 x g in 10 min cycles at 4^{o}C, also serving to separate out unencapsulated nisin [109]. This was continued until a 10x dilution of the original formulation volume was reached in order to lower residual ethanol content, at which point it was concentrated back down to 1 mL. This solution was then collected and syringe filtered through 0.45 μm membranes to remove contaminants and sterilize the liposomes, at which point they were stored at 4^{o}C until use [110].

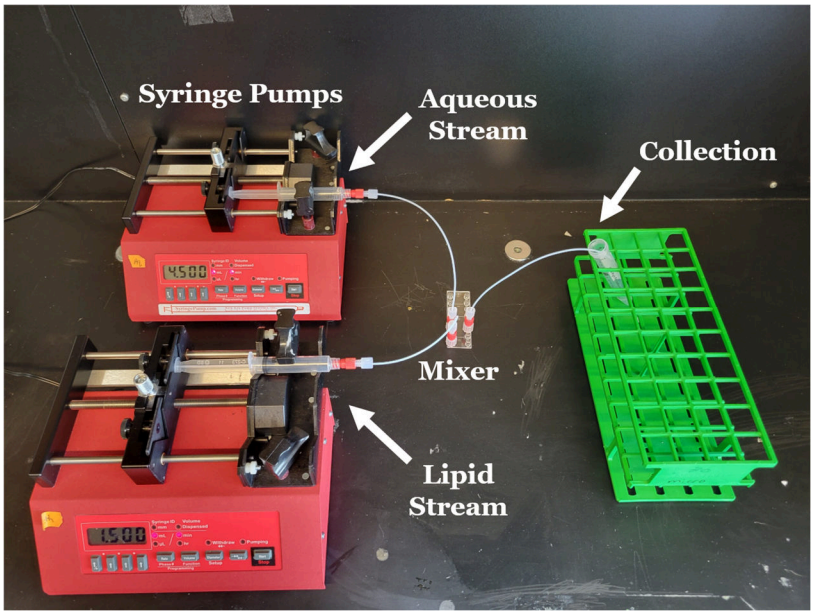


Figure 2.1. Experimental setup of the microfluidic system.

2.2.2 Dried Film Preparation

To prepare dried films, liposomal solutions were diluted in 96-well plates with Milli-Q water to desired concentrations at a final volume of 100 µL. Liposomal dosing was based on molarity as per Equation **(1)**:

$$Dosing\ Volume\ (\mu L) = \frac{Desired\ molarity * Molar\ mass * Assay\ volume * Initial\ liposome\ volume}{Lipid\ mass\ output} \quad \textbf{(1)}$$

where the liposomal molar mass (MM) was calculated as a mixture of the three lipid components based on their molar composition as per Equation **(2)**:

$$Liposomal\ MM\ (g/mol) = \left(\frac{MM_{EPC} * mol\%}{100}\right) + \left(\frac{MM_{Cholesterol} * mol\%}{100}\right) + \left(\frac{MM_{EPG} * mol\%}{100}\right) \quad \textbf{(2)}$$

Following mixing, the solution was evaporated at room temperature under continual air flow overnight until fully dried.

2.2.3 Physical Particle Characteristics

Liposomes were characterized for their PS and polydispersity index (PDI) via dynamic light scattering (DLS) and zeta potential (ZP) through M3-PALS measurements within the same instrument (Zetasizer Ultra Red, Malvern Panalytical). For all samples, the liposomes were diluted 1:80 in milli-Q water and triplicate measurements were taken.

2.2.4 Encapsulation Efficiency

Encapsulation efficiency (EE) of nisin was determined through a CBQCA assay according to manufacturer specifications (Molecular Probes) with some modifications. Briefly, 8.25 µL of liposomal suspension was mixed with 16.5 µL of 2% Triton, 115.5 µL of 0.05 M sodium borate, 156.75 µL of Milli-Q water, 11 µL of 20mM potassium cyanide, and 22 µL of 2 mM CBQCA reagent. The solution was vortexed to mix and incubated for 1 h at room temperature away from light, with fluorescence measurements conducted on a microplate reader (Varioskan LUX, Thermo Fisher Scientific) at an emission and excitation wavelength of 550 nm and 465 nm, respectively. To ensure accuracy, a new CBQCA calibration curve was developed for each independent measurement to account for potential fluctuations in CBQCA concentration.

Liposomal dilution for subsequent mass measurements was calculated based on the total volume of collected liposomes, the volume of liposomes utilized in the assay, and the total volume of the assay itself. Fluorescence readings were then compared with the calibration curve of free drug in suspension to calculate an experimental nisin mass encapsulated within the liposomes. This was contrasted with the initial mass of drug loaded in the aqueous phase to calculate a direct EE as per Equation **(3)**. Following this, loading capacity (LC) was determined using the aforementioned mass of nisin collected in the formulation as compared to the weight of liposomes recovered following microfluidic processing, as displayed in Equation **(4)**:

$$EE\%\ (direct) = \left(\frac{Mass\ of\ nisin\ in\ formulation}{Initial\ mass\ of\ nisin}\right) * 100 \quad \textbf{(3)}$$

$$LC\% = \left(\frac{Mass\ of\ nisin\ in\ formulation}{Mass\ of\ recovered\ liposomes}\right) * 100 \quad \textbf{(4)}$$

2.2.5 Physical Stability

To examine short-term physical stability of the liposomes, synthesized particles in triplicate were stored at both 4°C and 37°C in Milli-Q water. At specified intervals (0, 1, 3, 7, 14 days), DLS techniques were utilized as previously described to examine PS and PDI of the liposomes.

2.3 Box-Behnken Response Surface Design

A three-level, three-factor BBD was utilized to optimize liposomal formulations for desired outputs of the dependent variables using Minitab® 16.0 software. The produced second-order polynomial equations followed the form of Equation **(5)**:

$$Y = A_0 + \sum_{i=1}^{k} A_i X_i + \sum_{i=1}^{k} A_{ii} X_i^2 + \sum_{i=1}^{k-1} \sum_{j=2}^{k} A_{ij} X_i X_j \quad \textbf{(5)}$$

where X represents the independent factors, Y is the dependent variable being studied, A_o, A_i, A_{ii}, and A_{ij} are regression coefficients of constant, linear, quadratic, and interaction terms respectively, and k is the total number of independent factors [101]. The tested independent variables (X) were the FRR of the aqueous and ethanol stream during mixing, nisin concentration, and EPG molar composition as expressed in Table 2.1, along with their corresponding encoded levels in the software. These were evaluated by the following dependent variables (Y): EE, LC, PS, and PDI, with experiments performed in 15 randomized runs and repeated in triplicate. Coefficients were determined via least square regression followed by analysis of variance (ANOVA) to generate a series of polynomial equations capable of describing the relation between each independent variable and the responses. A series of contour plots were then developed based on these equations with continuous hold variables set to their median value.

Various optimization solutions were screened through user-defined response goals, with Minitab® 16.0 software using the generated model to fit values for each independent variable. For all optimization calculations, weight and importance values were set to 1. Using the fitted independent variables, each optimized formulation set was produced in triplicate and compared to predicted outputs. For all testing, the total cholesterol content was fixed at 60 mol%, while varying EPG content was accounted for through modulation of EPC content.

Table 2.1. Independent variables and their corresponding levels utilized in the BBD.

		Coded levels		
Independent Variables	**Symbol**	**-1**	**0**	**1**
FRR (aqueous:ethanol)	X_1	2:1	3:1	4:1
Nisin concentration (μM)	X_2	30	60	90
EPG molar composition (mol%)	X_3	1	4	7

2.4 Bacterial Studies

2.4.1 Bacterial Strains and Growth Conditions

Stock cultures of the antibiotic-resistant 23F-1 strain of *S. pneumoniae* and the Fussel strain of *S. epidermidis* were kept in a 15% glycerol solution supplemented with BHI broth and TSB respectively and stored at -80ºC. Prior to hemolytic or antibacterial testing, *S. epidermidis* was streaked onto a tryptic soy agar (TSA) plate, while *S. pneumoniae* was grown on a TSA plate supplemented with 5% defibrinated sheep blood according to handling specifications (ATCC). The plates were incubated for 24 h at 37ºC and 5% CO_2, at which point several individual colonies were transferred to their respective complete media for overnight growth. *S. pneumoniae* was grown using BHI broth supplemented with 2% yeast extract under static conditions in a 37 ºC environment at 5% CO_2, while *S. epidermidis* was grown with constant shaking at 250 rpm in TSB under 37ºC aerobic conditions [111, 112].

Following overnight growth, the bacterial concentration was adjusted to an optical density (OD) of 0.085 via spectrophotometer measurements (Genesys 20, Thermo Fisher Scientific) at 600 nm, corresponding to a 0.5 McFarland standard [113]. This was allowed to incubate until it reached log phase growth, corresponding to 5 h for *S. pneumoniae* and 2 h for *S. epidermidis*. These timings were determined through growth curve analysis for both bacteria, involving the removal of standardized inoculum at specified timepoints for subsequent serial dilution. Following dilution, 100 μL of bacterial suspension was spread onto agar plates and incubated for 24 h, at which point isolated colonies within viable ranges (30-300 colonies) were enumerated to determine the colony forming units (CFU)/mL for each timepoint [114]. These were then contrasted with corresponding OD readings at 600 nm, which were also collected for each timepoint. All experiments were conducted in triplicate. The conversion between counted colonies and CFU/mL was calculated according to Equation **(6)**:

$$CFU/mL = \frac{Counted\ colonies}{Inoculum\ volume\ for\ spread\ plate * Dilution\ factor} \quad \textbf{(6)}$$

Once the bacterial suspension had reached log phase growth, it was then diluted back to a 0.5 McFarland OD as a standardized inoculum for all subsequent experiments.

2.4.2 Hemolytic Activity Assay

For all hemolytic assays, RBCs were suspended in PBS to a final concentration of 2% [69]. For sequestration studies, liposomal samples were diluted in PBS at varying molarities, calculated as previously described in Equation **(1),** and added to the erythrocytes. For film studies, RBCs and PBS were added within pretreated 96-well plates containing liposomal films of known molarity to a final volume of 100 µL. The hemolytic reaction was then initiated through the addition of either cultured *S. pneumoniae* supernatant normalized to a 0.5 McFarland standard or recombinant PLY protein at the desired volume or concentration. For all sequestration studies conducted with bacterial supernatant in the presence of liposomes, the *S. pneumoniae* load was fixed at $3.0x10^7$ CFU/mL, or the equivalent of 70 µL of suspension. All bacterial loads were calculated assuming a 0.5 McFarland standard equated to $1.5x10^8$ CFU/mL of microbe in suspension [113]. For assays involving PLY, the toxin (10 µg/mL) was preincubated with 2 mM DTT for 1 h at room temperature prior to the assay in order to reduce the cysteine residue present in the undecapeptide sequence for protein activation [115].

The solution, at a final fixed volume of 350 µL, was then incubated in either a 1.5 mL Eppendorf microtube or, for film studies, a 96-well plate for 30 min at 37°C and non-lysed RBCs were pelleted via centrifugation at 1000 x g for 10 min at 4°C. The supernatant was then collected and transferred to a 96-well plate, with the extent of hemoglobin release determined via absorbance measurements at 450 nm. A control set was also included, involving a negative control of RBCs in only PBS and a positive control of RBCs in a 0.02% Triton solution (100% lysis). All experiments were conducted in triplicate. Percent lysis was determined from these readouts as per Equation **(7)**:

$$Hemolysis\ (\%) = \left(\frac{A_{450}(sample) - A_{450}(negative\ control)}{A_{450}(positive\ control) - A_{450}(negative\ control)}\right) * 100 \quad \textbf{(7)}$$

2.4.3 Morphological Analysis

Morphological analysis of liposomal structure was conducted through transmission electron microscopy (TEM). To examine the structural impact of PLY binding, liposomes were imaged both in the presence and absence of the purified toxin. Prior to use, PLY (10 µg/mL) was preincubated with 2 mM DTT for exactly 1 h [115]. The final solutions contained liposomes at a concentration of 200 µM, calculated as per Equation **(1)**, PLY at a concentration of 4 µg/mL where applicable, and Milli-Q water. For each solution, a 10 µL aliquot was placed on a 300-mesh formvar/carbon coated copper grid and allowed to adsorb, with any surplus volume removed via filter paper. Following this, the grids were submersed in a 3% (w/v) aqueous uranyl acetate solution and left in contact for 1 min, after which the grid was briefly washed to remove excess stain [116]. Surplus water was removed via filter paper and the sample was allowed to dry at ambient conditions overnight. The following day, the liposomes were imaged (CM10 TEM, Philips) at an accelerating voltage of 80 kV. ImageJ software was utilized to quantify PS and pore diameter of the collected micrographs.

2.4.4 Liposomal Release Assay

To measure the rate of nisin release from PLY interaction, liposomes were added to a microcentrifuge tube at a concentration of 200 µM. PLY toxin (10 µg/mL) was preincubated with 2 mM DTT for 1 h to activate the protein structure and then added at a final concentration of 4 µg/mL, with the total volume of the assay brought up to 200 µL through addition of PBS. The tubes were then immediately incubated at 37°C for varying timepoints, at which point they were collected and transferred to Amicon Ultra-0.5 centrifugal filters. These were immediately spun at 10,000 x g for 5 min at 4°C to separate out released nisin [109]. The concentrated solution remaining in the top filter was collected with PBS and 165 µL of this was then transferred for use in CBQCA protein measurements as previously described. A negative and positive control were included for each liposomal series, with the negative containing just liposomes and PBS and the positive containing a 0.2% Triton solution to fully disrupt the particles. All experiments were conducted in triplicate. The fluorescence readouts were converted to an experimental mass through use of a calibration curve, with percent release calculated via comparison to theoretical nisin mass as per Equation **(8)**:

$$Nisin\ Release\ (\%) = \left(\frac{Nisin\ mass\ collected\ in\ concentrate - Theoretical\ mass}{Theoretical\ mass}\right) * 100 \qquad \textbf{(8)}$$

2.4.5 Minimum Inhibitory and Bactericidal Concentrations

To determine the minimum inhibitory concentration (MIC) of free and encapsulated nisin, the broth microdilution method was utilized [117]. To each 1.5 mL microcentrifuge tube, either free nisin or liposomes were added to a desired concentration and the volume was normalized to 65 µL with milli-Q water. To this, 283 µL of either BHI broth for *S. pneumoniae* or TSB for *S. epidermidis* was added to allow for growth and bring the assay to a final volume of 350 µL. Encapsulated nisin concentration for liposomal dosing was calculated according to Equation **(9)**:

$$Liposomal\ Nisin\ Concentration\ (\mu g/mL) = \frac{Initial\ nisin\ mass * EE}{Volume\ of\ liposomes\ collected} \quad \textbf{(9)}$$

Following this, a 2 µL bacterial inoculum standardized to a 0.5 McFarland unit was added to each tube, corresponding to $8.6x10^5$ CFU/mL. Both a negative and growth control were included, with the former containing no bacterial suspension or therapeutic and the latter containing just bacterial suspension. The tubes were then incubated in each bacterium's preferred growth environment for 24 h, with subsequent transfer to a 96-well plate for OD readings at 600 nm. MIC values were taken as the lowest therapeutic concentration that produced an OD below or equal to the negative growth control after incubation, with all measurements conducted in triplicate [117].

Following MIC determinations, an inoculating loop was dipped into the media and streaked onto a marked quadrant of an agar plate, using TSA plates for *S. epidermidis* and TSA + 5% defibrinated sheep blood plates for *S. pneumoniae*. These plates were subsequently incubated for 24 h at 37ºC in a 5% CO_2 atmosphere, at which point they were visually inspected for the absence or presence of bacteria. The lowest concentration that resulted in 99.9% of bacterial population death was marked as the minimum bactericidal concentration (MBC) based on triplicate experiments [117].

2.4.6 Time-Kill Kinetics Assay

The bactericidal activity of both free and liposome-encapsulated nisin was evaluated through time-kill studies [118]. The effectiveness of free nisin was first investigated through its addition to 1.5 mL microcentrifuge tubes at various concentrations relative to the MIC (0X, 0.5X, 1X, 2X, and 4X). Effectiveness of the liposomal solutions was then evaluated through their addition at 1X the MIC, with the entrapped nisin concentration determined as previously discussed in Equation **(9)**. All therapeutic doses were normalized with Milli-Q water to a final volume of 80 µL, after which 914.29 µL of each

respective bacteria's desired growth media was added. Subsequently, a standardized bacterial inoculum of 5.71 µL was included such that it reached the same bacterial concentration as MIC experiments ($8.6x10^5$ CFU/mL) at a total assay volume of 1000 µL. The bacteria were then incubated in their preferred growth conditions, with suspension removed at various time intervals (0, 0.5, 1, 2, 4, 8, 12, and 24 h) to undergo serial dilution. Spread plates were prepared in the same manner as previously described, with isolated colonies enumerated following 24 h incubation to allow for calculation of CFU/mL at each timepoint. The plate-dilution method was capable of bacterial detection up to 100 CFU/mL, serving as the limit of quantitation. All experiments were conducted in duplicate.

2.5 Cell Studies

2.5.1 Cell Culturing

For cell studies, the adherent IMR-90 cell line consisting of human lung fibroblasts was utilized. These were cultured in EMEM supplemented with 10% heat-inactivated FBS and 1% P/S in surface-treated T-75 cell culture flasks according to handling specifications (ATCC). These were grown at 37°C in a fully humidified atmosphere containing 5% CO_2 (air jacketed CO_2 incubator basic, VWR), with medium renewal every 3 days as required. Cells were subcultured when they reached roughly 70% confluency. This process involved a brief rinse with 1X PBS to remove trace serum containing trypsin inhibitor, followed by the addition of 3 mL of 0.25% trypsin-EDTA solution for 3 min at 37°C. This step facilitated cell detachment from the culture flask, as monitored via an inverted microscope (Invertoscope 40C, Zeiss). Following this, 8 mL of complete growth medium was added to the flask and the suspension was centrifuged at 125 x g for 10 min. The supernatant was discarded and the remaining pellet was then resuspended in growth medium for further use. To prepare cells for cryopreservation, 5% DMSO (v/v) was added to the suspension and it was frozen overnight at -80°C, with subsequent transfer to liquid nitrogen for long-term storage [119]. Alternatively, to prepare subcultures the resuspended pellet was diluted with fresh complete medium at ratios between 1:2 to 1:4, depending on desired growth rates, to new culture vessels and incubated. Cell morphology was captured through brightfield measurements (EVOS® FL Auto Imaging System, Thermo Fisher Scientific).

2.5.2 Cell Viability Testing

To examine the toxicity of both free nisin and liposome-encapsulated therapeutic on cultured IMR-90 cells, MTS cell viability assays were performed [120]. Cells at 70% confluency were detached, pelleted, and reconstituted in 1 mL of growth medium as previously described. A 20 µL aliquot of cell suspension was mixed 1:1 with a 0.4% trypan blue solution for 3 min, with 10 µL of the resultant solution transferred to a chamber slide for use in an automated cell counter to determine live cell counts (Countess II Automated Cell Counter, Thermo Fisher Scientific). All cell seeding was conducted in sterile cell culture-treated 96-well plates at a volume of 100 µL and seeding density of 5000 cells/well, with plates incubated at 37ºC and 5% CO_2 for 24 h.

Following incubation, the cells were treated through removal of old medium and replacement with 75 µL of fresh complete growth medium. To this, a mixture of components was added as a therapeutic dose, depending on the assay, and standardized to a final volume of 25 µL with sterile Milli-Q water. These treatments included the addition of free nisin, ethanol, and both empty and loaded liposomes at varying concentrations, with vesicle dosing volumes calculated as previously described in Equation **(9)**. The treatment plates were then incubated for an additional 24 h under the same conditions, at which point the medium was swapped again, this time for 100 µL of fresh complete growth medium to avoid colour changes induced by pH and 20 µL of the tetrazolium reagent MTS. All assays were also conducted with control groups, where the negative growth control was treated with only complete medium and the positive growth control was treated with complete medium and 20 µL of DMSO on the third day. Blank measurements were also taken, which were identical to the negative and positive growth controls except there was no cell seeding. The treatment plate was then incubated away from light for 3 h and absorbance readings at 490 nm were taken using a microplate reader. All measurements were conducted in triplicate, with cell viability calculated using the relevant control groups and Equation **(10)**:

$$Cell\ Viability\ (\%) = \left(\frac{A_{490}(treatment\ well) - A_{490}(negative\ blank)}{A_{490}(negative\ growth\ control) - A_{490}(negative\ blank)}\right) * 100 \qquad \textbf{(10)}$$

For treatments involving the addition of bacterial supernatant to cell culture, there were some minor modifications to the previously described procedure. On treatment day, the replaced growth medium did not contain 1% P/S to allow for bacterial growth. Standardized bacterial inoculums suspended in their preferred growth media were added at specified loads, utilizing the same assumption that a 0.5 McFarland standard equated to $1.5x10^8$ CFU/mL of bacteria [113]. For all subsequent cell protection

assays, *S. pneumoniae* load was standardized at $7.5x10^6$ CFU/mL, equating to 5 µL of culture. For protection assays, empty liposomes were first concentrated to an equivalent level as their loaded counterpart and dosed at the same volume to ensure accuracy in lipid content. All measurements were conducted in triplicate.

2.6 Statistical Analysis

Data in this study was reported as mean ± standard deviation (SD) via triplicate measurements, with the exception of time-kill studies which were conducted in duplicate. Measurements examining the impact of cholesterol content variation on physical properties, short-term stability, cytotoxicity, and cellular protection upon bacterial challenge underwent one-way ANOVA with a post hoc Tukey multiple comparison test, where $p < 0.05$ was regarded as statistically significant.

Chapter 3: Results and Discussion

3.1 Liposomal Synthesis and Optimization

3.1.1 Microfluidic System Development

An in-house microfluidic setup was constructed to successfully formulate liposomal solutions, with several key parameter's worth further discussion. Two syringe pumps were necessary in the system to allow for alternation in pumping speeds between the two fluid streams, in this case being an ethanol and aqueous phase to ensure miscibility. Further, to avoid potential unwanted interactions between the liposomal constituents, nonreactive tubing was utilized. This tubing was also trimmed to minimize length, as remaining void volume in small-volume runs becomes a major source of sample loss. The mixer chip utilized in the system had an internal herringbone geometry to induce faster mixing rates between the aqueous and ethanolic fluid streams. One limitation of such a mixer chip is that the microstructures do not allow for high TFRs, however this only becomes relevant at scaled-up manufacturing [89]. Further, studies have found that TFR has a comparatively smaller impact on PS than other parameters, such as FRR [88]. Potential clogging of the herringbone grooves was avoided via a water/ethanol flush and subsequent air purge after each use.

Another major factor in the developed system was the choice of liposomal constituents and therapeutic. Regarding lipids, it is important to note the phase transition temperature (T_m), source, stability, charge, and mixture composition [84]. The T_m for phospholipids is the point where hydrocarbon chains switch from acting like a gel to a liquid, and this relies on the given lipids saturation, acyl chain length, packing efficiency, head group polarity, and ionic strength of the suspension medium [121]. The liposomes in this work incorporated EPC and EPG as structural phospholipids, and each of them have a wide fatty acid distribution due to their natural derivation. As a result, at room temperature both could be found in liquid-crystalline form, with T_m's often reported around -15^{o}C [122].

It is generally recommended to process liposomes incorporating natural lipids at a temperature greater than the T_m of any of the liposomal constituents to prevent aggregation. This made the chosen lipids more attractive in that there was less need for heating control and subsequently less potential for therapeutic degradation during formulation [123]. Conversely, natural lipids often suffer from poor stability due to issues in membrane fluidity, requiring the incorporation of cholesterol to fill in gaps left by imperfect packing between the lipid species present in the membrane. The inclusion of cholesterol

served to restrict fluidity, prevent hydrolysis, and improve overall stability of the developed liposomes, along with the added benefit that it acted as a binding point to facilitate PLY interactions [123]. Beyond this, saturating levels of cholesterol greatly increase the activation energy required for molecules, such as nisin, to diffuse across the lipid bilayer and thereby reduce leakiness of the liposome [124]. EPG, an anionic lipid, was incorporated into liposomes for two main goals: to facilitate attractive electrostatic interactions with cationic nisin, as well as prevent aggregation in solution to improve overall stability [125]. Another important consideration is that EPC, EPG, and cholesterol could all be dissolved in ethanol at concentrations suitable for microfluidic manufacture, while this same property is not shared among all synthetic lipids.

For choice of therapeutic, nisin Z was selected over its other variant, nisin A, due to its improved solubility at physiological pH. Milli-Q water was selected as the liposomal buffer, rather than PBS, to avoid potential long-term stability concerns with nisin, as the peptide shows hindered solubility in saline environments [126]. The liposomal solution was diluted 10x to reduce residual ethanol via Milli-Q washing, as its presence can increase cytotoxicity and impact bilayer conformation to reduce overall stability [127]. As can be seen in Figure 3.1, ethanol concentrations above 5% (v/v) led to a significant drop in IMR-90 cell viability. In comparison, after 10x dilution via buffer exchange the residual ethanol content in liposomes formulated at an FRR of 3:1 would be far below 2.5% (v/v).

To conduct the buffer exchange, centrifugal filtration techniques were adopted using filter units with a MWCO of 30 kDa. It is important to note the molecular weight of nisin is ~3.5 kDa, thereby allowing for any unencapsulated therapeutic to easily flow through the filter and prevent artificially high EE determinations. There are various separation techniques available, but it has been found that filtration can more effectively separate out small particle suspensions while simultaneously exerting less physical force on the liposomal suspension, avoiding potential particle damage [128]. Overall, through optimization of these key formulation aspects, a microfluidic system capable of liposomal manufacture was developed.

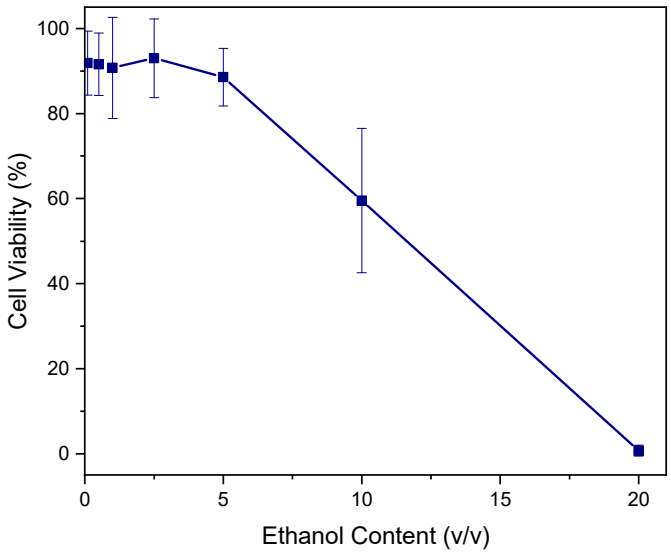


Figure 3.1. Impact of ethanol content on viability of cultured IMR-90 cells. Values represent mean ± SD (n=3).

Another key aspect of a successful liposome workflow is the ability to detect therapeutic in a reliable manner for EE determination. This can be measured either directly or indirectly, with the former quantifying the actual payload in the final sample and the latter quantifying non-encapsulated therapeutic in the filtrate after buffer exchange. Indirect measurements, while more common, typically have higher variability and a tendency to overestimate EE. In contrast, the major roadblock with direct EE measurements is potential interactions with the lipids present in the final solution and the need for a permeabilization agent, such as Triton [129].

There are various techniques available to quantify proteins like nisin, including absorption, fluorescent, and immunoassays, as well as chromatographic analysis. Of these, fluorescence-based assays are often utilized due to their rapidity and high sensitivity, with the reagent CBQCA being particularly notable for liposome systems. It is essentially non-fluorescent in solution but can react with primary amines when in the presence of cyanide to form a fluorescent adduct [130]. Importantly, this reaction is not sensitive to the presence of lipids or Triton in solution, unlike more common bicinchoninic acid or NanoOrange™ assays, allowing for effective determination of protein via direct methods. An example of a nisin standard curve, as measured by the developed CBQCA assay, can be

seen in Figure 3.2. Fluorescence intensity followed a linear relationship with nisin concentration and exhibited an R^2 of 0.997, demonstrating strong detection accuracy at nisin concentrations as low as 0.5 µg/mL.

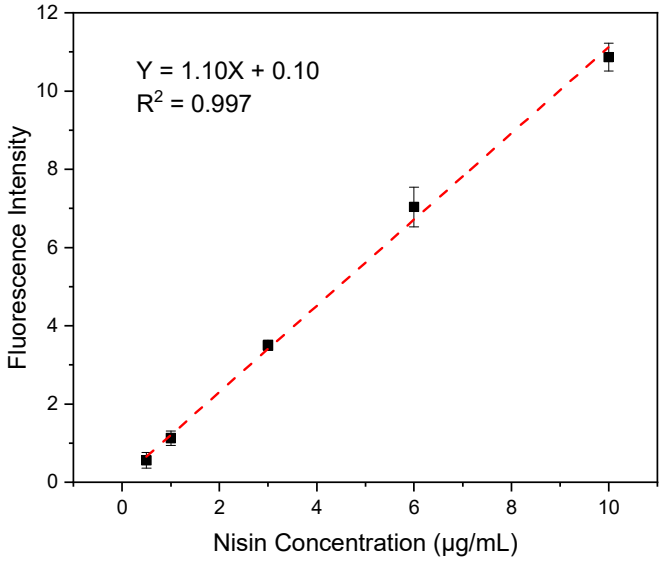


Figure 3.2. Standard curve of nisin measured via CBQCA assay, with the line of best fit, its equation, and R^2 value displayed. Values represent mean ± SD (n=3).

3.1.2 Box-Behnken Design Model Construction

In a given microfluidic system, there are various parameters that have a significant impact on particle properties, as previously described in Table 1.3. As such, to enhance the in-house developed system it was beneficial to conduct a BBD to improve the properties of cholesterol-rich liposomes. The design utilized independent variables of FRR, nisin concentration, and EPG molar content, as these all had major implications on particle characteristics. They were compared via the dependent variables EE, LC, PS, and PDI, with all responses displayed in Figure 3.3. For a full list of the encoded run design and response data, please refer to Table A1. It is important to note that for all formulations in the BBD, the composition of cholesterol was kept constant at 60 mol% as the desire was to fabricate cholesterol-rich liposomes. As seen from the wide range of response values for all four dependent variables, the

selection of independent variables for microfluidic optimization was warranted to improve liposomal properties. Importantly, there were several runs showcasing desirable properties, including high EE/LC and low PS/PDI, which served to demonstrate the ability of the workflow to make vesicles suitable for drug delivery applications. The low SD seen for all trials also served as an indication of strong replicative success of the microfluidic system, given that measurements were conducted in triplicate and fully randomized.

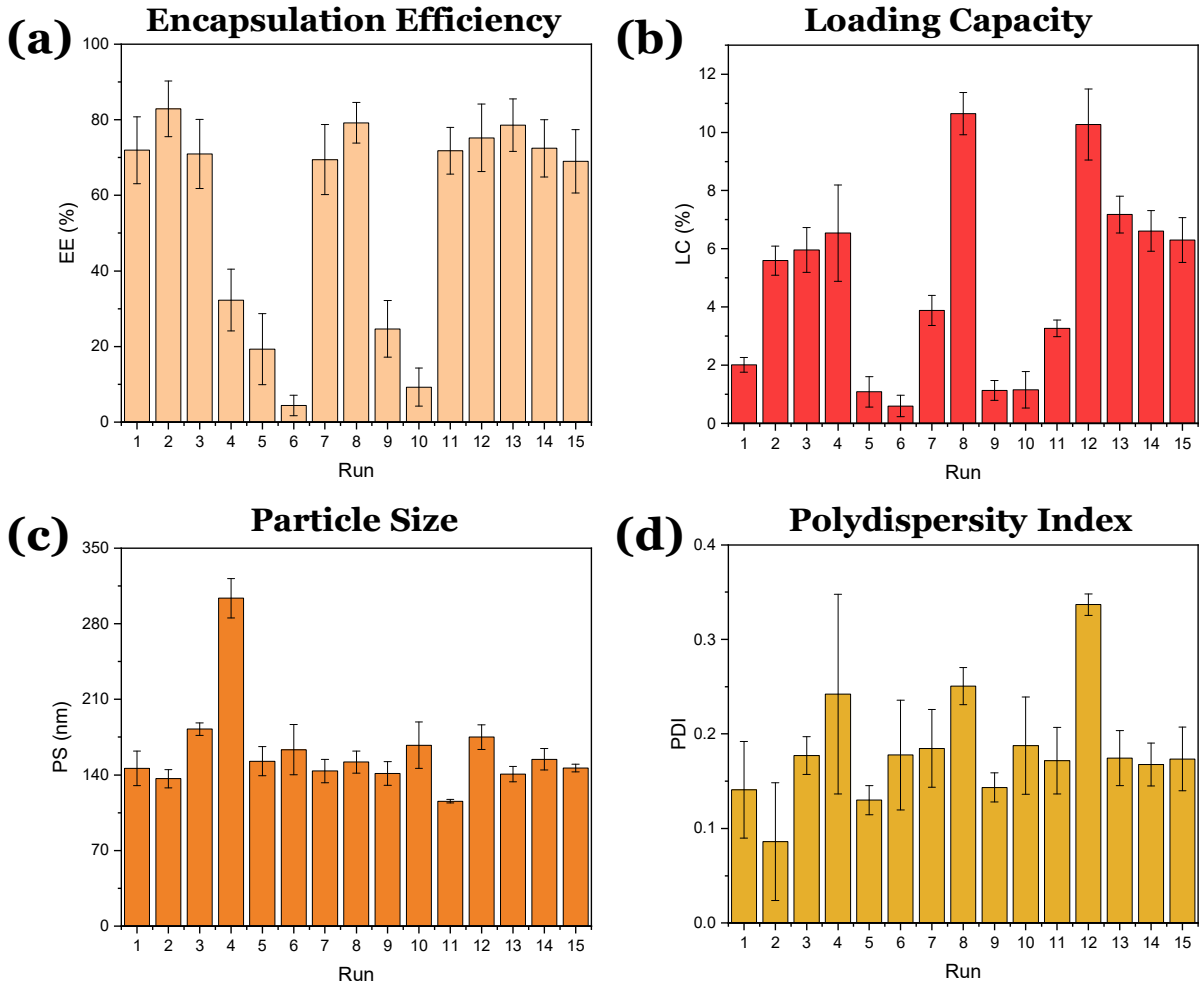


Figure 3.3. Measured responses of randomized three-factor BBD for **(a)** EE **(b)** LC, **(c)** PS, and **(d)** PDI. Values represent mean ± SD (n=3).

Based on the collected BBD data above, MiniTab® software was utilized to develop a second-order polynomial equation for each response variable via least square regression and subsequent ANOVA, as seen in Table 3.1. These quadratic equations each had 10 terms, with the coefficients and *p*-values lending insight into the influence and relationship between the independent factors and the associated response variable. Coefficients exhibiting a *p*-value < 0.05 were considered significant in subsequent analysis.

Table 3.1. Coefficients for the second-order polynomial equations for all four response variables (EE, LC, PS, PDI) and associated *p*-values as determined in Minitab® software (X_1 – FRR, X_2 – Nisin concentration, X_3 – EPG molar composition). All coefficients are displayed in coded units to maintain orthogonality, with each model's R^2 identified. All *p*-values < 0.05 have been highlighted under the assumption of significance.

Term	**EE**		**LC**		**PS**		**PDI**	
	Coefficient	*p*-val	Coefficient	*p*-val	Coefficient	*p*-val	Coefficient	*p*-val
$\mathbf{B_o}$	73.33	N/A	6.693	N/A	147.20	N/A	0.1700	N/A
$\mathbf{X_1}$	-4.11	0.208	1.305	**0.002**	16.30	0.114	0.01625	0.074
$\mathbf{X_2}$	-7.94	**0.038**	1.490	**0.001**	36.12	**0.008**	0.05125	**0.001**
$\mathbf{X_3}$	29.75	**0.000**	3.013	**0.000**	-4.82	0.596	0.03750	**0.003**
$\mathbf{X_1^2}$	-5.48	0.248	-0.787	0.054	24.00	0.114	-0.0163	0.186
$\mathbf{X_2^2}$	-3.34	0.461	-0.882	**0.038**	21.00	0.155	0.0088	0.447
$\mathbf{X_3^2}$	-24.76	**0.002**	-1.857	**0.002**	-18.30	0.205	0.0313	**0.032**
$\mathbf{X_1X_2}$	-12.39	**0.027**	-0.750	0.056	32.70	**0.042**	0.0275	**0.043**
$\mathbf{X_1X_3}$	6.16	0.187	1.810	**0.002**	-0.60	0.961	0.0050	0.644
$\mathbf{X_2X_3}$	4.70	0.296	1.745	**0.002**	8.30	0.521	0.0300	**0.032**
$\mathbf{R^2}$	0.9711		0.9878		0.8859		0.9570	

From the developed polynomial equations, it can be observed that EPG molar composition had the largest influence on EE, followed by nisin concentration. This follows logically, as the anionic nature of EPG would aid in facilitating interactions with the cationic nisin molecules. LC was directly influenced by all three studied factors, with FRR also having an impact since it adjusts the ratio between the two fluid streams and, consequently, the amount of lipid and recovered liposomes. PS was only significantly influenced by nisin concentration, while PDI was impacted by both the former and EPG molar composition. These findings likely relate to potential swelling and aggregation of the liposomes as a result of increased drug loading, as well as variation in membrane fluidity at different inclusions of EPG. Overall, the developed polynomial equations showed relatively good fits to the acquired data, with correlation coefficients (R^2) of 0.9711, 0.9878, 0.8859, and 0.9570 for EE, LC, PS, and PDI respectively.

This series of polynomial equations was then utilized to visualize the relationship between the dependent and independent variables via a series of contour plots, as seen in Figure 3.4. The EE data in Figures 3.4a-c confirmed previous indications that increasing EPG content led to improved EE through electrostatic interactions. Conversely, at high FRRs elevated nisin concentration led to diminished EE, likely due to saturated loading within the internal aqueous liposomal core and nisin-induced bilayer damage [131]. For LC data in Figures 3.4d-f, there appeared to be a linear relationship between all three factors, with higher values for each corresponding to greater drug loading. This follows logically, as high FRRs increase aqueous phase volume and thereby the amount of therapeutic able to be encapsulated in a similar fashion as elevating nisin molarity, while high EPG content improves liposomal association with nisin. The interactions between the variables became more complex with regards to PS in Figures 3.4g-i, although it can be noted that higher nisin concentration led to increased PS and overall dispersity through loading interactions. EPG incorporation had a lessened impact on PS but in general increased PDI, as seen in Figures 3.4j-l, while lower FRRs appeared to be optimal to reduce PS and showed little correlation with changes in PDI. These findings provide valuable insight into interactions between these three major microfluidic factors on given liposomal characteristics, and can be used to further optimize the system through statistical methods.

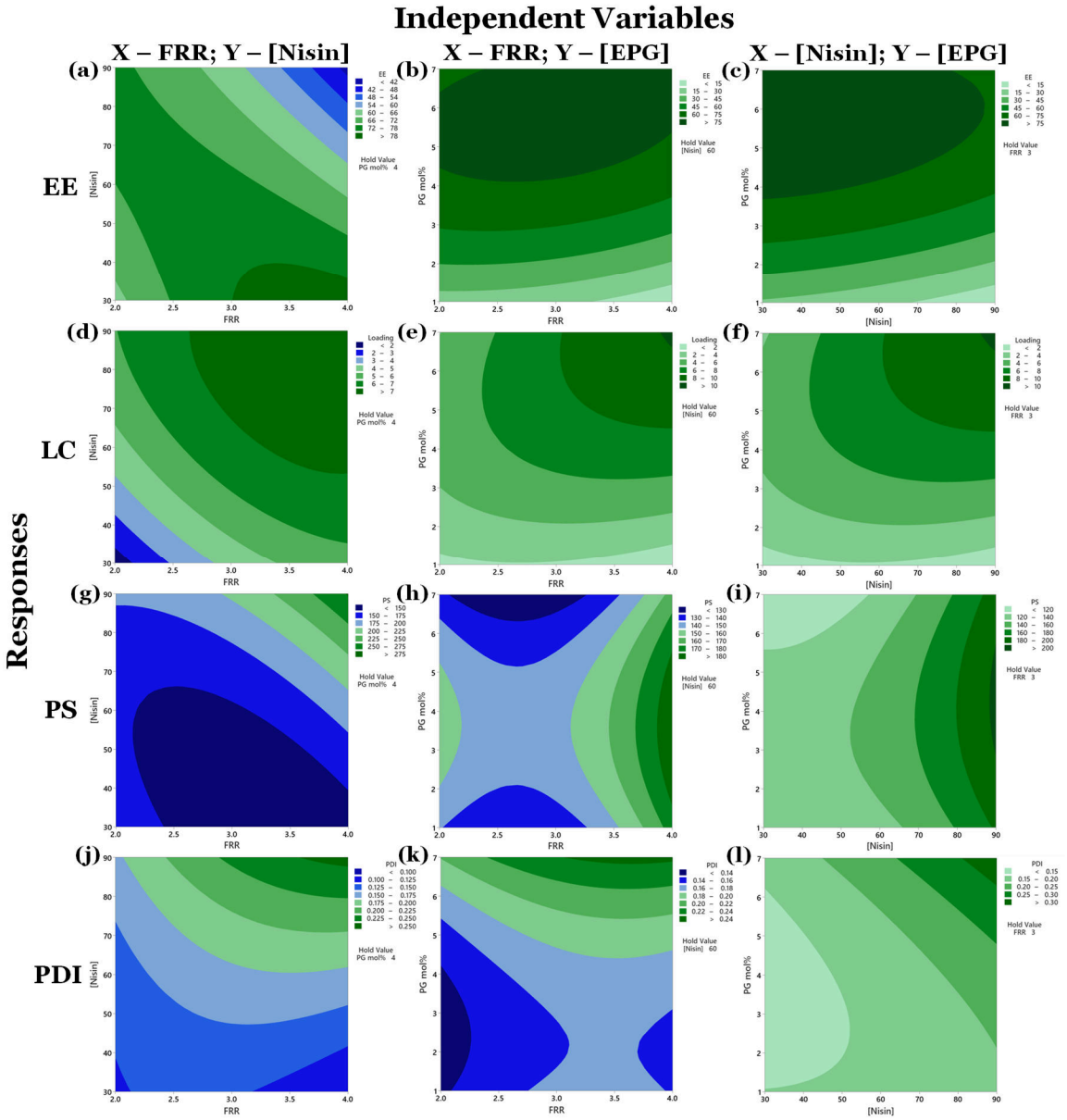


Figure 3.4. Contour plots highlighting the influence and interactions between different independent variables in the BBD model. This includes the correlation between **(a, d, g, j)** FRR and nisin concentration, **(b, e, h, k)** FRR and EPG molar concentration, and **(c, f, i, l)** nisin concentration and EPG molar concentration. Specifically, the contour plots give indications on the impact these variables have on **(a-c)** EE, **(d-f)** LC, **(g-i)** PS, and **(j-l)** PDI. All hold values were set to their median coded level. For interpretation, dark blue colours represent the lowest values for each response variable while dark green represents the highest, with legends displayed for each contour plot.

3.1.3 Optimization of Box-Behnken Design

The developed model was then used to predict optimum values for the given independent factors based on varying goals for each response variable. This was conducted for a series of optimization solutions, as seen in Table 3.2, which were then fabricated and compared to model predictions. For a full list of generated response targets, please refer to Table A2. Initial optimization attempts with the BBD model aimed to maximize EE and LC while simultaneously minimizing PS and PDI, as these properties are often desirable for a delivery system. However, this led to FRR and nisin concentration fits at upper and lower extremes respectively within the model, where BBD accuracy is known to be diminished [102]. This can be seen in the composite desirability of 0.85, which serves as an indication of how likely each predicted response will match the target requirements. To account for this, screening was conducted across a variety of additional optimization solutions through the use of different set target values. Of note is optimization solution 3 (coded O3), which had intermediary values for each response variable and delivered the highest composite desirability at 0.991.

Table 3.2. A series of optimization solutions given varying goals for each response variable in the developed polynomial model, including minimization (-), maximization (+), and set targets, along with corresponding fit and desirability values.

Code	**Goal**				**Fit**			**Composite Desirability**
	EE (%)	LC (%)	PS (nm)	PDI	FRR (aq:eth)	[Nisin] (μM)	EPG (mol%)	
O1	+	+	-	-	4:1	31.21	6.21	0.850
O2	75.0	+	140.0	-	3.35:1	50.00	4.00	0.811
O3	72.0	6.60	145.0	0.17	3.01:1	61.06	3.85	0.991
O4	+	+	130.0	-	4:1	31.21	5.42	0.861
O5	+	+	140.0	-	4:1	41.51	5.79	0.864
O6	+	+	150.0	-	4:1	43.94	5.18	0.864
O7	+	+	160.0	-	4:1	50.29	5.36	0.851

Each developed optimization solution was then fabricated and evaluated as per each response variable, as well as total encapsulated nisin mass and ZP, and displayed in Figure 3.5. General guidelines for desirable liposomal properties vary based on application, but for delivery purposes this generally involves PS < 260 nm, monodisperse populations, and elevated EE and LC [39]. From Figure 3.5a, it can be seen that all optimization solutions displayed over 70% EE, while O7 had the highest LC at 9.19 ± 0.66%. As identified in Figure 3.5b, all liposomal samples matched PS specifications but only O2 and O3 had PDIs ≤ 0.2. Further, O3 outperformed all other optimization solutions in terms of nisin mass encapsulated in Figure 3.5c, thereby making it the most efficacious therapeutic carrier. The O3 solution was capable of exhibiting an LC lower than O7 but still have more nisin physically encapsulated as it was synthesized at a lower FRR, providing a larger amount of lipids for nisin capture. It is also notable that all liposomes displayed a ZP within the range of -30 mV, which likely served to aid with electrical stabilization and prevent aggregation [132].

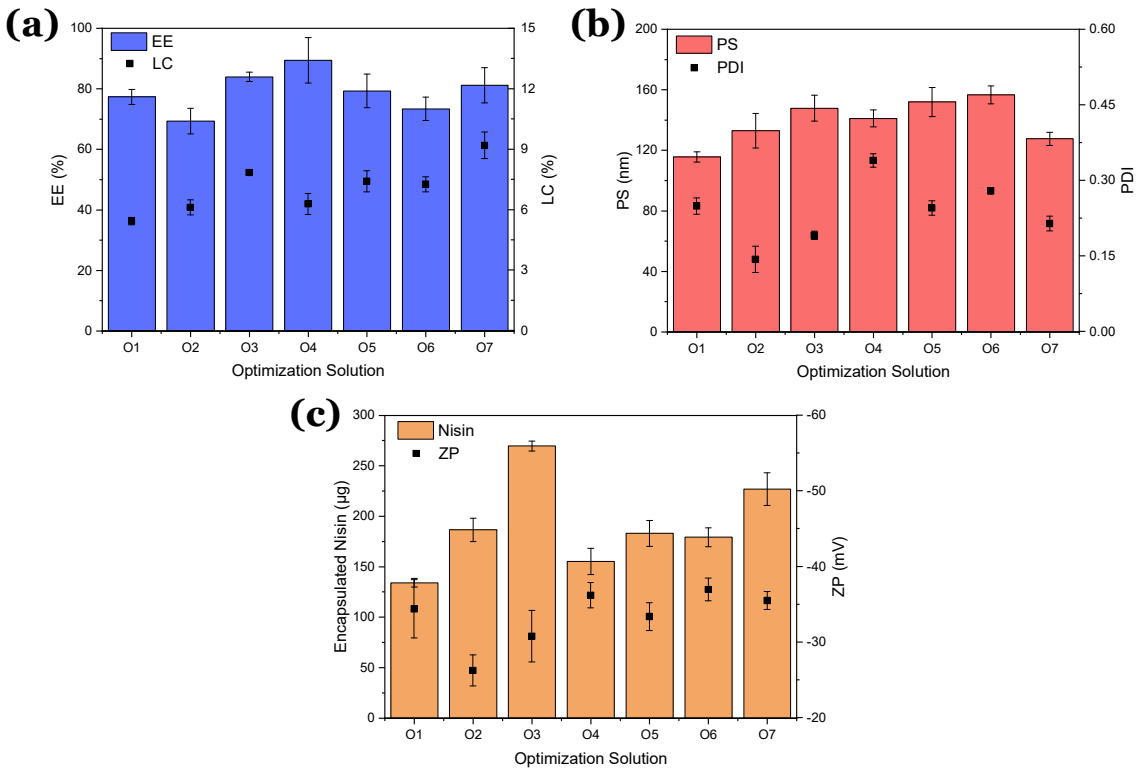


Figure 3.5. Liposomal characteristics of the optimization solutions, including **(a)** EE and LC, **(b)** PS and PDI, as well as **(c)** encapsulated nisin and ZP. Values represent mean ± SD (n=3).

Based on previous discussion, the optimized output for this model was determined to be O3, corresponding to a FRR, nisin concentration, and EPG molarity of 3.01:1, 61.06 μM, and 3.85 mol% respectively. Overall, greater than 80% agreeance was observed between experimental values and model predictions for all response variables, as displayed in Table 3.3. These results indicate that BBD methodology can be utilized to successfully optimize the microfluidic manufacture of liposomes, as well as predict and tailor particle characteristics given a set of formulation parameters. All subsequent liposomal samples utilized the optimized FRR, nisin concentration, and EPG molarity discussed.

Table 3.3. Response results of the O3 formulation and agreeance as compared to the predicted model outputs. Observed data values represent mean ± SD (n=3).

Response	Observed	Model Prediction	Agreeance (%)
EE (%)	84.04 ± 1.54	71.42 ± 4.64	85.0
LC (%)	7.84 ± 0.14	6.60 ± 0.35	84.2
PS (nm)	147.9 ± 8.62	148.9 ± 13.9	99.3
PDI	0.19 ± 0.01	0.17 ± 0.01	89.5

3.1.4 Variation of Liposomal Cholesterol

As the present work aimed to investigate the influence of cholesterol to facilitate PLY interactions and therapeutic release, the molar composition of cholesterol was then varied (30/45/60/75 mol%) in the optimized system and displayed in Figure 3.6. Cholesterol content had no significant influence on EE and only minor improvements in LC, as seen in Figure 3.6a. Cholesterol has been well documented to diminish EE in systems encapsulating hydrophobic cargo, but this has been avoided through selection of a molecule capable of inclusion within the internal aqueous core [133]. In comparison, there was a 19.6% increase in PS from the lowest to highest molar concentration of cholesterol studied, along with the lowest observed PDI of 0.17 ± 0.02 at 60 mol% in Figure 3.6b. This is likely owing to the ability of hydrophobic cholesterol to interact with acyl chains present in the naturally derived polysaturated phospholipids, with its inflexible nature imparting rigidity to the membrane and promoting a more spherical, monodisperse nature [81]. This additional rigidity also limits curvature of the bilayer and

consequently results in larger equilibrium liposome size [134]. However, at oversaturating levels of cholesterol there can be the formation of external cholesterol crystals, serving as a possible explanation for the PDI increase in the 75 mol% composition [124]. Overall, it appeared that 60 mol% led to optimal properties of all conditions tested.

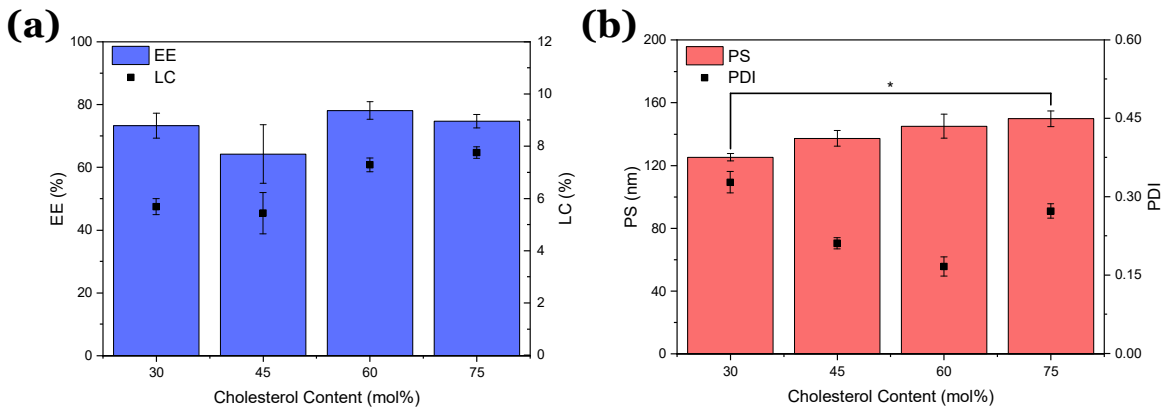


Figure 3.6. Impact of cholesterol content on liposomal **(a)** EE and LC, as well as **(b)** PS and PDI. Statistical analysis was carried out via one-way ANOVA followed by Tukey's multiple comparison test for both EE and PS, where $*p < 0.05$. Values represent mean ± SD (n=3).

It was also of interest to examine the impact of cholesterol content on short-term physical stability of the liposomes, with PS and PDI variation over a period of 14 days highlighted in Figure 3.7. This study was conducted at both fridge and physiological temperatures to examine the impact of storage conditions on natural phospholipids. Despite the low T_m's of EPC and EPG, storage temperature displayed no observable difference in stability for liposomes with 45 and 60 mol% cholesterol content, with these vesicles maintaining a comparable PS and PDI over the entire 14-day period. However, there was a notable increase in both vesicle size and dispersity for liposomes containing 30 mol% cholesterol at elevated storage temperatures. This was demonstrated in Figure 3.7b and Figure 3.7d by a respective 40.0% and 41.3% rise in PS and PDI after 14 days of storage relative to initial measurements. This indicates that incorporation of cholesterol played an important role in enhancing short-term stability of the formulations, as the sterol is known to enhance rigidity of the membrane and thereby prevent fusion and aggregation, especially in bilayers comprised of low T_m phospholipids [81]. In comparison, the 75 mol% samples only exhibited physical changes upon storage at 37°C, demonstrated in Figure 3.7d by

a 75.0% increase in PDI after 14 days relative to initial measurements. At excess concentrations and higher temperatures it is likely that oxidative degradation of external cholesterol led to the generation of byproducts capable of bilayer changes, such as 25-hydroxycholesterol [135]. Overall, these results indicate that incorporation of 45 and 60 mol% cholesterol led to optimal stability of the liposomal suspensions through packing within unsaturated regions of the bilayer. Expansion of these studies to examine both physical characteristics and nisin leakage over longer durations and in different buffers would be beneficial as an indicator of feasibility of this system for potential *in vivo* use.

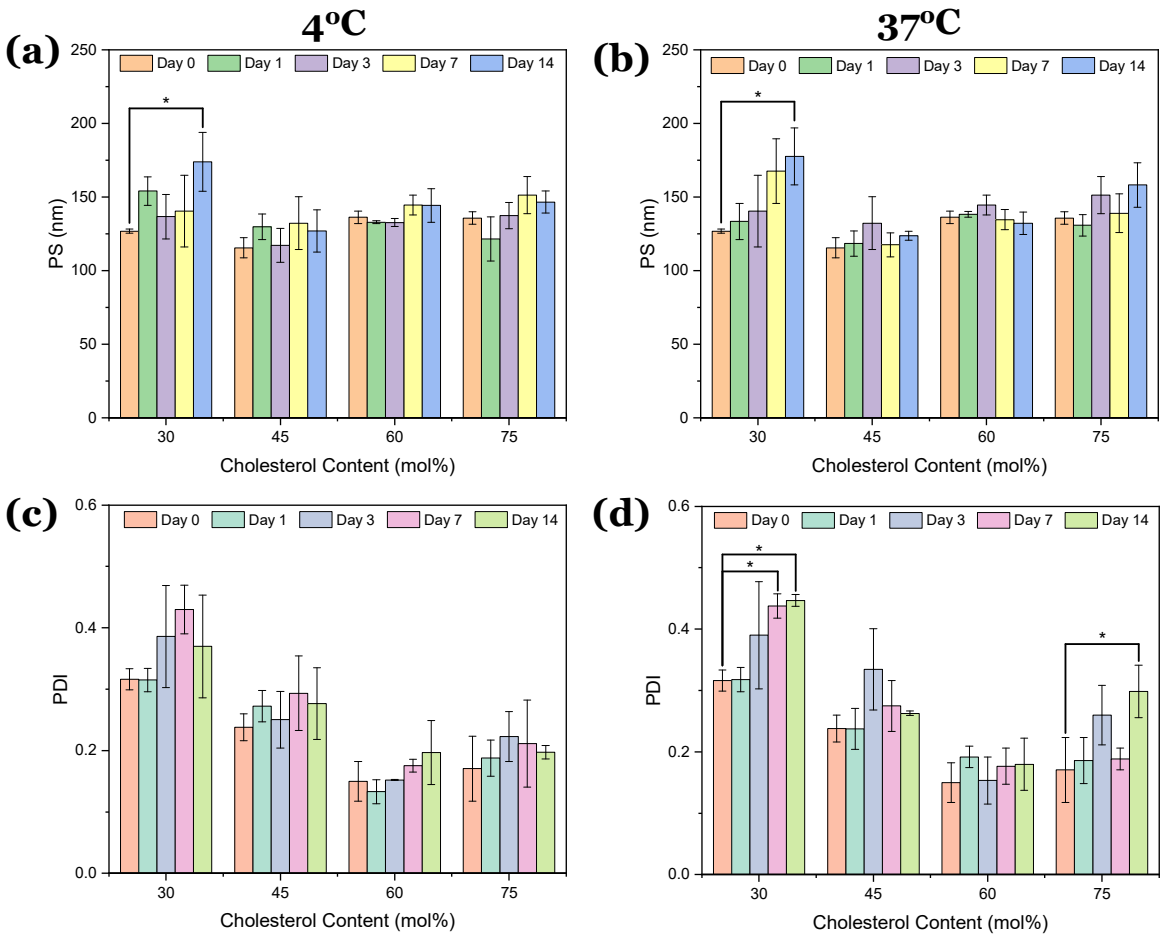


Figure 3.7. Physical stability of liposomes in terms of **(a,b)** PS and **(c,d)** PDI at storage temperatures of **(a,c)** 4°C and **(b,d)** 37°C, measured at varying timepoints over a 14-day period. Statistical analysis was carried out via one-way ANOVA followed by Tukey's multiple comparison test from initial measurements against each timepoint, where $*p < 0.05$. Values represent mean ± SD (n=3).

3.2 Pneumolysin Interactions

3.2.1 Optimization of Bacterial Culture

To examine the influence of PLY, it was desired to compare both purified recombinant protein and toxin present in cultured bacterial supernatant. To obtain the latter, *S. pneumoniae* had to be optimized with regards to culturing methodology and standardized for experiments. The essential nutrients required for growth relies heavily on the strain, and with over 97 available serotypes culturing media varies widely [136]. In this study, strain 23F-1 was cultured in BHI as per supplier specifications (ATCC), with a minor modification being the addition of 2% yeast extract to improve growth. In comparison, *S. epidermidis* was cultured in TSB and chosen as a control microbe due to its colonization of mucosal membranes and limited toxin production, allowing for the examination of liposomal specificity on PLY interactions [137].

To improve reproducibility of bacterial experiments it was imperative to utilize cultures within their logarithmic growth phase, as once inoculated into fresh media the initial lag phase was able to be bypassed [138]. As such, growth curves determined via OD measurements and serial plate dilution colony counting for both *S. pneumoniae* and *S. epidermidis* can be seen in Figure 3.8, with initial OD's standardized to 0.085. OD measurements are often the norm for examining bacterial growth due to their rapidity and non-destructive nature, while CFU counts are far more expensive and variable but can be desirable for viable cell counting [139]. Note that *S. pneumoniae* exhibited far lower densities than *S. epidermidis*, as demonstrated by both colony counting and OD measurements in Figure 3.8a-b, but nonetheless matched growth curves of the same strain in literature [140]. Despite this, both bacteria did demonstrate regions of logarithmic growth, corresponding to culture times between 4-8 h and 1-3 h for *S. pneumoniae* and *S. epidermidis*, respectively.

For all subsequent studies, both bacteria were harvested within their respective logarithmic growth phase and diluted in fresh inoculum to match OD readings equivalent to a 0.5 McFarland standard. These McFarland standards are solutions with known OD readings that are used as a reference for adjustment of suspension turbidity, thereby producing consistent bacterial counts to improve reproducibility of microbial testing [113]. Finally, OD measurements and CFU readings within regions of logarithmic growth were compared via a standardization curve for both *S. pneumoniae* and *S. epidermidis* in Figure 3.8c-d. The linear relationship and corresponding high R^2 values of 0.969 and

0.976 for *S. pneumoniae* and *S. epidermidis* respectively indicated the ability to make approximations of viable cell density through OD measurements.

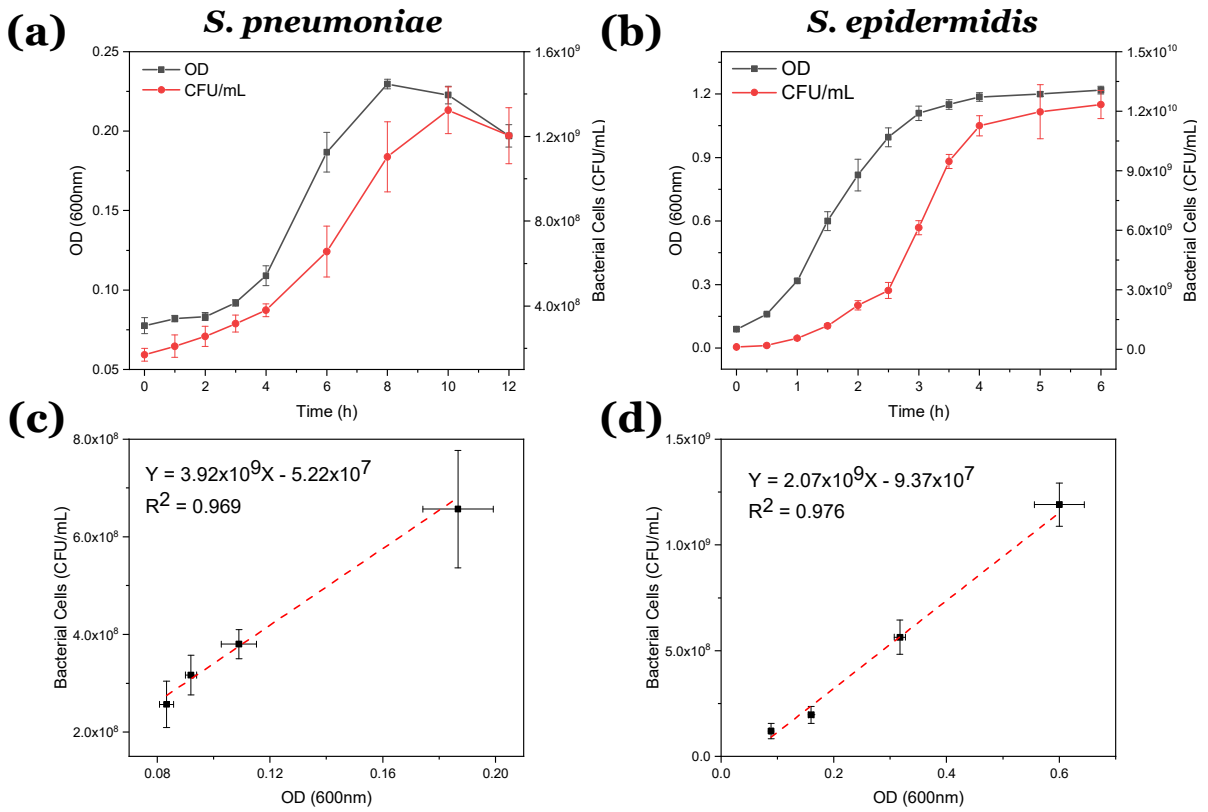


Figure 3.8. Growth curves of cultured **(a)** *S. pneumoniae* and **(b)** *S. epidermidis* as measured through both OD at 600 nm and CFU via serial plate dilutions, with initial inoculums diluted to a 0.5 McFarland standard density. A standardization curve within regions of logarithmic growth was then developed to contrast OD at 600 nm vs CFU/mL for both **(c)** *S. pneumoniae* and **(d)** *S. epidermidis*, with a line of best fit, its equation, and R^2 displayed for each. Values represent mean ± SD (n=3).

3.2.2 Hemolytic Activity

Purified PLY toxin and cultured *S. pneumoniae* were compared in their hemolytic ability, along with an investigation into the sequestration capabilities of the liposomal formulation in Figure 3.9. To begin,

recombinant PLY toxin displayed rapid hemolysis in Figure 3.9a, with almost complete lysis observed at 200 ng/mL. This falls within the range of toxin expression typically found in clinical *S. pneumoniae* infections [51]. In comparison, hemolytic activity from the bacterial culture reached maximal levels around a load of $3.0x10^7$ CFU/mL, equating to 70 μL of standardized *S. pneumoniae*. These results indicated that the cultured bacteria were capable of producing some form of virulence factors to induce RBC degradation, with activity levels matching well with that of purified PLY.

Using levels found sufficient to induce full hemolysis of human RBCs, the ability of the liposomal platform to sequester both PLY toxin and *S. pneumoniae* culture at varying molar compositions of cholesterol was examined in Figure 3.9b and Figure 3.9c respectively. Overall, there was little protective effect from liposomes containing less than 60 mol% cholesterol, while the cholesterol-rich formulations exhibited extremely effective toxin sequestration and neutralization at molarities as low as 10 μM. This equated to over a 90% reduction in hemolytic activity relative to solutions containing liposomes with 60 mol% versus 45 mol% cholesterol content in the presence of either PLY toxin or *S. pneumoniae* culture. There was little difference separating 60 and 75 mol% compositions, seemingly indicating that only a threshold cholesterol content was required to properly facilitate toxin binding. It has been suggested that PLY membrane binding is only triggered when cholesterol concentration exceeds the association capacity of the related phospholipids, as this excess is free to associate with the toxin [141]. One study found that only molar compositions of cholesterol above 50% in liposomes were able to form such independent domains within the bilayer, while at lower concentrations it preferred to associate only within the acyl chains [124].

It is of note that both bacterial culture and purified toxin exhibited similar trends in hemolytic activity as a function of liposomal molarity and cholesterol concentration. These results indicate that RBC degradation by *S. pneumoniae* culture was indeed caused by PLY production, as other virulence factors would not associate with liposomes in such a fashion. It also suggests that the level of PLY release at $3.0x10^7$ CFU/mL of pneumococcus culture was at or around 200 ng/mL. Overall, these findings provide strong evidence of rapid and preferential toxin uptake by the developed cholesterol-rich liposomal formulations, with neutralization activity serving to protect human RBCs in solution.

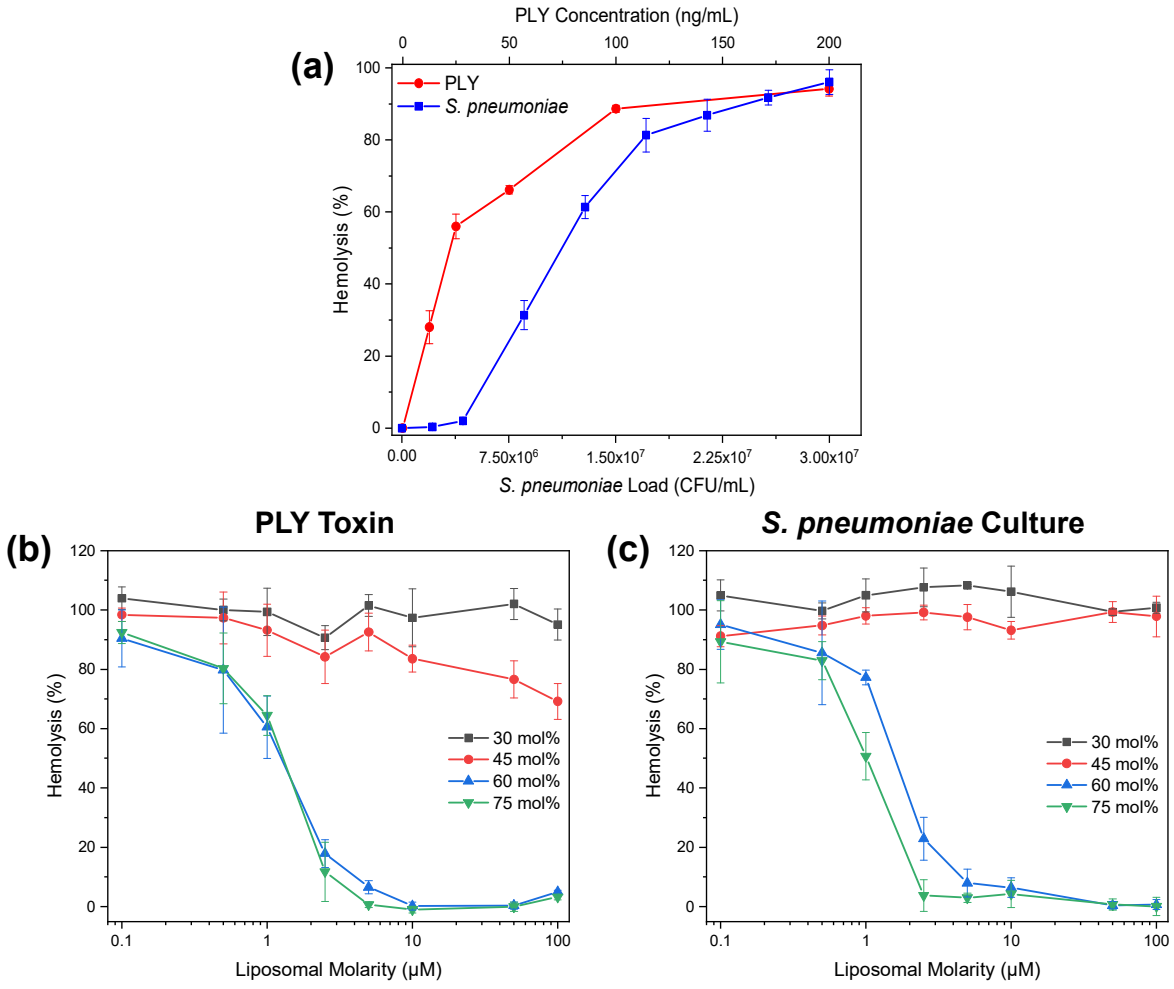


Figure 3.9. Hemolytic activity of **(a)** varying concentrations of purified PLY toxin and *S. pneumoniae* culture load against human RBCs. This was then compared to hemolytic activity of **(b)** purified PLY toxin (200 ng/mL) and **(c)** *S. pneumoniae* culture ($3.0x10^7$ CFU/mL) against RBCs in the presence of liposomes at varying cholesterol content. Values represent mean ± SD (n=3).

To demonstrate the potential for use in surface coating applications, liposomal solution was then air-dried under ambient conditions and at various molarities, with wells prepared at 1000 μM seen in Figure 3.10a. This formed uniform, opaque films on the polystyrene surface that were subsequently used for sequestration studies in Figure 3.10b under similar methodology as discussed above and a PLY concentration of 200 ng/mL. As can be observed, the overall trend of toxin neutralization and

erythrocyte protection at higher cholesterol content was maintained, with ≥ 60 mol% cholesterol limiting hemolytic rate due to the presence of available cholesterol for binding. It must be noted that higher liposome concentrations were required to observe a similar protective effect as the particles suspended in solution, with the lowest hemolytic rate of 30.1 ± 5.2% occurring at a lipid film molarity of 1000 µM. This is likely due to incomplete solubilization of the dried film and changes in the lipid aggregate structure upon dehydration and subsequent rehydration, which often result in fused vesicles and an increase in size [142]. This can serve to directly diminish the availability of surface cholesterol and thereby hamper toxin binding. Regardless, these results indicate that lipid films formed from liposomal solution were able to retain their toxin-neutralization activity when dried onto a plastic substrate, indicating potential for surface and packaging applications.

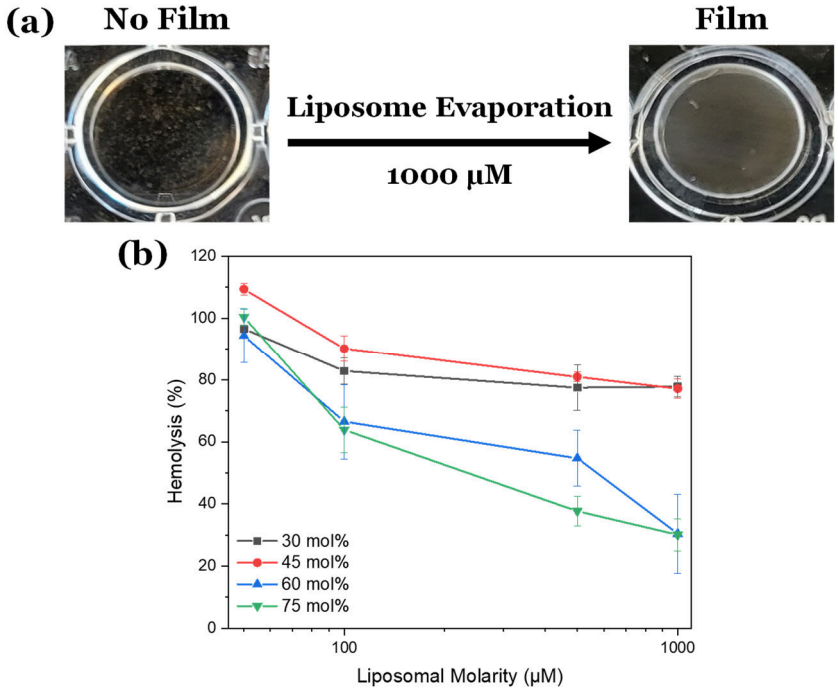


Figure 3.10. Liposomal solution at varying molarities were affixed to the bottom of a 96-well plate and fully dried, with **(a)** visible changes in opacity within the well evidence of lipid film formation at 1000 µM. Following this, the protective effect of the films was examined through **(b)** hemolytic assays of the treated wells at varying cholesterol content when incubated with PLY capable of inducing full lysis of human erythrocytes (200 ng/mL). Values represent mean ± SD (n=3).

3.2.3 Pneumolysin-Induced Liposomal Burst Release

After displaying potent toxin neutralization capabilities, the ability and rate of PLY to elicit disruption of liposomal structure was of interest. To date, CDC-induced liposomal release kinetics have been investigated for suilysin [143], perfringolysin O [144, 145], and PLY [146] and found to occur at rapid time-scales, although investigations had always utilized fluorescent biomarkers or real-time atomic force microscopy imaging rather than an antimicrobial therapeutic. As such, it was of interest in this study to examine release kinetics of liposome-encapsulated nisin. From the previous section it was found that full hemolytic protection was achieved at a liposomal concentration of 10 μM for 200 ng/mL of PLY. It was pertinent to examine activity at this sequestration limit, but due to the low liposomal molarity it was necessary to increase the concentration for proper detection of released nisin via CBQCA assay. As such, for release studies the liposomal molarity was increased to 200 μM and PLY was equivalently scaled to 4 μg/mL to maintain the same ratio. Both a positive lysis control (0.2% Triton) and negative control (PBS) were included for all samples over the tested timepoints, with full data visible in Figure A1. As expected, the positive control showed full lysis across all time-points, while the negative control exhibited negligible nisin release over the duration of the study.

The release profile of liposome-encapsulated nisin incubated with PLY toxin is visible in Figure 3.11. It was apparent that there was little nisin release from formulations containing both 30 and 45 mol% cholesterol, while the two cholesterol-rich formulations displayed rapid leakage of over 60% therapeutic after just 5 min and full release after ~ 30 min. These findings corroborate the protection assays in that only cholesterol-rich formulations are likely to have surface-exposed cholesterol domains available to facilitate binding interactions with the toxin. Beyond that, this demonstrates the ability of the toxin to disrupt liposomal structure via formation of a transmembrane pore, thereby eliciting leakage of encapsulated nisin in a responsive and rapid fashion [146]. It is important to note that peptide separation from the liposomal suspension was conducted through an active technique, being centrifugal filtration, which can indicate more rapid release than passive approaches that rely on diffusion, such as dialysis [147].

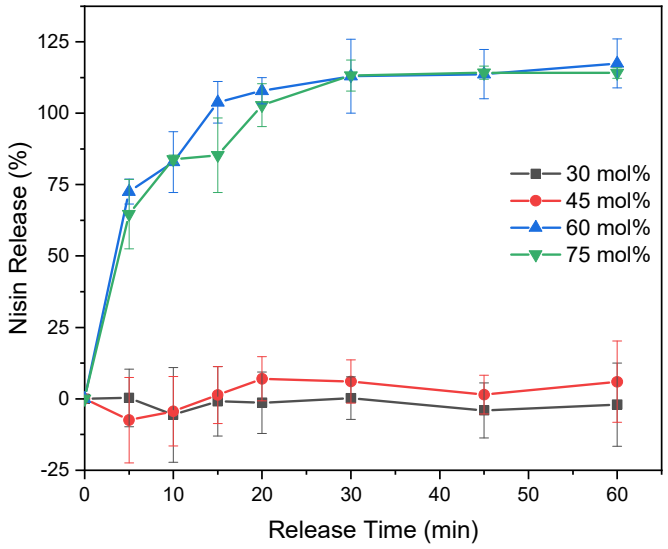


Figure 3.11. Liposomal release of nisin induced by PLY incubation (4 µg/mL) at 37°C, measured at varying timepoints over a 1 h duration at differing molar cholesterol content (200 µM liposomal dose). Values represent mean ± SD (n=3).

3.2.4 Morphological Analysis of Liposomal Pneumolysin Binding

To determine the impact of PLY binding on structural morphology of the produced liposomes, 4 µg/mL of toxin was incubated with 200 µM of particles at varying molar compositions of cholesterol for 1 h. Structural analysis was then conducted via negative-stain TEM, with individual liposomes identified both with and without PLY treatment in Figure 3.12. The sizes of the imaged vesicles were determined through ImageJ analysis and ranged between 100-150 nm, correlating well with data obtained from light-scattering measurements. Note that, while single-particle analysis has been presented, the displayed images were good representatives of the sample morphology as a whole.

As seen in Figure 3.12a, at low cholesterol inclusion there was more evidence of irregularities in the shape of the liposomal vesicles due to reduced rigidity of the bilayer [134]. Beyond 30 mol%, the particles demonstrated a far more uniform, spherical nature. Another important finding was that after PLY treatment, liposomes with both 30 and 45 mol% cholesterol inclusion demonstrated no evidence of significant morphological change to the untreated version, as seen in Figures 3.12a-d. Conversely,

at 60 and 75 mol% cholesterol there was indications of potential structural irregularities on the surface of the liposomes incubated with PLY, denoted by red arrows in Figures 3.12e-h. It is hypothesized that these irregularities may be due to the presence of PLY pre- or transmembrane pores. Size analysis through ImageJ indicated an average diameter of 25.1 ± 9.8 nm between all marked structures, which closely agrees with known PLY pore size [45].

As a comparison, the morphological impact of PLY presence in bilayers, giant vesicles, and liposomes have been studied via TEM morphology by several groups previously [44, 45, 146, 148–151]. While the micrographs obtained in this study lacked the resolution to concretely identify characteristic features, the spherical nature and diameters of the potential pores were consistent with literature. The elevated brightness of these structures may be a result of unwanted interactions with the staining agent uranyl acetate, as it has been reported to produce misleading bright and dark regions within liposomal samples [152]. As such, future studies are warranted to examine this system under cryo-TEM, as this technique not only avoids the potential for liposomal damage during fixation and staining, but can also provide more in-depth structural information about lamellarity of the particles and PLY pore structure [152]. Regardless, initial findings indicate that these structural abnormalities may be through PLY-induced liposomal degradation, consistent with hemolytic and release assay data to support the hypothesis that only cholesterol-rich formulations can facilitate toxin interaction.

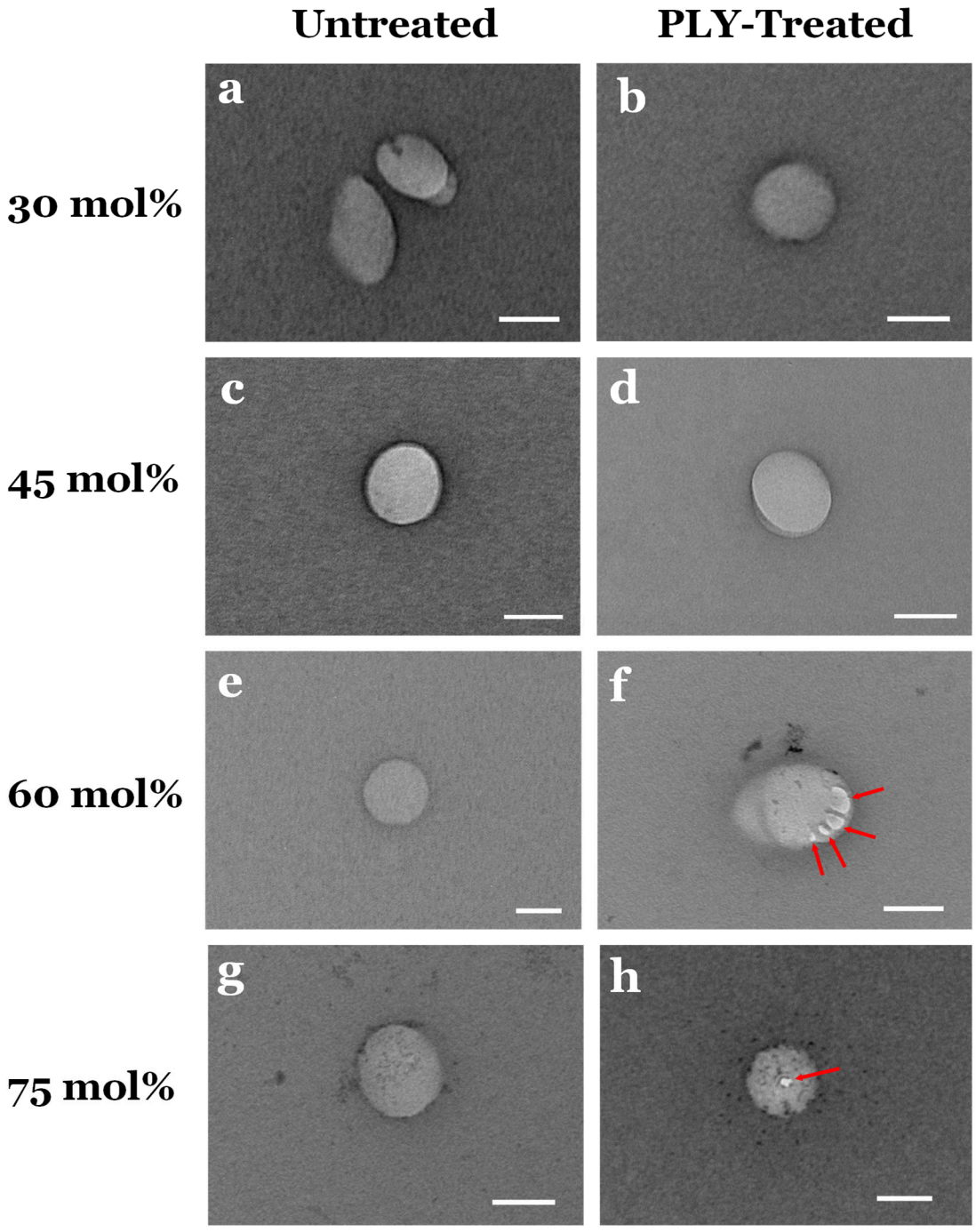


Figure 3.12. TEM images of both **(a,c,e,g)** untreated and **(b,d,f,h)** PLY-incubated (4 µg/mL) liposomes at varying molar cholesterol compositions (200 µM), ranging from **(a,b)** 30 mol%, **(c,d)** 45 mol%, **(e,f)** 60 mol%, and **(g,h)** 75 mol%. Red arrows indicate potential PLY-induced liposomal pores. All scale bars are equivalent to 100 nm.

3.3 Antibacterial Activity

3.3.1 Minimum Inhibitory and Bactericidal Concentrations

The antibacterial efficacy of free and encapsulated nisin was examined through MIC and MBC measurements against both *S. pneumoniae* and *S. epidermidis*. The former examines what level of therapeutic is required to prevent bacterial growth, while the latter quantifies what level is required for complete bacterial clearance. Following incubation with $8.6x10^5$ CFU/mL of standardized bacterial inoculum, OD measurements, as seen in Figure A2, were obtained to determine MIC through solution turbidity. To assess the system's bactericidal capacity, MIC cultures were then plated and incubated overnight, followed by examination for bacterial presence. Images of the physical plate growth at varying nisin concentrations has been included in Figure A3 for *S. pneumoniae* and Figure A4 for *S. epidermidis*. A summary of MIC and MBC measurements for both bacteria can be seen in Table 3.4.

Free nisin was determined to be bactericidal against *S. pneumoniae*, as the MBC of 4 µg/mL was within a close ratio of the MIC at 1.5 µg/mL [153]. This antimicrobial activity arises from nisin's ability to bind to the precursor lipid II within gram-positive bacteria and inhibit cell wall biosynthesis, leading to cell membrane permeation [154]. In comparison to free drug, liposome-encapsulated nisin showed varying levels of effectiveness against *S. pneumoniae*, with low molar compositions less capable of bacterial inhibition and clearance than those at 60 or 75 mol%. This is likely attributable to higher release of nisin from cholesterol-rich liposomes as a result of PLY-induced vesicle damage.

While prolonged release profiles are often considered advantageous to protect the therapeutic from degradation and increase serum concentrations, controlled release of high local drug concentrations at the infection site is often preferred to elicit rapid clearance of bacterial populations [155]. Cationic liposomes are by far the most utilized variation for treatment of bacterial infections, as they can facilitate fusion and therapeutic release through electrostatic adsorption to negatively charged bacterial membranes, thereby lowering MICs [156]. However, these carriers suffer from nonspecific interactions *in vivo*, leading to high cytotoxicity, low serum stability, and reduced activity [125]. Conversely, anionic liposomes, while more stable and less cytotoxic, have been found to display higher MICs than free drug in solution due to their unfavourable electrostatic interactions, making a triggered release system mandatory to boost efficacy [125, 157]. As such, the ability of cholesterol-rich liposomal formulations in this study to closely match the bactericidal activity of free nisin in solution served as an indication that encapsulated drug was being successfully released in proximity to *S. pneumoniae*

culture *in vitro*. One caveat to such a system is that rapid release profiles can often lead to toxicity *in vivo*, but as nisin has been approved by the FDA and is generally regarded as safe for use as a food additive, this is postulated to have less significance [158, 159].

Unlike with *S. pneumoniae*, free nisin acted in a bacteriostatic fashion against *S. epidermidis*, with the MIC of 3 µg/mL far lower than the observed 96 µg/mL MBC. This discrepancy in activity between the microbes may result from a variety of factors, such as difference in growth media, cell membrane composition, and microenvironment within the grown culture, with bacteriostatic activity against *S. epidermidis* observed elsewhere [160]. In contrast, liposome-encapsulated nisin was less effective at bacterial inhibition and could not demonstrate complete clearance within the concentration regime for all tested molar compositions of cholesterol, likely owing to poor release in solution and unfavourable electrostatic interactions. It should however be noted that there was still some form of inhibitory effect seen, likely attributable to the presence of surface adsorbed nisin or therapeutic leakage in solution.

Table 3.4. MIC and MBC for *S. pneumoniae* and *S. epidermidis* against both free and liposome-encapsulated nisin at varying molar compositions of cholesterol (n=3). Initial bacterial load equated to $8.6x10^5$ CFU/mL.

Formulation	***S. pneumoniae***		***S. epidermidis***	
	MIC (µg/mL)	MBC (µg/mL)	MIC (µg/mL)	MBC (µg/mL)
Free Nisin	1.5	4	3	96
30 mol%	8	32	12	> 96
45 mol%	6	16	12	> 96
60 mol%	2	4	12	> 96
75 mol%	2	4	12	> 96

One indication of surface adsorption of therapeutic is through examination of ZP, as changes in surface potential between an unloaded and loaded NP may arise due to the outward presence of therapeutic [161]. As such, a comparison of the properties between nisin-containing and empty

liposomes has been included in Table A3, where ZP was displayed to remain constant regardless of loading. As such, it is likely that the residual inhibitory activity seen was largely a result of nisin leakage in the bacterial growth media over the duration of the assay and warrants further investigation. Regardless, the ubiquitous lowered activity seen in *S. epidermidis* serves as further evidence that liposomal release of nisin was consequential on the presence of PLY in solution.

3.3.2 Time-Kill Kinetics

To complement bactericidal studies, it was then of interest to examine time kinetics for nisin-induced bacterial killing in Figure 3.13. The activity of free nisin in solution was first examined at varying factors of the MIC for both *S. pneumoniae* and *S. epidermidis*, visible in Figure 3.13a and Figure 3.13b respectively. For both, the introduction of nisin led to a sharp decline in viable bacteria over the first 2 h, but only in the case of 4X MIC treatment on *S. pneumoniae* was complete clearance observed to the limit of detection of 100 CFU/mL. This matches well with the determined MBC of 4 μg/mL, as 4x MIC treatment correlated to a nisin dose of 6 μg/mL. Nisin has been characterized previously to elicit fast bactericidal effect against various strains via lipid II binding and subsequent arrest of cell wall biosynthesis and pore formation [162]. Conversely, *S. epidermidis* appeared less susceptible to nisin as it showed efficient recovery of bacterial populations 24 h after initial exposure. To explain this, findings suggest that some bacteria are more capable of recovery from nisin than others through adaptations in minor cell populations, however generally still remain sensitive upon subsequent exposure [163]. As expected, treatment at and above the MIC for both bacteria led to populations that were equivalent or below the original CFU due to the inhibitory effect of nisin.

Following this, loaded liposomes dosed at concentrations equivalent to the MIC were compared to free nisin in solution for both *S. pneumoniae* and *S. epidermidis* in Figure 3.13c and Figure 3.13d respectively. In the case of *S. pneumoniae*, bactericidal activity of liposomes containing 60 and 75 mol% cholesterol closely mimicked free nisin in solution, owing to their previously characterized rapid therapeutic release in proximity to PLY toxin. Comparatively, low molar compositions of cholesterol exhibited little bactericidal impact, with final colony counts being similar to that of the growth control. Meanwhile, for *S. epidermidis* the compositional molarity of cholesterol had insignificant influence on bactericidal activity, as all tested compositions exhibited little clearance as compared to free nisin in solution. This arose from the aforementioned unfavourable electrostatic interactions between the

anionic liposomes and bacterial membrane, with any potential leakage of nisin unable to overcome recovery rates of the fast-growing *S. epidermidis*. Overall, these results indicate antibacterial efficacy and specificity of cholesterol-rich liposomes for PLY-producing *S. pneumoniae* as compared to an *S. epidermidis* control.

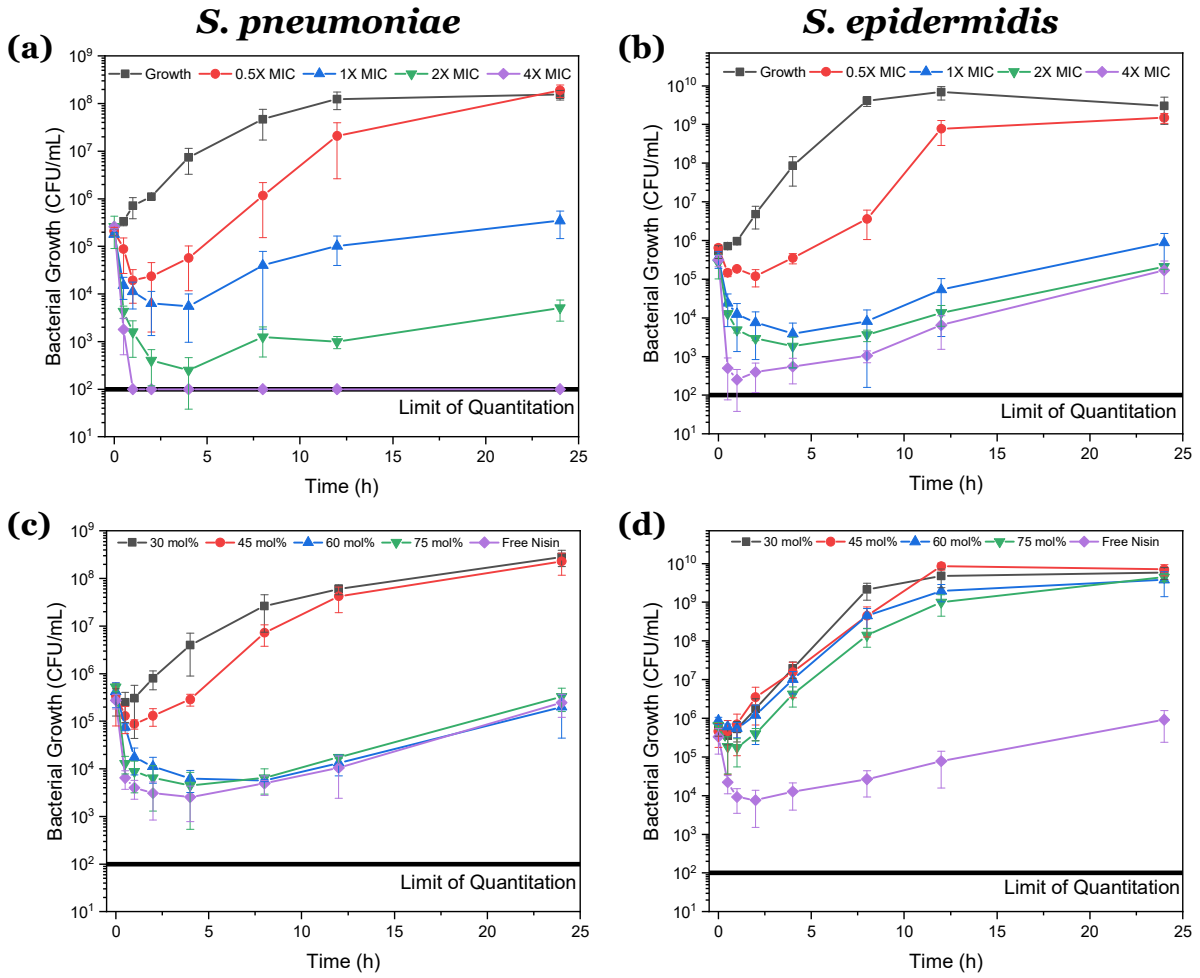


Figure 3.13. Time-kill plots for both **(a,c)** *S. pneumoniae* and **(b,d)** *S. epidermidis* over a 24 h incubation period and initial load of 8.6×10^5 CFU/mL. The effectiveness of **(a-b)** free nisin at various factors of the MIC was examined, as well as **(c-d)** liposome-encapsulated nisin at varying molar compositions of cholesterol at a concentration of 1X the MIC. Values represent mean ± SD (n=3), with a limit of quantitation of 100 CFU/mL.

3.4 Cell Protective Impact

3.4.1 Nisin Cytotoxicity

An MTS assay was conducted to investigate the impact of free and liposome-encapsulated nisin on the proliferation of IMR-90 cells, with results displayed in Figure 3.14. To examine the cell structure of the affixed cell line within 96-well plates, please refer to Figure A5. Note that all calculations of cell viability were normalized to the negative growth control as per Equation **(10)**. As observed, nisin exhibited little cytotoxic effect on the cultured IMR-90 cells until reaching a concentration of 150 μg/mL, at which point there was a dramatic absolute reduction in viability of 45.2%. This is likely attributable to receptor-mediated nisin uptake once the bacteriocin was concentrated enough in solution, leading to membrane alteration, calcium influx, and overall modulation of cell physiology [164, 165]. However, the dosing regime where nisin exhibits cytotoxic impact is far beyond that of the 4 μg/mL MBC against *S. pneumoniae*, indicating its high specificity for bacterial membranes. The impact of nisin on various cell lines has also been documented in literature, with significant drops in viability occurring within a similar dosing regime to this study [166, 167].

The cytotoxicity of loaded liposomes at varying molar compositions of cholesterol was then examined. It can be seen that, in general, liposomes with either 60 or 75 mol% cholesterol did elicit a mild cytotoxic impact on the IMR-90 cells, though not in an expected dose-dependent manner. The only exception to this trend was at the highest dosing condition of 150 μg/mL of nisin, where liposomes displayed higher viability through diminished leakage of the encapsulated therapeutic. To explain these findings, recall previous discussion that identified cholesterol saturation within liposomal membranes can result in the formation of external crystals. These cholesterol crystals can be readily oxidized, with the range of oxysterol byproducts capable of inducing toxicity within biological systems [168, 169]. It is also possible that residual cholesterol may elicit enhanced exocytosis of formazan granules, the enzymatic reduction product of MTS, thereby reducing absorbance readings and consequently displaying artificially lowered viability [170]. While all wells were thoroughly washed to remove residual liposomes and cholesterol prior to the addition of MTS reagent in an attempt to account for this, validation through alternative techniques like trypan blue or flow cytometry may be beneficial.

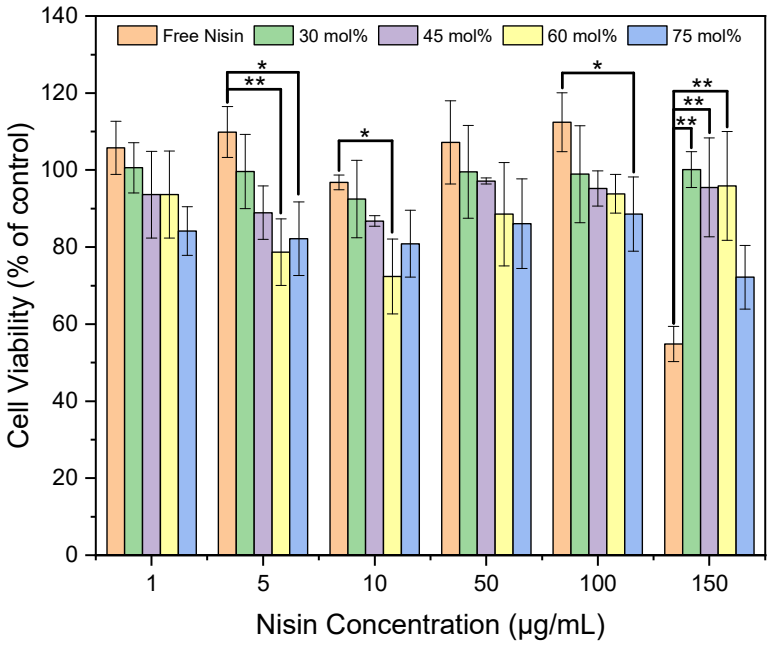


Figure 3.14. Cytotoxicity assay examining the impact of unencapsulated and liposome-encapsulated nisin on cultured IMR-90 cell viability at varying concentrations over a 24 h incubation period. Statistical analysis was carried out through one-way ANOVA followed by Tukey's multiple comparison test between free nisin and the liposomal samples at each concentration, where $*p < 0.05$, $**p < 0.01$. Values represent mean ± SD (n=3).

3.4.2 Bacterial Challenge Protection

To examine the ability of both free and liposome-encapsulated nisin to protect cultured IMR-90 cells from bacterial infection, the impact of both *S. pneumoniae* and *S. epidermidis* on cell survival was first examined. To do this, IMR-90 cells were challenged with varying loadings of each bacterium for 24 h and the impact on cell viability was examined via MTS. As seen in Figure 3.15, *S. pneumoniae* potently induced cell death even at low bacterial populations, with full clearance seen past 6.0×10^6 CFU/mL. This impact on cell survival has been well documented for various cell lines and is largely dependent on PLY and various other virulence factors possessed by the pathogen [171]. Conversely, *S. epidermidis* did not exhibit as strong of a cellular response, with a maximum absolute decrease in viability of 40.4% at a bacterial load of 3.0×10^6 CFU/mL. However, at elevated loading the viability

remained constant, likely owing to the fact that *S. epidermidis* can reach its stationary phase after 6 h of growth and final bacterial counts in the 24 h challenge would be similar regardless of initial challenge load. This indicates that cytotoxicity likely arose through nutrient competition and culture interactions, as *S. epidermidis* lacks any form of aggressive virulence factor to induce cell death [172, 173].

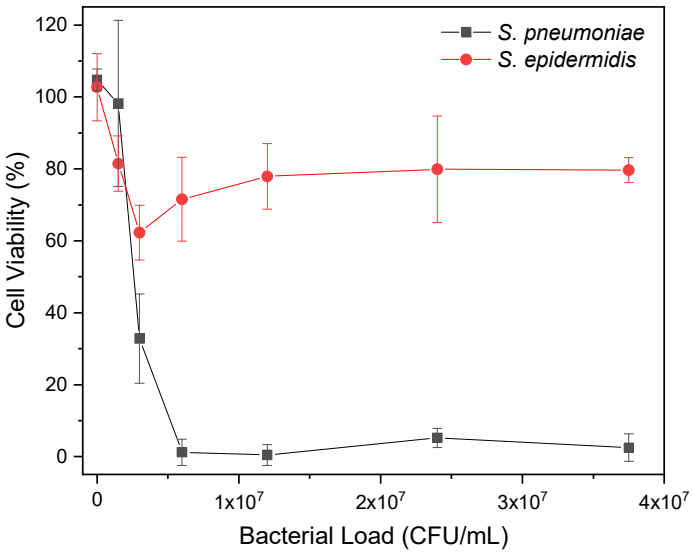


Figure 3.15. Impact on IMR-90 cell viability through inoculation with varying bacterial loads of cultured *S. pneumoniae* and *S. epidermidis* for 24 h. Values represent mean ± SD (n=3).

Following examination of the ability for either bacterium to induce IMR-90 death upon challenge, protection assays were performed with *S. pneumoniae* at an initial bacterial load of 7.5×10^6 CFU/mL. This assay was conducted as described before, but now also in the presence of either free nisin, unloaded liposomes, or loaded liposomes at varying molar compositions for 24 h, with results displayed in Figure 3.16. One difficulty in the treatment of *S. pneumoniae* is that lysis of the bacterium causes burst release of internalized PLY, the main produced pathogenic factor responsible for cell death [174]. As such, free nisin in solution, even at concentrations known to be bactericidal, was not able to fully protect IMR-90 cells from pneumococci challenge, with the highest dose resulting in a cell viability of 57.7 ± 4.2%. Conversely, Figures 3.16a-b display that unloaded particles incorporating either 30 or 45 mol%

cholesterol exhibited little protective impact at all, supporting previous evidence that cholesterol content ≤ 45 mol% was insufficient to facilitate PLY binding. It should also be noted that unloaded liposomes in this assay were concentrated to the same volume and treated equivalently to those with encapsulated nisin to ensure lipid content remained consistent. In comparison, loaded formulations incorporating low cholesterol did demonstrate improvements to IMR-90 viability, although protective impact either matched or underperformed free drug in solution. This observed activity likely originated from some level of nisin leakage from the more fluid liposomal bilayer [124].

Liposomes synthesized with 60 and 75 mol% cholesterol exhibited a strong, dose-dependent protective impact on IMR-90 cells upon *S. pneumoniae* challenge, as seen in Figures 3.16c-d. At high dosing levels, empty particles elicited a similar boost in IMR-90 viability as free nisin in solution and significantly more than unloaded liposomes formulated with low molar cholesterol. This again supports the claim that surface-exposed cholesterol domains at high molar inclusion were sufficient to induce PLY binding and subsequent toxin neutralization. This acted synergistically with nisin encapsulation, as both loaded liposomes brought viability over 90% at a nisin dosing level of 32 μg/mL through rapid release of therapeutic in contact with *S. pneumoniae* culture. When compared to an equivalent dose of free nisin in solution, this represented an absolute increase in viability of 36.1% and 33.5% for the 60 and 75 mol% formulations, respectively. This high protective impact arises from the ability of the cholesterol-rich system to efficiently induce *S. pneumoniae* clearance while simultaneously neutralizing additional internalized PLY released as a result of bacterial lysis. One limitation of this study, however, is that *S. epidermidis* could not be used to examine specificity of the liposomal platform for the presence of PLY, as the microbe was not able to induce sufficient toxicity to IMR-90 cells.

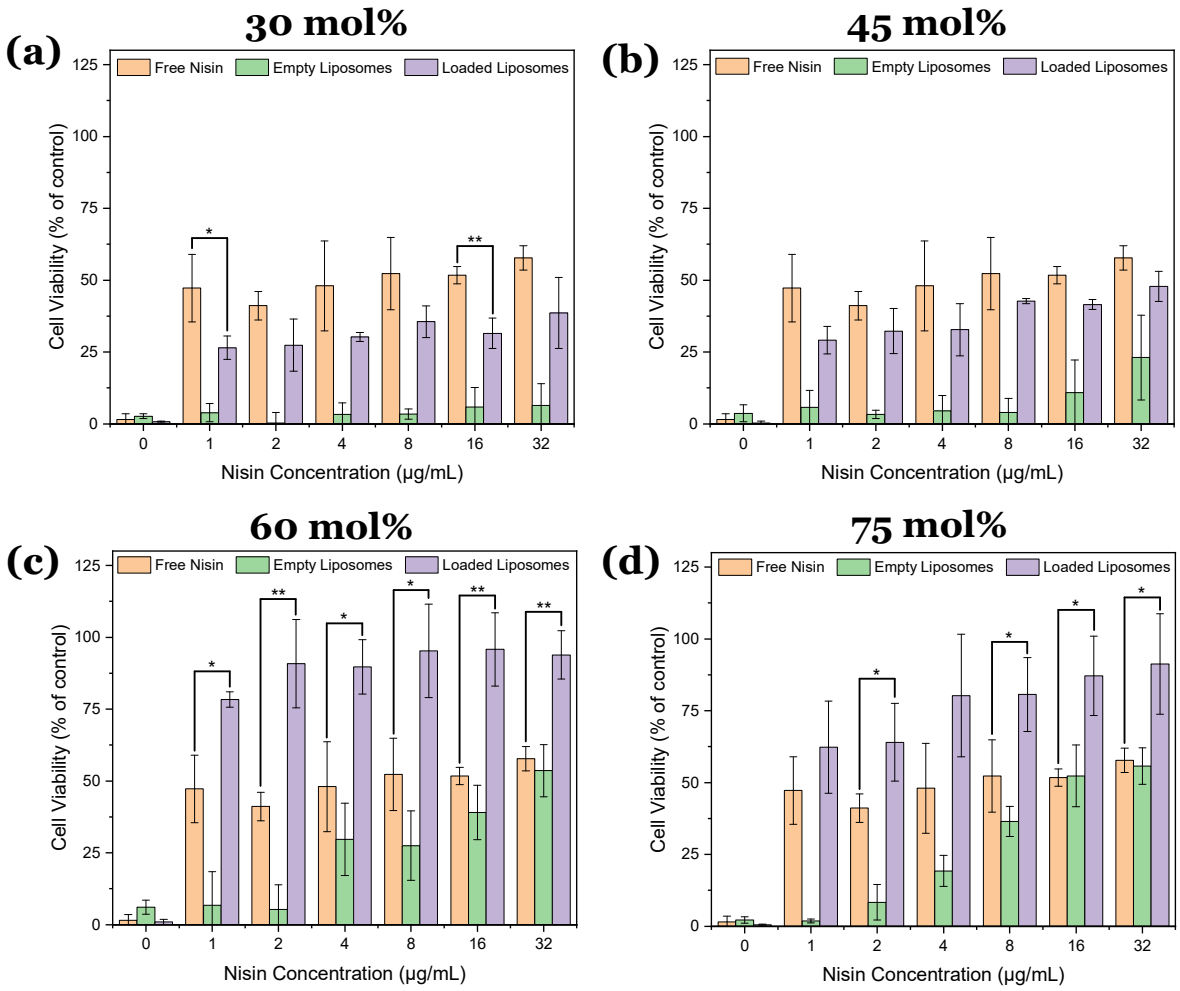


Figure 3.16. Protection studies examining viability of IMR-90 cells challenged by 7.5×10^6 CFU/mL of *S. pneumoniae* culture in the presence of free nisin, empty liposomes, or nisin-loaded liposomes. This study was conducted for liposomes containing a molar composition of **(a)** 30 mol%, **(b)** 45 mol%, **(c)** 60 mol%, and **(d)** 75 mol% cholesterol. Statistical analysis was carried out through one-way ANOVA followed by Tukey's multiple comparison test between free nisin and loaded liposomal samples at each concentration, where $*p < 0.05$, $**p < 0.01$. Values represent mean ± SD (n=3).

Chapter 4: Conclusions

4.1 Findings and Significance

This study aimed to utilize microfluidic techniques to optimize synthesis of liposomes at varying molar ratios of cholesterol to examine PLY-induced release of nisin for treatment of pneumococcal infections. In particular, there was interest in examining the impact of cholesterol on PLY binding and the ability of the system to protect against the toxicity of *S. pneumoniae* infection. It was found that a BBD was suitable to optimize microfluidic parameters for the formulation of cholesterol-rich liposomes within desirable limits of EE, LC, PS, and PDI. These parameters corresponded to a FRR, nisin concentration, and EPG molar content of 3.01:1, 61.06 μM, and 3.85 mol% respectively, with a total composite desirability of 0.991.

A variety of assays were then conducted on liposomes at varying molar compositions of cholesterol to elucidate the impact of membrane saturation on PLY binding kinetics, through both application of purified toxin and cultured *S. pneumoniae*. Liposomes incorporating 60 mol% cholesterol demonstrated acceptable short-term stability and complete neutralization of toxin in hemolytic assays at a concentration of 10 μM. Furthermore, these vesicles exhibited specific and rapid bactericidal activity against *S. pneumoniae* culture with an MIC of 2 μg/mL. Finally, they elicited over a 30% improvement in absolute cell viability compared to free nisin within IMR-90 cells challenged by pneumococcus infection. Beyond this, it was identified in all conducted studies that cholesterol levels above 45 mol% were required to facilitate significant interactions with PLY toxin, which is postulated to arise through membrane saturation and subsequent formation of surface-exposed cholesterol domains within the liposome.

To the author's knowledge, this is the first study examining direct therapeutic release induced by PLY for treatment of *S. pneumoniae* infection. Given further development, this cholesterol-rich liposomal platform presents itself as a potential specified treatment strategy for IPD to address the ongoing concern of bacterial resistance. These applications could also be extended to diagnostic use through the encapsulation of fluorescent dyes, as an adjunct therapy with antibiotics, or for potential packaging applications via film coatings.

4.2 Limitations and Future Directions

While the results obtained in this study were promising for development of a PLY-responsive liposomal platform utilizing microfluidic synthesis, several key limitations should be addressed, as well as proposed alternative strategies and future directions. To begin, modification of the materials chosen for both liposomal synthesis and therapeutic effect may have proven beneficial. Natural lipids often suffer from stability issues due to their polyunsaturated fatty acids increasing membrane fluidity, as identified in short-term stability studies for liposomes containing 30 mol% cholesterol. PEGylation is one option to improve stability, although it is unknown how surface modifications would impact PLY binding ability to exposed cholesterol domains [175]. Extending stability studies to more closely examine structural changes after several months of storage would be beneficial, as well as examining for potential nisin leakage at different pH and in relevant buffers utilized in the study, including PBS, BHI, TSB, and EMEM. However, due to time limitations these studies could not be conducted. Natural lipids are typically not recommended for *in vivo* use regardless due to the possibility of viral contamination, making synthetic lipids a better choice for expanding studies [81].

Two synthetic lipids with a T_m above 37°C that still maintain solubility in ethanol at relevant concentrations for microfluidic synthesis includes 1,2-dipalmitoyl-sn-glycero-3-phosphocholine and 1,2-dipalmitoyl-sn-glycero-3-phospho-(1'-rac-glycerol) (sodium salt), often referred to as DPPC and DPPG respectively. It should be noted, however, that it may prove more difficult to incorporate greater than 50% molar compositions of cholesterol in a highly saturated bilayer as there is less room for packing, warranting further study. In addition to this, it may be of interest to examine the potential for nisin degradation through a combination of liquid chromatography and nuclear magnetic resonance techniques, as the peptide has displayed solubility issues in saline environments [126]. Should stability issues be observed, various alternative antimicrobial peptides have been summarized elsewhere [176].

Beyond this, there were various changes and improvements to the microfluidic system that would have benefited the study. One limitation of the current system is void volume left in the tubing between each run, leading to loss of therapeutic and lipid. To improve scalability, the design could be altered such that the syringes are affixed directly to the Leur adapters on the microfluidic chip through a vertical geometry and a modified pumping system, thereby eliminating the need for tubing. Another improvement is complete automation of the system based on the user's desired input of FRR, TFR, and formulation volume. Such a system could improve throughput and avoid collection of the very start and

end of the mixing cycle, as these are the most likely sections to have inconsistent particle properties as a result of incomplete mixing. In-house design of the micromixer may also be of interest, as different geometries highlighted elsewhere can lower synthesis time through higher TFRs, improve particle properties, and reduce potential for clogging [177]. Beyond just the microfluidic system, the BBD model displayed limitations in system optimization, as initial screening led to fitted parameters at the extremes of the design space, thereby limiting model accuracy. As such, CCD may have proven more effective at modeling the system, or alternatively, machine learning techniques like artificial neural networks have been gaining popularity for NP optimization [178].

One major limitation of the conducted studies was in the choice of *S. epidermidis* as a control to examine specificity of the developed system. Firstly, nisin acted in a bacteriostatic fashion on this culture, thereby limiting MBC comparisons because liposomes could not be dosed at a sufficient concentration to elicit bactericidal effect. Beyond this, *S. epidermidis* was unable to eradicate IMR-90 upon challenge, hence making subsequent protective assays impossible. It would be helpful to test additional bacterial strains that do demonstrate pathogenic behaviour, thereby allowing for cellular clearance without the production of CDC toxins, such that specificity of the liposomes may be examined more thoroughly. Ideally, this bacterium would also be susceptible to nisin at similar concentrations to *S. pneumoniae* so more relevant comparisons could be drawn. One such candidate could be *Staphylococcus aureus*, as it displays potent pathogenic activity through various virulence factors, excluding CDCs, and has shown nisin susceptibility [179, 180]. Beyond this, comparison of cellular viability through alternative methods would be useful to validate MTS measurements, as potential interactions between residual cholesterol and formazan may have had implications in absorbance readings. These assays could include direct trypan blue cell counting, flow cytometry methods, or real-time techniques utilizing luciferase.

Some limitations in therapeutic release and detection also arose during this study. Firstly, centrifugal filtration may not have been optimal to study nisin release, as the separation process relied on the application of centrifugal force that does not naturally mimic *in vivo* environments. However, alternative release methodologies, such as dialysis, were unsuitable as the CBQCA detection limit for nisin was 0.5 μg/mL and thereby not sensitive enough for high-volume dilution. As such, it may be of interest to examine the use of ultra-performance liquid chromatography for nisin detection, as these techniques can provide high specificity and sensitivity for protein analysis [130]. It may also be possible

to tag the nisin peptide with a fluorescent molecule, as performed elsewhere, such that real-time release could be examined in a plate-reader [181].

Morphological analysis would have benefited from utilization of different preparation techniques. Due to availability, negative-staining was carried out, involving room temperature affixation of the liposomes to sample grids prior to TEM analysis. One key drawback of this method is that, due to liposomal structure largely arising from the inner aqueous core, dehydration of the samples can lead to morphological changes [152]. Further, washing steps were required to remove residual uranyl acetate stain, which served to dilute the sample such that only individual particles could be imaged within a single micrograph. As such, it would be beneficial to conduct future morphological analysis via freeze-fracture cryo-TEM to preserve structure and gain better resolution of internal structures within the vesicle. It may also be of interest to oversaturate the liposomes with PLY and examine how toxin concentration directly impacts surface structure.

There are various future directions to investigate in regards to the developed liposomal system. Beyond addressing the above-mentioned limitations, it would be pertinent to examine potential pulmonary delivery platforms for liposomes should *in vivo* studies be planned. These can include dry powder, soft mist, and pressurized inhalers, as well as medical nebulizers [182]. The chosen inhalation device has direct consequences on the storage form of liposomes, as any requiring a powder would likely require lyophilization of the particles. This process can have a significant impact on vesicle properties, stability, and therapeutic efficacy, thereby necessitating the use of some form of lyoprotectant [183]. To further examine potential cytotoxicity of the system, testing of additional cell lines encountered during pulmonary delivery would be warranted. Finally, expansion of the system to other CDC-producing bacteria would indicate if the developed cholesterol-rich liposomal formulations can elicit broad-spectrum targeted release against a variety of pathogenic strains.

References

[1] Geno KA, Gilbert GL, Song JY, et al. Pneumococcal capsules and their types: past, present, and future. *Clin Microbiol Rev* 2015; 28: 871–899.

[2] Brooks LRK, Mias GI. Streptococcus pneumoniae's virulence and host immunity: aging, diagnostics, and prevention. *Front Immunol* 2018; 9: 1366.

[3] Loughran AJ, Orihuela CJ, Tuomanen EI. Streptococcus pneumoniae: invasion and inflammation. *Microbiol Spectr* 2019; 7: 1128.

[4] Mehr S, Wood N. Streptococcus pneumoniae – a review of carriage, infection, serotype replacement and vaccination. *Paediatr Respir Rev* 2012; 13: 258–264.

[5] Roth A, Reichmann P, Hakenbeck R. The capsule of Streptococcus pneumoniae contributes to virulence in the insect model Manduca sexta. *J Mol Microbiol Biotechnol* 2012; 22: 326–334.

[6] Sura T, Gering V, Cammann C, et al. Streptococcus pneumoniae and influenza A virus co-infection induces altered polyubiquitination in A549 cells. *Front Cell Infect Microbiol* 2022; 12: 817532.

[7] Bartlett JG, Dowell SF, Mandell LA, et al. Practice guidelines for the management of community-acquired pneumonia in adults. *Clin Infect Dis* 2000; 31: 347–382.

[8] Troeger C, Forouzanfar M, Rao PC, et al. Estimates of the global, regional, and national morbidity, mortality, and aetiologies of lower respiratory tract infections in 195 countries: a systematic analysis for the Global Burden of Disease Study 2015. *Lancet Infect Dis* 2017; 17: 1133–1161.

[9] Wunderink RG, Waterer GW. Community-acquired pneumonia. *N Engl J Med* 2014; 370: 543–551.

[10] Weiser JN, Ferreira DM, Paton JC. Streptococcus pneumoniae: transmission, colonization and invasion. *Nat Rev Microbiol* 2018; 16: 355–367.

[11] Frost I, Sati H, Garcia-Vello P, et al. The role of bacterial vaccines in the fight against antimicrobial resistance: an analysis of the preclinical and clinical development pipeline. *The Lancet Microbe* 2023; 4: e113–e125.

[12] Heras B, Scanlon MJ, Martin JL. Targeting virulence not viability in the search for future antibacterials. *Br J Clin Pharmacol* 2015; 79: 208–215.

[13] Vögele M, Bhaskara RM, Mulvihill E, et al. Membrane perforation by the pore-forming toxin

pneumolysin. *Proc Natl Acad Sci* 2019; 116: 13352–13357.

[14] Nishimoto AT, Rosch JW, Tuomanen EI. Pneumolysin: pathogenesis and therapeutic target. *Front Microbiol* 2020; 11: 1543.

[15] Frias MJ, Melo-Cristino J, Ramirez M. The autolysin LytA contributes to efficient bacteriophage progeny release in Streptococcus pneumoniae. *J Bacteriol* 2009; 191: 5428–5440.

[16] Kadioglu A, Weiser JN, Paton JC, et al. The role of Streptococcus pneumoniae virulence factors in host respiratory colonization and disease. *Nat Rev Microbiol* 2008; 6: 288–301.

[17] Domenech M, García E, Moscoso M. Biofilm formation in Streptococcus pneumoniae. *Microb Biotechnol* 2012; 5: 455–465.

[18] Barocchi MA, Ries J, Zogaj X, et al. A pneumococcal pilus influences virulence and host inflammatory responses. *PNAS* 2006; 103: 2857–2862.

[19] Gosink KK, Mann ER, Guglielmo C, et al. Role of novel choline binding proteins in virulence of Streptococcus pneumoniae. *Infect Immun* 2000; 68: 5690–5695.

[20] Li N, Yang XY, Guo Z, et al. Varied metal-binding properties of lipoprotein PsaA in Streptococcus pneumoniae. *J Biol Inorg Chem* 2014; 19: 829–838.

[21] Manco S, Hernon F, Yesilkaya H, et al. Pneumococcal neuraminidases A and B both have essential roles during infection of the respiratory tract and sepsis. *Infect Immun* 2006; 74: 4014–4020.

[22] Wholey WY, Abu-Khdeir M, Yu EA, et al. Characterization of the competitive pneumocin peptides of Streptococcus pneumoniae. *Front Cell Infect Microbiol* 2019; 9: 55.

[23] Di Guilmi AM, Dessen A. New approaches towards the identification of antibiotic and vaccine targets in Streptococcus pneumoniae. *EMBO Rep* 2002; 3: 728–734.

[24] Alouf JE, Billington SJ, Jost BH. Repertoire and general features of the family of cholesterol-dependent cytolysins. In: Alouf JE, Popoff MR (eds) *The Comprehensive Sourcebook of Bacterial Protein Toxins*. Oxford: Elsevier, pp. 643–658.

[25] Shewell LK, Day CJ, Jen FEC, et al. All major cholesterol-dependent cytolysins use glycans as cellular receptors. *Sci Adv* 2020; 6: eaaz4926.

[26] Chang B, Kinjo Y, Morita M, et al. Distribution and variation of serotypes and pneumococcal surface protein A clades of Streptococcus pneumoniae strains isolated from adult patients with invasive pneumococcal disease in Japan. *Front Cell Infect Microbiol* 2021; 11: 617573.

[27] Ricketson LJ, Bettinger JA, Sadarangani M, et al. Vaccine effectiveness of the 7-valent and 13-valent pneumococcal conjugate vaccines in Canada: An IMPACT study. *Vaccine* 2022; 40: 2733–2740.

[28] Shimbashi R, Suzuki M, Chang B, et al. Effectiveness of 23-valent pneumococcal polysaccharide vaccine against invasive pneumococcal disease in adults, Japan, 2013–2017. *Emerg Infect Dis* 2020; 26: 2378–2386.

[29] Ono T, Watanabe M, Hashimoto K, et al. Serotypes and antibiotic resistance of Streptococcus pneumoniae before and after the introduction of the 13-valent pneumococcal conjugate vaccine for adults and children in a rural area in Japan. *Pathogens* 2023; 12: 493.

[30] Nasreen S, Wang J, Kwong JC, et al. Population-based incidence of invasive pneumococcal disease in children and adults in Ontario and British Columbia, 2002–2018: A Canadian Immunization Research Network (CIRN) study. *Vaccine* 2021; 39: 7545–7553.

[31] Blaschke AJ. Interpreting assays for the detection of Streptococcus pneumoniae. *Clin Infect Dis* 2011; 52: 331–337.

[32] Leonard A, Möhlis K, Schlüter R, et al. Exploring metabolic adaptation of Streptococcus pneumoniae to antibiotics. *J Antibiot* 2020; 73: 441–454.

[33] Tang J, Ouyang Q, Li Y, et al. Nanomaterials for delivering antibiotics in the therapy of pneumonia. *Int J Mol Sci* 2022; 23: 15738.

[34] Kumar M, Sarma DK, Shubham S, et al. Futuristic non-antibiotic therapies to combat antibiotic resistance: a review. *Front Microbiol* 2021; 12: 609459.

[35] Ji S, An F, Zhang T, et al. Antimicrobial peptides: an alternative to traditional antibiotics. *Eur J Med Chem* 2024; 265: 116072.

[36] Shin JM, Gwak JW, Kamarajan P, et al. Biomedical applications of nisin. *J Appl Microbiol* 2016; 120: 1449–1465.

[37] Majchrzykiewicz JA, Kuipers OP, Bijlsma JJE. Generic and specific adaptive responses of Streptococcus pneumoniae to challenge with three distinct antimicrobial peptides, bacitracin, LL-37, and nisin. *Antimicrob Agents Chemother* 2010; 54: 440–451.

[38] Makabenta JM V, Nabawy A, Li CH, et al. Nanomaterial-based therapeutics for antibiotic-resistant bacterial infections. *Nat Rev Microbiol* 2022; 19: 23–36.

[39] Azarmi S, Roa WH, Löbenberg R. Targeted delivery of nanoparticles for the treatment of lung diseases. *Adv Drug Deliv Rev* 2008; 60: 863–875.

[40] Chen D, Liu J, Wu J, et al. Enhancing nanoparticle penetration through airway mucus to improve drug delivery efficacy in the lung. *Expert Opin Drug Deliv* 2021; 18: 595–606.

[41] Ferreira M, Ogren M, Dias JNR, et al. Liposomes as antibiotic delivery systems: a promising nanotechnological strategy against antimicrobial resistance. *Molecules* 2021; 26: 2047.

[42] Wang X, Shan M, Zhang S, et al. Stimuli-responsive antibacterial materials: molecular structures, design principles, and biomedical applications. *Adv Sci* 2022; 9: 2104843.

[43] Shah NR, Voisin TB, Parsons ES, et al. Structural basis for tuning activity and membrane specificity of bacterial cytolysins. *Nat Commun* 2020; 11: 5818.

[44] Tilley SJ, Orlova EV, Gilbert RJC, et al. Structural basis of pore formation by the bacterial toxin pneumolysin. *Cell* 2005; 121: 247–256.

[45] Aziz UBA, Saoud A, Bermudez M, et al. Targeted small molecule inhibitors blocking the cytolytic effects of pneumolysin and homologous toxins. *Nat Commun* 2024; 15: 3537.

[46] Anchisi L, Dessì S, Pani A, et al. Cholesterol homeostasis: a key to prevent or slow down neurodegeneration. *Front Physiol* 2013; 3: 486.

[47] Anderson R, Feldman C. Pneumolysin as a potential therapeutic target in severe pneumococcal disease. *J Infect* 2017; 74: 527–544.

[48] Thapa R, Ray S, Keyel PA. Interaction of macrophages and cholesterol-dependent cytolysins: the impact on immune response and cellular survival. *Toxins* 2020; 12: 531.

[49] Chao Y, Marks LR, Pettigrew MM, et al. Streptococcus pneumoniae biofilm formation and dispersion during colonization and disease. *Front Cell Infect Microbiol* 2015; 4: 194.

[50] Gilley RP, Orihuela CJ. Pneumococci in biofilms are non-invasive: implications on nasopharyngeal colonization. *Front Cell Infect Microbiol* 2014; 4: 163.

[51] Jacques LC, Panagiotou S, Baltazar M, et al. Increased pathogenicity of pneumococcal serotype 1 is driven by rapid autolysis and release of pneumolysin. *Nat Commun* 2020; 11: 1892.

[52] Anderson R, Nel JG, Feldman C. Multifaceted role of pneumolysin in the pathogenesis of myocardial injury in community-acquired pneumonia. *Int J Mol Sci* 2018; 19: 1147.

[53] Surve MV, Bhutda S, Datey A, et al. Heterogeneity in pneumolysin expression governs the fate of Streptococcus pneumoniae during blood-brain barrier trafficking. *PLoS Pathog* 2018; 14: e1007168.

[54] Hirst RA, Kadioglu A, O'Callaghan C, et al. The role of pneumolysin in pneumococcal pneumonia and meningitis. *Clin Exp Immunol* 2004; 138: 195–201.

[55] Zysk G, Schneider-Wald BK, Hwang JH, et al. Pneumolysin is the main inducer of cytotoxicity to brain microvascular endothelial cells caused by Streptococcus pneumoniae. *Infect Immun* 2001; 69: 845–852.

[56] Keller LE, Bradshaw JL, Pipkins H, et al. Surface proteins and pneumolysin of encapsulated and nonencapsulated Streptococcus pneumoniae mediate virulence in a chinchilla model of otitis media. *Front Cell Infect Microbiol* 2016; 6: 55.

[57] Wade KR, Hotze EM, Briles DE, et al. Mouse, but not human, ApoB-100 lipoprotein cholesterol is a potent innate inhibitor of Streptococcus pneumoniae pneumolysin. *PLoS Pathog* 2014; 10: e1004353.

[58] Han C, Zhang M. Genetic diversity and antigenicity analysis of Streptococcus pneumoniae pneumolysin isolated from children with pneumococcal infection. *Int J Infect Dis* 2019; 86: 57–64.

[59] Scott NR, Mann B, Tuomanen EI, et al. Multi-valent protein hybrid pneumococcal vaccines: a strategy for the next generation of vaccines. *Vaccines* 2021; 9: 209.

[60] Aceil J, Avci FY. Pneumococcal surface proteins as virulence factors, immunogens, and conserved vaccine targets. *Front Cell Infect Microbiol* 2022; 12: 832254.

[61] Lu J, Jiao Y, Cao G, et al. Multimode CaCO3/pneumolysin antigen delivery systems for inducing efficient cellular immunity for anti-tumor immunotherapy. *Chem Eng J* 2021; 420: 129746.

[62] Shen Q, Xiong Q, Zhou K, et al. Functionalized DNA-origami-protein nanopores generate large transmembrane channels with programmable size-selectivity. *J Am Chem Soc* 2023; 145: 1292–1300.

[63] Blanco-Covián L, Montes-García V, Girard A, et al. Au@Ag SERRS tags coupled to a lateral flow immunoassay for the sensitive detection of pneumolysin. *Nanoscale* 2017; 9: 2051–2058.

[64] Salvador M, Marqués-Fernández JL, Bunge A, et al. Magnetic nanoclusters increase the sensitivity of lateral flow immunoassays for protein detection: application to pneumolysin as a biomarker for Streptococcus pneumoniae. *Nanomaterials* 2022; 12: 2044.

[65] Sabirovas T, Valiuniene A, Gabriunaite I, et al. Mixed hybrid bilayer lipid membranes on mechanically polished titanium surface. *BBA - Biomembr* 2020; 1862: 183232.

[66] Henry BD, Neill DR, Becker KA, et al. Engineered liposomes sequester bacterial exotoxins and protect from severe invasive infections in mice. *Nat Biotechnol* 2015; 33: 81–88.

[67] Baumgartner D, Aebi S, Grandgirard D, et al. Clinical Streptococcus pneumoniae isolates induce differing CXCL8 responses from human nasopharyngeal epithelial cells which are reduced by liposomes. *BMC Microbiol* 2016; 16: 154–161.

[68] Koffel R, Wolfmeier H, Larpin Y, et al. Host-derived microvesicles carrying bacterial pore-forming toxins deliver signals to macrophages: a novel mechanism of shaping immune responses. *Front Immunol* 2018; 9: 1688.

[69] Besançon H, Babiychuk V, Larpin Y, et al. Tailored liposomal nanotraps for the treatment of Streptococcal infections. *J Nanobiotechnology* 2021; 19: 46.

[70] Müller A, Lekhuleni C, Hupp S, et al. Meningitis-associated pneumococcal serotype 8, ST 53, strain is hypervirulent in a rat model and has non-haemolytic pneumolysin which can be attenuated by liposomes. *Front Cell Infect Microbiol* 2023; 12: 1106063.

[71] Laterre PF, Colin G, Dequin PF, et al. CAL02, a novel antitoxin liposomal agent, in severe pneumococcal pneumonia: a first-in-human, double-blind, placebo-controlled, randomised trial. *Lancet Infect Dis* 2019; 19: 620–630.

[72] Coburn PS, Miller FC, LaGrow AL, et al. Disarming pore-forming toxins with biomimetic nanosponges in intraocular infections. *mSphere* 2019; 4: e00262-19.

[73] Kwon K, Lee J, Lee S, et al. Pneumolysin/plasma protein adsorption, bacterial adherence, and cell adhesion characteristics of a cell-membrane-mimicking polymer system. *ACS Appl Bio Mater* 2022; 5: 2240–2252.

[74] Provoda CJ, Stier EM, Lee KD. Tumor cell killing enabled by listeriolysin O-liposome-mediated delivery of the protein toxin gelonin. *J Biol Chem* 2003; 278: 35102–35108.

[75] Sun R, Liu Y. Listeriolysin O as a strong immunogenic molecule for the development of new anti-tumor vaccines. *Hum Vaccines Immunother* 2013; 9: 1058–1068.

[76] Lin L, Zhang X, Zhao C, et al. Liposome containing nutmeg oil as the targeted preservative against Listeria monocytogenes in dumplings. *RSC Adv* 2016; 6: 978–986.

[77] Cui HY, Wu J, Lin L. Inhibitory effect of liposome-entrapped lemongrass oil on the growth of Listeria monocytogenes in cheese. *J Dairy Sci* 2016; 99: 6097–6104.

[78] Subramanian K, Iovino F, Tsikourkitoudi V, et al. Mannose receptor-derived peptides neutralize pore-forming toxins and reduce inflammation and development of pneumococcal disease. *EMBO Mol Med* 2020; 12: e12695.

[79] Kammann T, Hoff J, Yildirim I, et al. Intracellularly released cholesterol from polymer-based

delivery systems alters cellular responses to pneumolysin and promotes cell survival. *Metabolites* 2021; 11: 821.

[80] Tewabe A, Abate A, Tamrie M, et al. Targeted drug delivery - from magic bullet to nanomedicine: principles, challenges, and future perspectives. *J Multidiscip Healthc* 2021; 14: 1711–1724.

[81] Nsairat H, Khater D, Sayed U, et al. Liposomes: structure, composition, types, and clinical applications. *Heliyon* 2022; 8: e09394.

[82] Leitgeb M, Knez Ž, Primožič M. Sustainable technologies for liposome preparation. *J Supercrit Fluids* 2020; 165: 104984.

[83] Andra VVSNL, Pammi SVN, Bhatraju LVKP, et al. A comprehensive review on novel liposomal methodologies, commercial formulations, clinical trials and patents. *Bionanoscience* 2022; 12: 274–291.

[84] Lombardo D, Kiselev MA. Methods of liposomes preparation: formation and control factors of versatile nanocarriers for biomedical and nanomedicine application. *Pharmaceutics* 2022; 14: 543.

[85] Yu B, Lee RJ, Lee LJ. Microfluidic methods for production of liposomes. *Methods Enzymol* 2009; 465: 129–141.

[86] Has C, Sunthar P. A comprehensive review on recent preparation techniques of liposomes. *J Liposome Res* 2020; 30: 336–365.

[87] Zhang G, Sun J. Lipid in chips: a brief review of liposomes formation by microfluidics. *Int J Nanomedicine* 2021; 16: 7391–7416.

[88] Carugo D, Bottaro E, Owen J, et al. Liposome production by microfluidics: potential and limiting factors. *Sci Rep* 2016; 6: 25876.

[89] Osouli-Bostanabad K, Puliga S, Serrano DR, et al. Microfluidic manufacture of lipid-based nanomedicines. *Pharmaceutics* 2022; 14: 1940.

[90] Williams MS, Longmuir KJ, Yager P. A practical guide to the staggered herringbone mixer. *Lab Chip* 2008; 8: 1121–1129.

[91] Tóth EL, Holczer EG, Iván K, et al. Optimized simulation and validation of particle advection in asymmetric staggered herringbone type micromixers. *Micromachines* 2015; 6: 136–150.

[92] Iakovlev AP, Erofeev AS, Gorelkin PV. Novel pumping methods for microfluidic devices: a comprehensive review. *Biosensors* 2022; 12: 956.

[93] Wallace SJ, Li J, Nation RL, et al. Drug release from nanomedicines: selection of appropriate encapsulation and release methodology. *Drug Deliv Transl Res* 2012; 2: 284–292.

[94] Nele V, Holme MN, Kauscher U, et al. Effect of formulation method, lipid composition, and PEGylation on vesicle lamellarity: a small-angle neutron scattering study. *Langmuir* 2019; 35: 6064–6074.

[95] Nasab NA, Kumleh HH, Beygzadeh M, et al. Delivery of curcumin by a pH-responsive chitosan mesoporous silica nanoparticles for cancer treatment. *Artif Cells, Nanomedicine, Biotechnol* 2018; 46: 75–81.

[96] Choi S, Kang B, Yang E, et al. Precise control of liposome size using characteristic time depends on solvent type and membrane properties. *Sci Rep* 2023; 13: 4728.

[97] Joguparthi V, Feng S, Anderson BD. Determination of intraliposomal pH and its effect on membrane partitioning and passive loading of a hydrophobic camptothecin, DB-67. *Int J Pharm* 2008; 352: 17–28.

[98] Toh MR, Chiu GNC. Liposomes as sterile preparations and limitations of sterilisation techniques in liposomal manufacturing. *Asian J Pharm Sci* 2013; 8: 88–95.

[99] Boafo GF, Magar KT, Ekpo MD, et al. The role of cryoprotective agents in liposome stabilization and preservation. *Int J Mol Sci* 2022; 23: 12487.

[100] Jaradat E, Weaver E, Meziane A, et al. Synthesis and characterization of paclitaxel-loaded PEGylated liposomes by the microfluidics method. *Mol Pharm* 2023; 20: 6184–6196.

[101] Rane S, Prabhakar B. Optimization of paclitaxel containing pH-sensitive liposomes by 3 factor, 3 level Box-Behnken design. *Indian J Pharm Sci* 2013; 75: 420–426.

[102] Kazemian ME, Nassab SAG, Javaran EJ. Comparative study of Box–Behnken and central composite designs to investigate the effective parameters of ammonia–water absorption refrigerant system. *Proc Inst Mech Eng Part C J Mech Eng Sci* 2021; 235: 3095–3108.

[103] Ranade SS, Thiagarajan P. Selection of a design for response surface. *IOP Conf Ser Mater Sci Eng* 2017; 263: 022043.

[104] Breig SJM, Luti KJK. Response surface methodology: a review on its applications and challenges in microbial cultures. *Mater Today Proc* 2021; 42: 2277–2284.

[105] Huang S, Xu D, Zhang L, et al. Therapeutic effects of curcumin liposomes and nanocrystals on inflammatory osteolysis: in vitro and in vivo comparative study. *Pharmacol Res* 2023; 192: 106778.

[106] Ikuta KS, Swetschinski LR, Aguilar GR, et al. Global mortality associated with 33 bacterial pathogens in 2019: a systematic analysis for the Global Burden of Disease Study 2019. *Lancet* 2022; 400: 2221–2248.

[107] Kim GL, Seon SH, Rhee DK. Pneumonia and Streptococcus pneumoniae vaccine. *Arch Pharm Res* 2017; 40: 885–893.

[108] Khoshmanesh K, Almansouri A, Albloushi H, et al. A multi-functional bubble-based microfluidic system. *Sci Rep* 2015; 5: 9942.

[109] Sant'Anna V, Malheiros PS, Brandelli A. Liposome encapsulation protects bacteriocin-like substance P34 against inhibition by Maillard reaction products. *Food Res Int* 2011; 44: 326–330.

[110] Johnson TF, Jones K, Iacoviello F, et al. Liposome sterile filtration characterization via X-ray computed tomography and confocal microscopy. *Membranes* 2021; 11: 905.

[111] Restrepo AV, Salazar BE, Agudelo M, et al. Optimization of culture conditions to obtain maximal growth of penicillin-resistant Streptococcus pneumoniae. *BMC Microbiol* 2005; 5: 34.

[112] Kohda K, Li X, Soga N, et al. An in vitro mixed infection model with commensal and pathogenic staphylococci for the exploration of interspecific interactions and their impacts on skin physiology. *Front Cell Infect Microbiol* 2021; 11: 712360.

[113] Leber AL. Preparation of routine media and reagents used in antimicrobial susceptibility testing. In: Leber AL (ed) *Clinical Microbiology Procedures Handbook*. Washington DC: ASM Press, 2016, pp. 5.20.1.1-5.20.3.10.

[114] O'Toole GA. Classic spotlight: plate counting you can count on. *J Bacteriol* 2016; 198: 3127–3127.

[115] Billington S. Thiol-activated cytolysins: structure, function and role in pathogenesis. *FEMS Microbiol Lett* 2000; 182: 197–205.

[116] Baxa U. Imaging of liposomes by transmission electron microscopy. In: McNeil S (ed) *Characterization of Nanoparticles Intended for Drug Delivery*. New York: Humana Press, 2018, pp. 73–88.

[117] Mitsuwan W, Olaya-Abril A, Calderón-Santiago M, et al. Integrated proteomic and metabolomic analysis reveals that rhodomyrtone reduces the capsule in Streptococcus pneumoniae. *Sci Rep* 2017; 7: 2715.

[118] Lister PD, Sanders CC. Pharmacodynamics of levofloxacin and ciprofloxacin against

Streptococcus pneumoniae. *J Antimicrob Chemother* 1999; 43: 79–86.

[119] Jang TH, Park SC, Yang JH, et al. Cryopreservation and its clinical applications. *Integr Med Res* 2017; 6: 12–18.

[120] Yu SH, Kumar M, Kim IW, et al. A comparative analysis of in vitro toxicity of synthetic zeolites on IMR-90 human lung fibroblast cells. *Molecules* 2021; 26: 3194.

[121] Schönfeldová T, Piller P, Kovacik F, et al. Lipid melting transitions involve structural redistribution of interfacial water. *J Phys Chem B* 2021; 125: 12457–12465.

[122] Liang X, Mao G, Ng KYS. Mechanical properties and stability measurement of cholesterol-containing liposome on mica by atomic force microscopy. *J Colloid Interface Sci* 2004; 278: 53–62.

[123] Jash A, Ubeyitogullari A, Rizvi SSH. Synthesis of multivitamin-loaded heat stable liposomes from milk fat globule membrane phospholipids by using a supercritical-CO_2 based system. *Green Chem* 2020; 22: 5345–5356.

[124] Subczynski WK, Pasenkiewicz-Gierula M, Widomska J, et al. High cholesterol/low cholesterol: effects in biological membranes review. *Cell Biochem Biophys* 2017; 75: 369–385.

[125] Tseu GYW, Kamaruzaman KA. A review of different types of liposomes and their advancements as a form of gene therapy treatment for breast cancer. *Molecules* 2023; 28: 1498.

[126] Rollema HS, Kuipers OP, Both P, et al. Improvement of solubility and stability of the antimicrobial peptide nisin by protein engineering. *Appl Environ Microbiol* 1995; 61: 2873–2878.

[127] Maeki M, Kimura N, Okada Y, et al. Understanding the effects of ethanol on the liposome bilayer structure using microfluidic-based time-resolved small-angle X-ray scattering and molecular dynamics simulations. *Nanoscale Adv* 2024; 6: 2166–2176.

[128] Gomez AG, Syed S, Marshall K, et al. Liposomal nanovesicles for efficient encapsulation of staphylococcal antibiotics. *ACS Omega* 2019; 4: 10866–10876.

[129] Muso-Cachumba JJ, Ruiz-Lara G, Monteiro G, et al. Challenges in estimating the encapsulation efficiency of proteins in polymersomes – which is the best method? *Brazilian J Pharm Sci* 2023; 59: e23365.

[130] Song JG, Baral KC, Kim GL, et al. Quantitative analysis of therapeutic proteins in biological fluids: recent advancement in analytical techniques. *Drug Deliv* 2023; 30: 2183816.

[131] Were LM, Bruce BD, Davidson PM, et al. Size, stability, and entrapment efficiency of

phospholipid nanocapsules containing polypeptide antimicrobials. *J Agric Food Chem* 2003; 51: 8073–8079.

[132] Németh Z, Csóka I, Jazani RS, et al. Quality by design-driven zeta potential optimisation study of liposomes with charge imparting membrane additives. *Pharmaceutics* 2022; 14: 1798.

[133] Castañeda-Reyes ED, Perea-Flores MJ, Davila-Ortiz G, et al. Development, characterization and use of liposomes as amphipathic transporters of bioactive compounds for melanoma treatment and reduction of skin inflammation: a review. *Int J Nanomedicine* 2020; 15: 7627–7650.

[134] Kaddah S, Khreich N, Kaddah F, et al. Cholesterol modulates the liposome membrane fluidity and permeability for a hydrophilic molecule. *Food Chem Toxicol* 2018; 113: 40–48.

[135] Abucayon EG, Sweeney S, Matyas GR. A reliable quantification of cholesterol and 25-hydroxycholesterol in liposomal adjuvant formulation by liquid chromatography high-resolution tandem mass spectrometry. *ACS Omega* 2024; 9: 19637–19644.

[136] Sanchez-Rosario Y, Johnson MDL. Media matters, examining historical and modern Streptococcus pneumoniae growth media and the experiments they affect. *Front Cell Infect Microbiol* 2021; 11: 613623.

[137] Vuong C, Otto M. Staphylococcus epidermidis infections. *Microbes Infect* 2002; 4: 481–489.

[138] Ughy B, Nagyapati S, Lajko DB, et al. Reconsidering dogmas about the growth of bacterial populations. *Cells* 2023; 12: 1430.

[139] Beal J, Farny NG, Haddock-Angelli T, et al. Robust estimation of bacterial cell count from optical density. *Commun Biol* 2020; 3: 512.

[140] Tóthpál A, Desobry K, Joshi SS, et al. Variation of growth characteristics of pneumococcus with environmental conditions. *BMC Microbiol* 2019; 19: 304.

[141] Flanagan JJ, Tweten RK, Johnson AE, et al. Cholesterol exposure at the membrane surface is necessary and sufficient to trigger perfringolysin O binding. *Biochemistry* 2009; 48: 3977–3987.

[142] Guimarães D, Noro J, Silva C, et al. Protective effect of saccharides on freeze-dried liposomes encapsulating drugs. *Front Bioeng Biotechnol* 2019; 7: 424.

[143] Leung C, Dudkina NV, Lukoyanova N, et al. Stepwise visualization of membrane pore formation by suilysin, a bacterial cholesterol-dependent cytolysin. *eLife* 2014; 3: e04247.

[144] Heuck AP, Tweten RK, Johnson AE. Assembly and topography of the prepore complex in cholesterol-dependent cytolysins. *J Biol Chem* 2003; 278: 31218–31225.

[145] Evans JC, Johnstone BA, Lawrence SL, et al. A key motif in the cholesterol-dependent cytolysins reveals a large family of related proteins. *mBio* 2020; 11: e02351-20.

[146] Faraj BHA, Collard L, Cliffe R, et al. Formation of pre-pore complexes of pneumolysin is accompanied by a decrease in short-range order of lipid molecules throughout vesicle bilayers. *Sci Rep* 2020; 10: 4585.

[147] Jose J, Kanniyappan H, Muthuvijayan V. A novel, rapid and cost-effective method for separating drug-loaded liposomes prepared from egg yolk phospholipids. *Process Biochem* 2022; 115: 80–91.

[148] van Pee K, Mulvihill E, Müller DJ, et al. Unraveling the pore-forming steps of pneumolysin from Streptococcus pneumoniae. *Nano Lett* 2016; 16: 7915–7924.

[149] Bonev BB, Gilbert RC, Andrew PW, et al. Structural analysis of the protein/lipid complexes associated with pore formation by the bacterial toxin pneumolysin. *J Biol Chem* 2001; 276: 5714–5719.

[150] Drücker P, Iacovache I, Bachler S, et al. Membrane deformation and layer-by-layer peeling of giant vesicles induced by the pore-forming toxin pneumolysin. *Biomater Sci* 2019; 7: 3693–3705.

[151] van Pee K, Neuhaus A, D'Imprima E, et al. CryoEM structures of membrane pore and prepore complex reveal cytolytic mechanism of pneumolysin. *eLife* 2017; 6: e23644.

[152] Robson AL, Dastoor PC, Flynn J, et al. Advantages and limitations of current imaging techniques for characterizing liposome morphology. *Front Pharmacol* 2018; 9: 80.

[153] Pankey GA, Sabath LD. Clinical relevance of bacteriostatic versus bactericidal mechanisms of action in the treatment of gram-positive bacterial infections. *Clin Infect Dis* 2004; 38: 864–870.

[154] Scherer KM, Spille JH, Sahl HG, et al. The lantibiotic nisin induces lipid II aggregation, causing membrane instability and vesicle budding. *Biophys J* 2015; 108: 1114–1124.

[155] Ghosh R, De M. Liposome-based antibacterial delivery: an emergent approach to combat bacterial infections. *ACS Omega* 2023; 8: 35442–35451.

[156] Wang DY, van der Mei HC, Ren Y, et al. Lipid-based antimicrobial delivery-systems for the treatment of bacterial infections. *Front Chem* 2020; 7: 872.

[157] Drulis-Kawa Z, Gubernator J, Dorotkiewicz-Jach A, et al. In vitro antimicrobial activity of liposomal meropenem against Pseudomonas aeruginosa strains. *Int J Pharm* 2006; 315: 59–66.

[158] Liu P, Chen G, Zhang J. A review of liposomes as a drug delivery system: current status of

approved products, regulatory environments, and future perspectives. *Molecules* 2022; 27: 1372.

[159] Younes M, Aggett P, Aguilar F, et al. Safety of nisin (E 234) as a food additive in the light of new toxicological data and the proposed extension of use. *EFSA J* 2017; 15: 5063.

[160] Twomey E, Hill C, Field D, et al. Bioengineered nisin derivative M17Q has enhanced activity against Staphylococcus epidermidis. *Antibiotics* 2020; 9: 305.

[161] Singh S. Liposome encapsulation of doxorubicin and celecoxib in combination inhibits progression of human skin cancer cells. *Int J Nanomedicine* 2018; 13: 11–13.

[162] Chi H, Holo H. Synergistic antimicrobial activity between the broad spectrum bacteriocin garvicin KS and nisin, farnesol and polymyxin B against gram-positive and gram-negative bacteria. *Curr Microbiol* 2018; 75: 272–277.

[163] Jensen C, Li H, Vestergaard M, et al. Nisin damages the septal membrane and triggers DNA condensation in methicillin-resistant Staphylococcus aureus. *Front Microbiol* 2020; 11: 1007.

[164] Molujin AM, Abbasiliasi S, Nurdin A, et al. Bacteriocins as potential therapeutic approaches in the treatment of various cancers: a review of in vitro studies. *Cancers* 2022; 14: 4758.

[165] Murinda SE, Rashid KA, Roberts RF. In vitro assessment of the cytotoxicity of nisin, pediocin, and selected colicins on simian virus 40-transfected human colon and Vero monkey kidney cells with trypan blue staining viability assays. *J Food Prot* 2003; 66: 847–853.

[166] Kamarajan P, Hayami T, Matte B, et al. Nisin ZP, a bacteriocin and food preservative, inhibits head and neck cancer tumorigenesis and prolongs survival. *PLoS One* 2015; 10: e0131008.

[167] Paiva AD, de Oliveira MD, de Paula SO, et al. Toxicity of bovicin HC5 against mammalian cell lines and the role of cholesterol in bacteriocin activity. *Microbiology* 2012; 158: 2851–2858.

[168] Inglut CT, Sorrin AJ, Kuruppu T, et al. Immunological and toxicological considerations for the design of liposomes. *Nanomaterials* 2020; 10: 190.

[169] Maldonado-Pereira L, Schweiss M, Barnaba C, et al. The role of cholesterol oxidation products in food toxicity. *Food Chem Toxicol* 2018; 118: 908–939.

[170] Ahmad S, Ahmad A, Schneider K, et al. Cholesterol interferes with the MTT assay in human epithelial-like (A549) and endothelial (HLMVE and HCAE) cells. *Int J Toxicol* 2006; 25: 17–23.

[171] Rashwan R, Varano della Vergiliana JF, Lansley SM, et al. Streptococcus pneumoniae potently induces cell death in mesothelial cells. *PLoS One* 2018; 13: e0201530.

[172] Mountcastle SE, Cox SC, Sammons RL, et al. A review of co-culture models to study the oral microenvironment and disease. *J Oral Microbiol* 2020; 12: 1773122.

[173] Otto M. Staphylococcus epidermidis – the "accidental" pathogen. *Nat Rev Microbiol* 2009; 7: 555–567.

[174] Rai P, He F, Kwang J, et al. Pneumococcal pneumolysin induces DNA damage and cell cycle arrest. *Sci Rep* 2016; 6: 22972.

[175] Taher M, Susanti D, Haris MS, et al. PEGylated liposomes enhance the effect of cytotoxic drug: a review. *Heliyon* 2023; 9: e13823.

[176] Huan Y, Kong Q, Mou H, et al. Antimicrobial peptides: classification, design, application and research progress in multiple fields. *Front Microbiol* 2020; 11: 582779.

[177] Prakash G, Shokr A, Willemen N, et al. Microfluidic fabrication of lipid nanoparticles for the delivery of nucleic acids. *Adv Drug Deliv Rev* 2022; 184: 114197.

[178] Hoseini B, Jaafari MR, Golabpour A, et al. Application of ensemble machine learning approach to assess the factors affecting size and polydispersity index of liposomal nanoparticles. *Sci Rep* 2023; 13: 18012.

[179] Okuda KI, Zendo T, Sugimoto S, et al. Effects of bacteriocins on methicillin-resistant Staphylococcus aureus biofilm. *Antimicrob Agents Chemother* 2013; 57: 5572–5579.

[180] DuMont AL, Torres VJ. Cell targeting by the Staphylococcus aureus pore-forming toxins: it's not just about lipids. *Trends Microbiol* 2014; 22: 21–27.

[181] Imran M, Revol-Junelles AM, Bruin M, et al. Fluorescent labeling of nisin Z and assessment of anti-listerial action. *J Microbiol Methods* 2013; 95: 107–113.

[182] Rudokas M, Najlah M, Alhnan MA, et al. Liposome delivery systems for inhalation: a critical review highlighting formulation issues and anticancer applications. *Med Princ Pract* 2016; 25: 60–72.

[183] Ghanbarzadeh S, Valizadeh H, Zakeri-Milani P. The effects of lyophilization on the physico-chemical stability of sirolimus liposomes. *Adv Pharm Bull* 2013; 3: 25–29.

Appendix

Table A1. Complete BBD, including coded levels for the independent factors per run (X_1 – FRR; X_2 – nisin concentration; X_3 – EPG molar composition) and all dependent variable outputs. Values represent mean ± SD (n=3).

Run	Coded Level			Response			
	X_1	X_2	X_3	Y_1 – EE (%)	Y_2 – LC (%)	Y_3 – Size (nm)	Y_4 – PDI
1	-1	-1	0	71.94 ± 8.85	2.01 ± 0.25	146.18 ± 16.09	0.14 ± 0.05
2	1	-1	0	82.87 ± 7.40	5.59 ± 0.50	136.50 ± 8.50	0.09 ± 0.06
3	-1	1	0	70.94 ± 9.14	5.96 ± 0.77	182.46 ± 5.75	0.18 ± 0.02
4	1	1	0	32.30 ± 8.18	6.54 ± 1.66	303.58 ± 18.14	0.24 ± 0.11
5	-1	0	-1	19.32 ± 9.37	1.08 ± 0.53	152.71 ± 13.50	0.13 ± 0.02
6	1	0	-1	4.42 ± 2.71	0.60 ± 0.37	163.41 ± 23.24	0.18 ± 0.06
7	-1	0	1	69.46 ± 9.30	3.88 ± 0.52	143.66 ± 10.88	0.18 ± 0.04
8	1	0	1	79.19 ± 5.39	10.64 ± 0.73	151.91 ± 10.18	0.25 ± 0.02
9	0	-1	-1	24.66 ± 7.49	1.13 ± 0.34	141.33 ± 10.96	0.14 ± 0.02
10	0	1	-1	9.27 ± 5.05	1.15 ± 0.63	167.51 ± 21.46	0.19 ± 0.05
11	0	-1	1	71.80 ± 6.21	3.27 ± 0.28	115.70 ± 1.72	0.17 ± 0.04
12	0	1	1	75.20 ± 8.95	10.27 ± 1.22	175.11 ± 11.40	0.34 ± 0.01
13	0	0	0	78.57 ± 6.96	7.17 ± 0.64	140.76 ± 7.14	0.17 ± 0.03
14	0	0	0	72.44 ± 7.60	6.61 ± 0.69	154.53 ± 9.99	0.17 ± 0.02
15	0	0	0	68.99 ± 8.41	6.30 ± 0.77	146.32 ± 3.51	0.17 ± 0.03

Table A2. Target values for each studied response variable from the series of optimization solutions, used as a basis for parameter fitting through the liposomal BBD model.

Response	Target Value						
	O1	**O2**	**O3**	**O4**	**O5**	**O6**	**O7**
PS (nm)	115.7	140.0	145.0	130.0	140.0	150.0	160.0
PDI	0.09	0.09	0.17	0.09	0.09	0.09	0.09
LC (%)	10.64	10.64	6.60	10.64	10.64	10.64	10.64
EE (%)	82.87	75.00	72.00	82.87	82.87	82.87	82.87

Table A3. Comparison of PS, PDI, and ZP of loaded and unloaded liposomes at varying molar compositions of cholesterol. Values represent mean ± SD (n=3).

Cholesterol (mol%)		PS (nm)	PDI	ZP (mV)
30	Loaded	125.27 ± 2.35	0.33 ± 0.02	-25.32 ± 2.46
	Unloaded	120.19 ± 5.72	0.37 ± 0.11	-31.42 ± 5.31
45	Loaded	137.36 ± 5.04	0.21 ± 0.01	-35.73 ± 2.41
	Unloaded	126.43 ± 14.45	0.27 ± 0.05	-29.06 ± 3.77
60	Loaded	145.13 ± 7.68	0.17 ± 0.02	-33.00 ± 7.28
	Unloaded	104.36 ± 6.14	0.18 ± 0.03	-28.52 ± 3.08
75	Loaded	149.84 ± 5.06	0.27 ± 0.01	-31.89 ± 1.81
	Unloaded	121.09 ± 10.97	0.25 ± 0.01	-32.84 ± 12.76

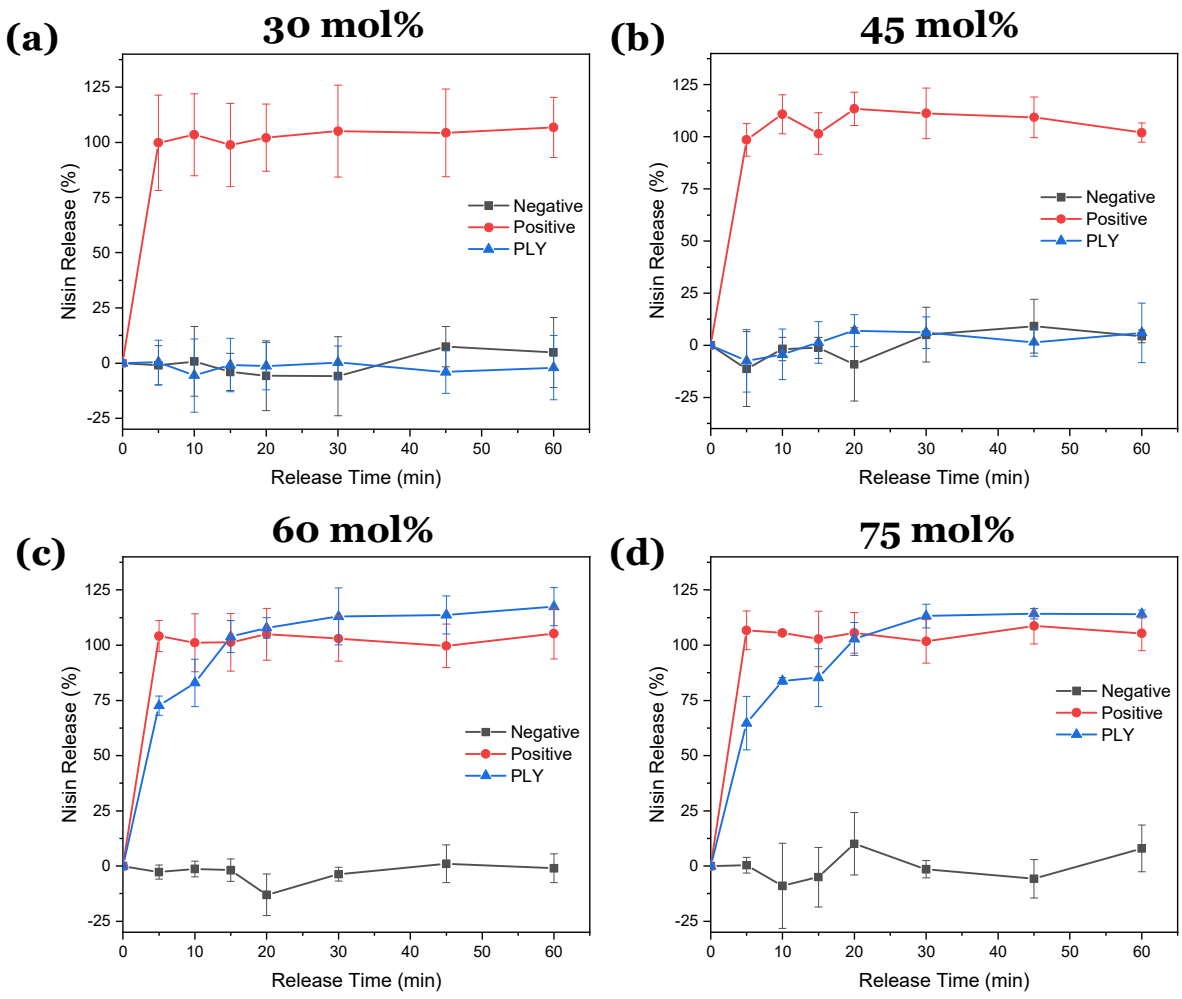


Figure A1. Liposomal release of nisin at various timepoints following incubation with PLY (4 µg/mL) at 37ºC, including a negative control with no toxin and positive release control containing 0.2% Triton. These assays were conducted on liposomes containing **(a)** 30 mol%, **(b)** 45 mol%, **(c)** 60 mol%, and **(d)** 75 mol% cholesterol (200 µM dose). Values represent mean ± SD (n=3).

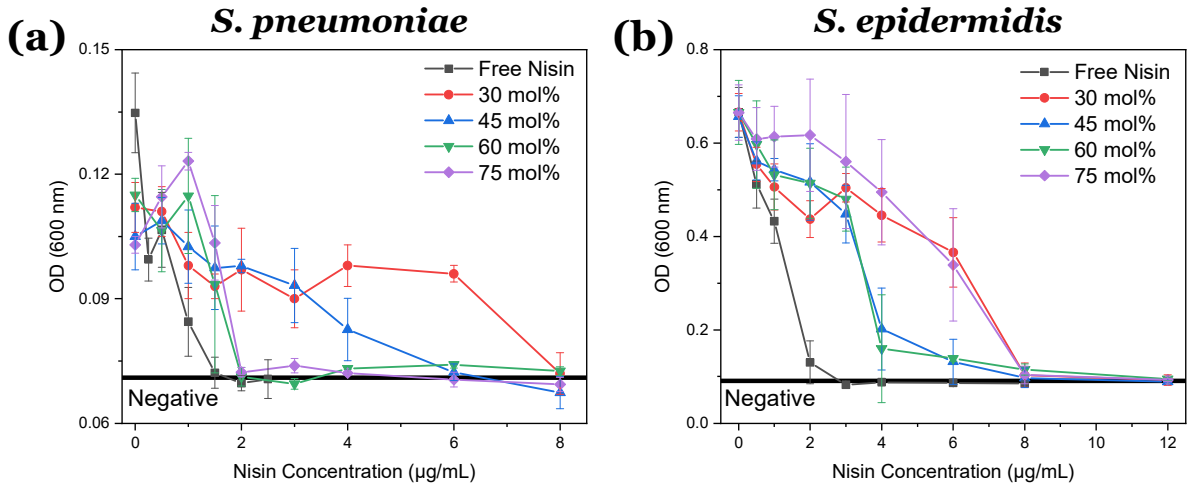


Figure A2. OD measurements at 600 nm to monitor bacterial susceptibility of **(a)** *S. pneumoniae* and **(b)** *S. epidermidis* to free and liposome-encapsulated nisin as compared to a negative control at an initial load of 8.6×10^5 CFU/mL. The molar composition of cholesterol present in the liposomes was varied between 30 and 75 mol% as indicated. Values represent mean ± SD (n=3).

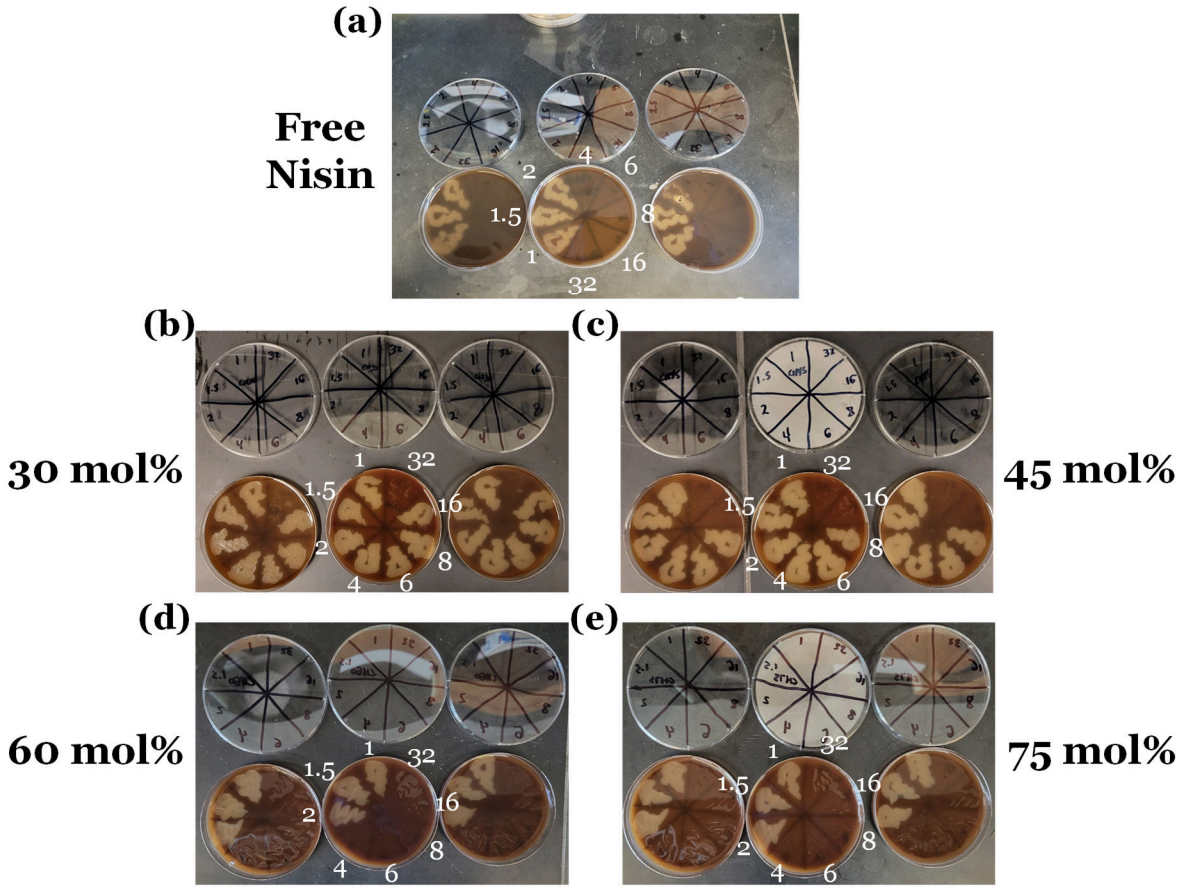


Figure A3. Determination of MBC against *S. pneumoniae* for **(a)** free nisin, as well as liposomes with a molar content of **(b)** 30 mol%, **(c)** 45 mol%, **(d)** 60 mol%, and **(e)** 75 mol% cholesterol via growth of 24 h MIC culture on TSA plates supplemented with defibrinated sheep blood. Relevant concentrations have been indicated in a white overlay, with all units being in µg/mL. Triplicate measurements are displayed.

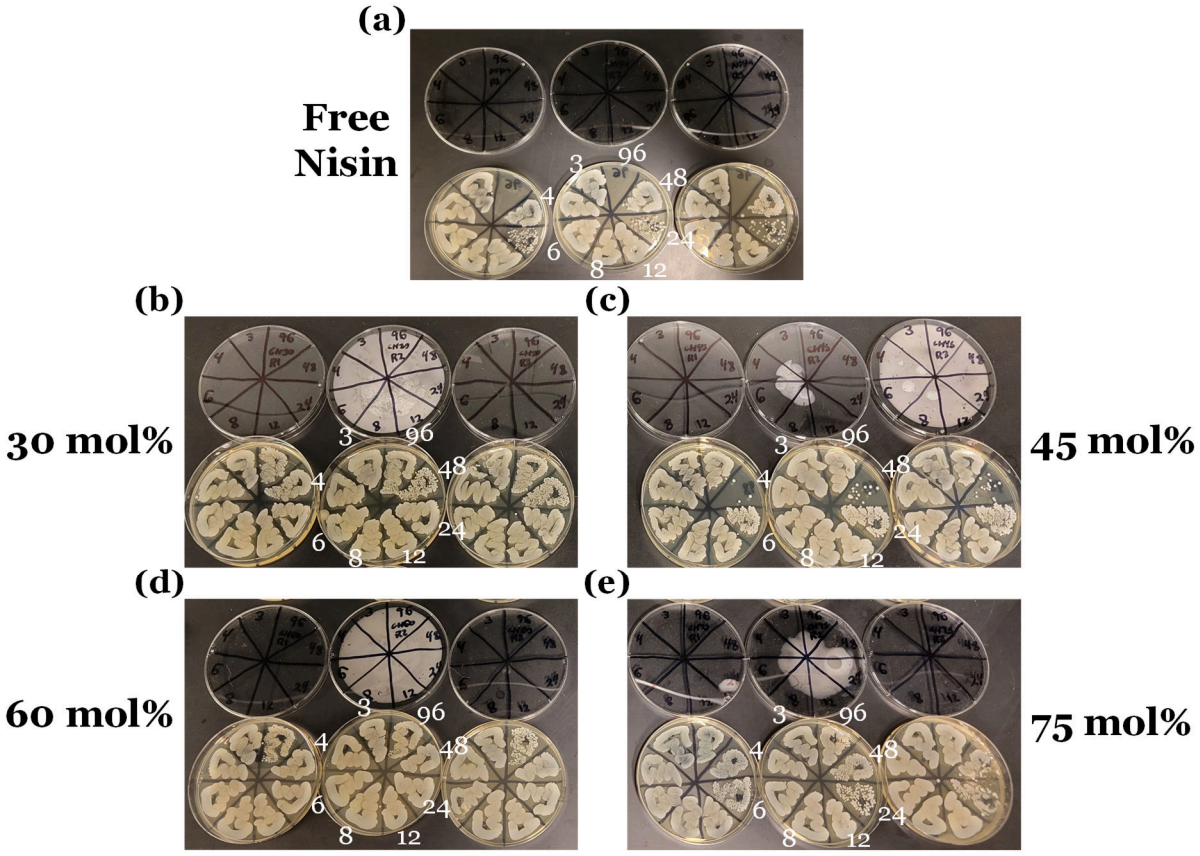


Figure A4. Determination of MBC against *S. epidermidis* for **(a)** free nisin, as well as liposomes with a molar content of **(b)** 30 mol%, **(c)** 45 mol%, **(d)** 60 mol%, and **(e)** 75 mol% cholesterol via growth of 24 h MIC culture on TSA plates. Relevant concentrations have been indicated in a white overlay, with all units being in µg/mL. Triplicate measurements are displayed.

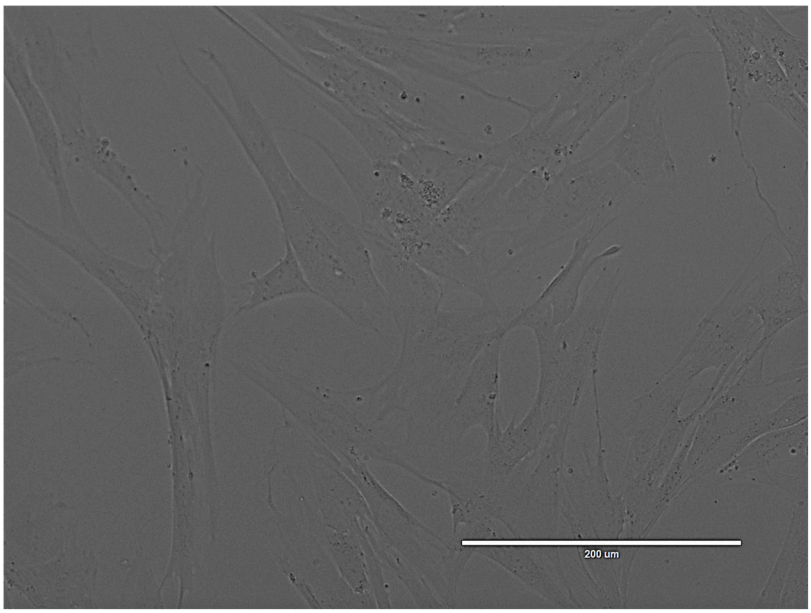


Figure A5. Optical microscope image of cultured IMR-90 cells affixed to a surface-treated 96-well plate. The scale bar represents 200 μm.